Diffusion of CaM, CaMKIIα and CaMKIIβ in neurons revealed by fluorescence correlation spectroscopy

March 2018

Seyed Morteza HEIDARINEJAD MOHAMMADI

ヘイダリネジャド　モハマデイ　セイエド モルテザ

Diffusion of CaM, CaMKIIα and CaMKIIβ in neurons revealed by fluorescence correlation spectroscopy

March 2018

Waseda University

Graduate School of Advanced Science and Engineering

Major in Life Science and Medical Bioscience

Research on Neurophysiology

Seyed Morteza HEIDARINEJAD MOHAMMADI

ヘイダリネジャド モハマデイ セイエド モルテザ

Contents

Summary

Calcium/calmodulin-dependent protein kinase II (CaMKII) is one of the important proteins in the neurons. Its unique oligomer formation property plays the leading part of the "molecular memory" hypothesis in synaptic plasticity. CaMKIIα translates the intracellular Ca^{2+} level to different molecular responses. Another important protein, which is serving as a signaling protein in neurons, is calmodulin (CaM). CaM cooperatively binds to Ca^{2+} and spreads extracellular signals through CaM-binding substrates. It triggers CaMKII activation by binding to CaMKII holoenzyme in cooperation with four Ca^{2+} ions and leads CaMKII to autonomy state. Therefore, elucidating the dynamics of CaM and CaMKII in both cytosol and nucleus of living neurons is essential for understanding the role of CaM/CaMKII pathway in relation to the regulations of synaptic plasticity and transcriptions in the nucleus.

In this study, I recruited the two-photon fluorescence correlation spectroscopy (FCS) technique to reveal the details of molecular dynamics of CaM and CaMKII expressed in human embryonic kidney 293 (HEK293) cells and in rat hippocampal neurons. In addition, a simultaneous multi-point FCS (MFCS) recording system was developed in this study owing to the benefit of the high-speed random scanning system. MFCS was able to monitor the behavior of those proteins in different compartments of neurons simultaneously, which is beneficial for understanding of molecular mechanisms independently operating in different cellular compartments.

Here, I showed that diffusion of CaM was altered by stimulation. Upon stimulation, CaM proteins started to diffuse faster. This change in diffusion pattern of CaM was possibly due to the dissociation from substrates. The change in diffusion of CaM was reversible and was recovered after washing out the stimuli. On the other hand, my

results showed that the molecular structure of CaMKII proteins was different in the cytosol and nucleus. The cytosolic structure of CaMKIIα and CaMKIIβ was composed of multi subunits in consistent with known homo- or heteromeric structure for this protein. Diffusing fragments in the nucleus were much faster. It implies existence of monomeric or degraded forms of CaMKIIα and β proteins in nucleus.

This study showed that the dodecameric holoenzyme structure of CaMKII is not stable, and is possibly degraded by Ca^{2+} dependent intracellular proteolytic activity. Upon activation of neurons, the CaMKIIα and CaMKIIβ holoenzyme structures split into small pieces. Such a liberation or degradation has a different mechanism than the cluster formation by CaMKII holoenzymes in the cytosol. The changes in structure of these molecules after stimulation in neurons showed different consequences for the protein in responding to external stimuli. Such structural changes of CaMKII proteins may be occurring in response to neuronal excitation, which would raise up new questions about the consequences of the function of CaMKII proteins in the neuron specifically in synaptic plasticity and cell death. In addition, this study showed that the measurement of protein diffusion from multiple points by MFCS would be a potent tool to investigate molecular dynamics of proteins in the neuron.

1 Introduction

1.1 Theory of diffusion

Early in the 19th century Joseph Fourier introduced the equations which explained the heat conduction (Fourier, J, 1822). Later Robert Brown coined the "Brownian motion" phrase and explained how randomly particles diffuse (Brown, R, 1828). In 1855, Adolf Fick developed the mathematics of diffusion equation, while Norbert Weiner in parallel connected the kinetic theory to the Brownian motion (Fick, 1855). In 1872, Ludwig Boltzmann introduced the transport equations, which provided basics of the random walk theory. At last in 1905, Albert Einstein unified all the former theories and used the function of random walk theory to explain relation between microscopic diffusion and the collision concept with macroscopic parameters such as diffusion coefficient (Einstein, A, 1905).

1.1.1 Fick's law

According to the Fick's law, flux of particles in space is proportional to the concentration gradient, and the proportional constant is the diffusion coefficient. If I suppose a non-uniform concentration function of $C(x)$ in the x direction, I will have a rightward flux of particles (Fig. 1-1).

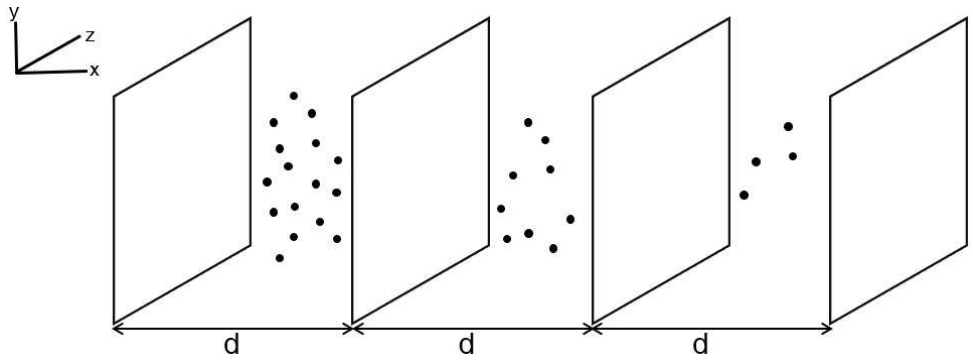

Figure 1-1. Representative example of non-uniform concentration distribution. Equally spaced planes perpendicular to x axis with distance of d. $C(x)$ is function of concentration in x direction.

Imagine the planes in perpendicular orientation to the x-axis each with known area (*S*). If I define *N(x,t)* as the number of particles between x and *x+dx* at time *t*, for the flux of particles across the planes, I could write:

$$j(x) = \frac{-\frac{1}{2}d\frac{d}{dx}N(x)}{\Delta t.S} \quad (1)$$

For number of particles, if the distance between the planes is *d*, one could write *N(x) = S.d.C(x)*, then flux of particles could be represented as follow:

$$j(x) = \frac{-\frac{1}{2}d^2}{\Delta t}\frac{d}{dx}C(x) \quad (2)$$

Here diffusion coefficient is defined as a proportional constant of the formula:

$$D = \frac{\frac{1}{2}d^2}{\Delta t} \quad (3)$$

Then the Fick's low in 3D dimension is written as:

$$\vec{j} = -D\nabla C(\vec{r}, t) \quad (4)$$

The Fick's law is valid in the media where diffusion properties of media at any position (*r*) are the same. Otherwise, in complex media, it may fail to describe the diffusion.

On the other hand, independent of Fick's law, the continuity equation for 3D space is expressed as follows:

$$\frac{\partial}{\partial t}C(\vec{r}, t) = -\nabla.\vec{j}(\vec{r}, t) \quad (5)$$

The continuity equation is showing that any change in the particle concentration is equal to the gradient of the flux of particles or in simpler words, any change in the number of particles at any given volume only depends on the diffusion of particles in and out of that space. By using the Fick's law, the continuity equation gives a new

diffusion equation:

$$\frac{\partial C(\vec{r},t)}{\partial t} = D\nabla^2 C(\vec{r},t) \tag{6}$$

1.1.2 The Stokes-Einstein equation

The Stokes-Einstein equation connects macroscopic quantities such as the diffusion coefficient and the viscosity to microscopic parameters such as the hydrodynamic radius and the Boltzmann's constant. Assuming a particle in spherical shape with a radius (R_h) moving in a stationary continuous viscous medium with viscosity of η, Stokes introduced the force of viscous medium on a sphere with the steady state velocity (υ) of medium as follows:

$$F = 6\pi\eta R_h \upsilon \tag{7}$$

Using definition of Fick in Eq (7), the Stokes-Einstein equation comes up for diffusion coefficient:

$$D = \frac{kT}{6\pi\eta R_h} \tag{8}$$

Where k is the Boltzmann's constant and T is the absolute temperature. By performing a random walk experiment, one can calculate the Boltzmann constant from the Stokes-Einstein equation.

1.2 Diffusion in biological systems

Since diffusion of macromolecules and in particular proteins is a topic which is connecting the classical view of physics to biology, it has gathered great interests of biophysicists. It is a tempting area to know how the biomolecules are behaving in the complex system, i.e., living cells. Looking for diffusion patterns of proteins is one of the

subjects, which is used to disclose the mysteries of structure and function of the proteins. Thanks to developed theories and techniques, nowadays there are several approaches to monitor behaviors of proteins *in vitro* and *in vivo*.

1.2.1 Importance of diffusion

Passive diffusion is the dominant way for intracellular transport of proteins. Such a mechanism is reasonable for any biological system, since saving energy is a very critical issue. Energy-free transports such as entropic based diffusions are more preferred than active transport, which costs adenosine triphosphate (ATP) (Philip Nelson, 2003). Proteins with stochastic diffusion patterns move in the entire cell volume within a few seconds. Therefore, diffusion of proteins is a critical parameter for the function of cells. Molecular functions such as signaling steps, gene transcription, intramolecular reactions and self-assembly of molecular structures in the cell are influenced by diffusion characteristics. All these events depend on the diffusion rate, thus better understanding of diffusion profiles of proteins is a necessary step to understand those mechanisms. Knowing the nature of the diffusion and then choosing the best mathematical model to extract the governing roles is the aim of the diffusion studies. 2D or 3D free diffusion, anomalous or confined diffusion with or without triplet transitions need different mathematical models to be analyzed.

1.2.2 Diffusion studies in living cells

For the intracellular diffusion studies, different methods have been used to quantify the behavior of macromolecules such as fluorescence recovery after photobleaching (FRAP) (Axelrod et al., 1976; Peters et al., 1974) and fluorescence fluctuation spectroscopy (FFS) (Magde et al., 1972). FRAP is the first method widely used in

diffusion studies due to its simplicity in terms of the technical aspects (Carisey et al., 2011; Mullineaux and Kirchhoff, 2007). Bleaching region of interest by high power light and recording the recovery rate over the time and space and then using proper fitting model is the approach to disclose the translational diffusion information. First it was introduced as a method to monitor the lateral diffusion of proteins and lipids of the membranes two-dimensionally (Axelrod et al., 1976; Mullineaux and Kirchhoff, 2007; Schlessinger et al., 1977; Waters, 2007). Then the technique was adopted to record from the cytoplasm, and to find out the mobility and binding properties of proteins in cytoplasm. The FRAP technique has been used in many neurobiological researches such as studying mobility of synaptic vesicles or transporters (Eriksen et al., 2009; Shtrahman et al., 2005), axonal transports (Gaffield et al., 2006; Orenbuch et al., 2012; Scott and Roy, 2012), synaptic structure (Tsuriel et al., 2006) and axonal skeleton characteristics (Gauthier-Kemper et al., 2012; Koskinen et al., 2012). FRAP yields two types of information. The recovery rate which is used to extract the diffusion coefficient and the recovery percentage to distinguish the mobile and immobile fractions of target molecules (De Los Santos et al., 2015). Photoswitching, photobleaching and overheating are the limitations of the FRAP technique (De Los Santos et al., 2015; Mueller et al., 2012; Sinnecker et al., 2005).

FFS or FCS has been used in enormous number of studies in living cells. The first intracellular record with FCS was done using microinjection of dye into cells (Brock et al., 1999). FCS has been used to record from different compartments of the cell such as the cytoplasm and the nucleus (Brock et al., 1999; Politz et al., 1998; Schwille et al., 1999). FCS analyses are able to discriminate between the active and passive diffusions, as it was used in the axon of squids to monitor the tubulin transportation profile (Köhler

et al., 2000; Terada et al., 2000). Later in this chapter, I will focus more on the FCS method and its applications.

1.2.3 Dynamics of proteins

Protein dynamics could affect the intracellular regulations in two distinct ways. The first way is the intrinsic motions such as conformational changes, which is important in reaction rates especially for the enzymes and regulatory proteins. The second way is diffusion of proteins which is an important factor for intracellular regulations and interactions in the cell. For this purpose, each protein could sweep all possible points of the intracellular space by a cost-free process within several seconds (Philip Nelson, 2003).

Various intracellular functions are influenced by diffusion rate such as oligomerization of proteins or rate of binding (Misteli, 2001). Therefore both types of motions should be taken into account for better understanding of the function of proteins in the cells (Henzler-Wildman et al., 2007).

1.3 Physics of fluorescence imaging

Fluorescence microscopy has been a rapidly expanding method in biology in last decades. Non-invasive nature of fluorescent probes and their wide range of applications have made it popular among biochemists and biophysicists. High spatial and temporal resolution of optical recordings at the molecular level has led to introduction of many useful techniques for study of biological systems such as fluorescence resonance energy transfer (FRET), fluorescence lifetime imaging microscopy (FLIM), single particle tracking (SPT), FRAP and FCS. Invention of these techniques has been accompanied with developing a lot of fluorescent tags and proteins, which have been recruited to

answer a wide range of questions from macromolecules conformational changes to the electrical activity of cells *in vitro* and *in vivo*. High signal to noise ratio with high specificities have led to doing experiments at the single molecule level. Here I provide a brief description about theory of fluorescence imaging related to FCS.

1.3.1 Basics of fluorescence

Photon emission by molecules or atoms that have absorbed photon or other electromagnetic radiations is called fluorescence. It occurs when the energy state is stimulated to higher energy levels by any radiant energy sources. Release of these absorbed energy is accompanied by emission of photons. In a general term, molecules with ability to emit photons upon excitation with light are called fluorophore.

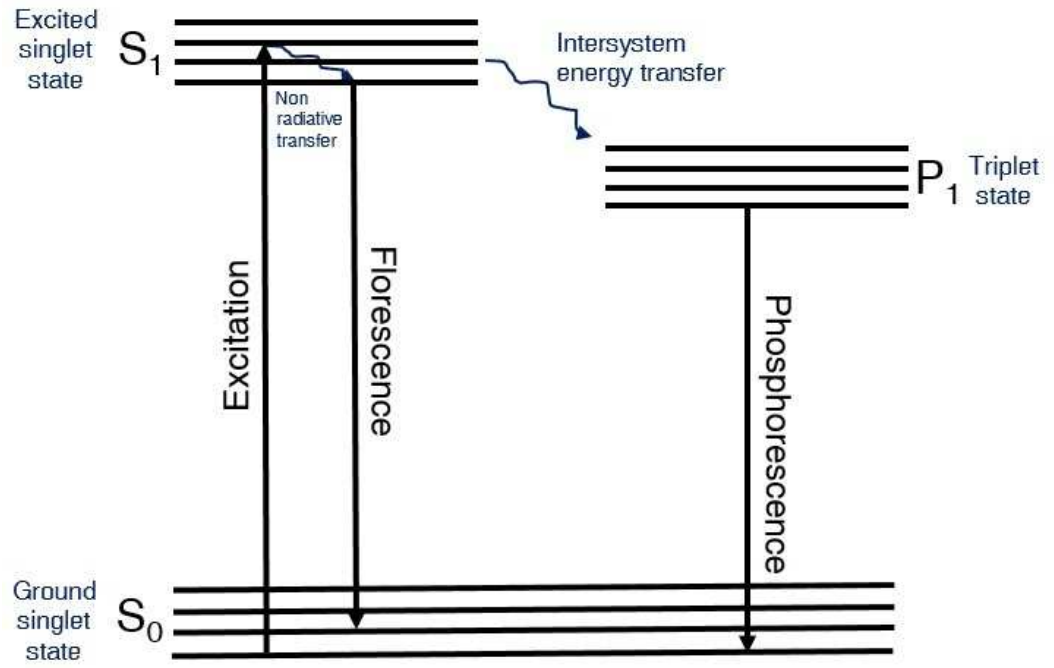

Figure 1-2. Diagram of the Jablonski for molecular energy levels.
Cycle of energy absorption and emission between ground state (S_0) and first singlet state (S_1). Because of non-radiative energy transfer within the state, energy of emitted photon is smaller than absorbed one. An intersystem energy transfer happens between the singlet state and the triplet state (P_1) which traps the electron much longer than S_1 and causes an on and off switch effect in light emission.

The Jablonski diagram explains the energy structure of photon emission from

energy levels and sublevels (Fig. 1-2). In principle, the electrons, which absorb energy from outside sources, may raise in energy levels within permitted energy states. Electrons after a while give back the energy and emit photon. In singlet state, electrons lose part of their energy due to conversion to other forms of energy, which results emission of photons with lower energy than absorbed ones. Due to this mechanism and according to the inverse relation between energy of photons and their wavelength (λ), wavelength of the emitted photons is longer than the absorbed one. The peak to peak difference between absorbed and emitted spectrum is called Stokes shift. Elevation of the electron energy and relaxing to the ground state is not a fixed pathway, and the existence of sublevels alters amount of absorbed and emitted energy in each cycle. Therefore, there are ranges of energies which stimulate the electrons between two specific energy levels and sublevels, and therefore there is spectrum of wavelengths which is emitted from fluorophores. In addition to the mentioned mechanism, sometimes there is an intersystem energy transfer in the molecule which receives the energy of elevated electron known as intersystem crossing or in particular triplet transition.

1.3.2 Triplet transitions

Triplet intersystem transitions convert part of energy of electrons to heat instead of photon in transition from an excited energy level to an intermediate energy state. Lifetime of electrons in the excited singlet states is in order of nanosecond while the triplet levels are long-live states and electrons are trapped in those levels in microsecond order. The emission of light from triplet states is called phosphorescence. The trapped electrons in the triplet state are out of fluorescence emission cycle, until they decay back to ground state and are stimulated again to a singlet energy level (S_1). The phenomenon

that a fraction of emission efficiency is trapped in triplet state is called “triplet state blinking” which changes the fluorescence emission from a constant manner to a flicker pattern. The blinking effect is a general term, which is used for any on and off switch phenomena of the dyes (Bagshaw and Cherny, 2006; Dickson et al., 1997).

In FCS experiments, triplet system is a subject of interest due to its microsecond time scale, which may interfere with FCS results directly. There are some environmental factors such as PH, which may change the triplet state characteristics. In other words, if the time scale of intracellular events be comparable with the blinking time scale, the FCS results will be affected by the interference of triplet state, which should be taken into account in analyzing FCS results.

1.3.3 Photobleaching

For fluorophores, losing the ability of emitting photons is called photobleaching. It is a serious issue for the methods, which are collecting high numbers of fluorescence photons from a sample. Molecules such as O_2 absorb energy of elevated electrons in triplet state. Such an energy transfer from the electron in the triplet state to other molecules produces free radicals such as singlet oxygen, which lead to damage to other molecules.

To avoid photobleaching, light intensity and duration of irradiation are two key parameters. Target molecules with slower diffusion rate or immobile targets are more in risk to be photobleached by light. The outcome of photobleaching is decrease in number of target molecules. On the other hand, photobleaching switches off the fluorophores, which resembles the fraction of fluorophores in “off” state by reducing the efficient irradiating time of fluorophores inside the exciting space. This is a serious problem for techniques such as FCS that is analyzed based on temporal information of excitations.

The best way to avoid photobleaching is reducing the light intensity, which should be determined for each fluorophore in different setups. It is a tradeoff for choosing optimum power to avoid photobleaching and to have enough photon number.

1.3.4 Fluorescent proteins

Acceptable fluorophores for imaging experiments emit around 10^9 photons per second (Maiti et al., 1997). Basically, stability and brightness are the two factors that are required for FCS experiments. Among fluorophores, fluorescent proteins have specific interest. They are expressed in cells without necessity of using invasive methods such as injection for labeling. Doubtless among the fluorescence proteins, the most popular one is green fluorescent protein (GFP) which was discovered in 1962 from jellyfish *Aequorea Victoria*, and 32 years later was expressed in bacteria (Weber, 2007). The structure of GFP keeps it resistant against bleaching. The chromophore part of GFP sequence contains a few amino acids (Ser-Tyr-Gly) in an α-helix, which is surrounded by a cylindrical β-sheet. For having more appropriate fluorophores, mutations in the GFP sequence have been introduced to make different variations in terms of absorption and emission spectra, quantum yield, photostability and dimerization properties. The enhanced GFP (EGFP) is the most common variant of GFP. It contains several mutations, and is brighter and more photostable. Besides, there are other fluorescent proteins such as DsRed with different spectrums.

1.4 Fluorescence Correlation Spectroscopy

The basic idea of fluorescence correlation spectroscopy is investigation of thermal fluctuation of macromolecules to gather their dynamic and kinetic information at equilibrium (Koppel, 1974; Krichevsky and Bonnet, 2002; Magde et al., 1972). FCS has

been recruited in the last three decades for analyzing diffusion, binding, estimation of concentration, translocation and conformational changes of bio-molecules (Chen et al., 2008; Schwille, 2001). In FCS experiments, a finely tuned laser spot within the sample reports fluorescence intensity fluctuations by a small number of labeled target molecules passing through the small volume (typically less than one femtoliter) of light (Fig. 1-3) (Kim et al., 2007; Schwille et al., 1999).

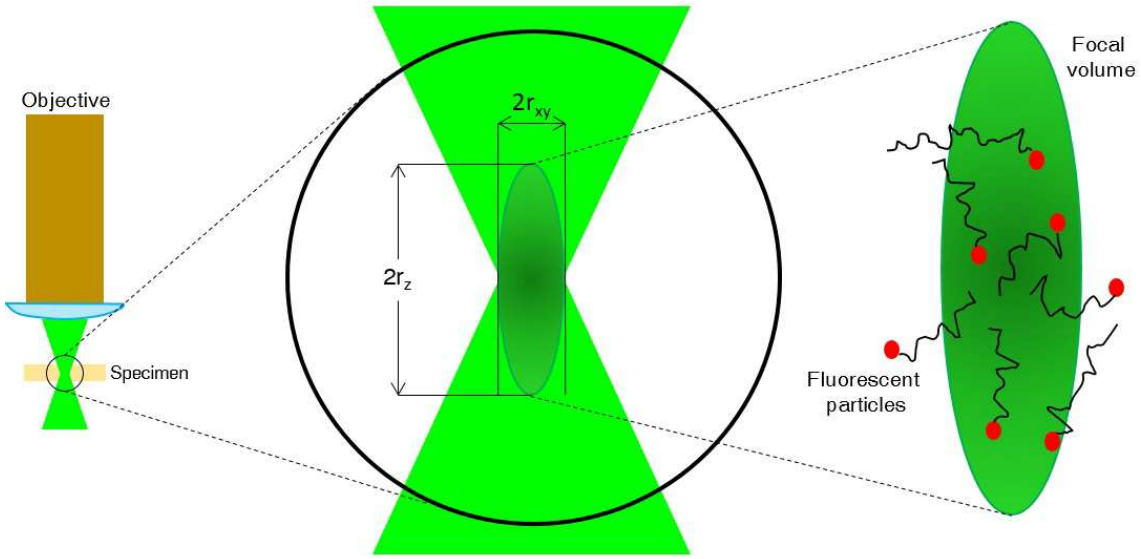

Figure 1-3. Schematic view of focused laser beam at specimen and fluctuations of light intensity recorded from laser focal volume.
The fluorescent particles are moving in and out of focal volume. The dimension of focal volume is estimated by radial (r_{xy}) and axial (r_z) radii.

Autocorrelation analyses of changes of fluorescence intensity reveal number, brightness and the diffusion time of the target molecule species (Müller et al., 2003; Schwille et al., 1999). The FCS technique is advantageous in its high sensitivity in concentration. The applicable range of target molecule concentration in the FCS technique is low, which avoids problems resulting from overexpression of proteins (Müller et al., 2003). In this section, I explain the theoretical and experimental aspects of the technique and discuss its advantages and disadvantages.

1.4.1 A historical view to FCS technique

FCS was introduced for study of chemical reactions and used for finding the diffusion coefficient in the early 1970s. It was proposed by the group of Douglas Magde, Elliot Elson and Watt W. Webb (Magde et al., 1972). They used the technique to study the binding between ethidium bromide (EtBr) and DNA strands. Due to the lack of appropriate facilities to focus the laser light in a femto liter scale, FCS experiments were started practically from early 90's by the adoption of the confocal microscopy. Inventions of lasers with high spatial and temporal stability to form a tiny femto liter volume for excitation and highly sensitive detectors were major developments for FCS experiments.

1.5 Theory of fluorescence correlation spectroscopy

FCS is an experimental method capable of sensing and converting fluctuations on emitted fluorescence to physical parameters. The most common usage of FCS is measuring diffusion of macromolecules, but in addition, there are other studies on observing the concentration, active transport, rotational diffusion, conformational changes and also photophysical phenomena such as photobleaching, light-induced blinking and intersystem crossing between singlet and triplet states (Schwille and Haustein, 2006).

Practically, FCS provides a measure for the self-similarity of a time series with different time lags. It is called autocorrelation when one signal is compared with itself and called cross-correlation when one signal is compared with another signal. After having auto or cross correlation graph, the graph is fitted to an appropriate model. In addition to the geometry of observation volume which is the most important factor for selecting the right model, other variations may be applied in the model according to

single or multi-photon excitation, free Brownian or anomalous diffusion, recording from intracellular medium or membrane and number of distinguishable diffusing targets.

To quantify the fluctuations, first I defined fluctuation of fluorescence intensity as *I(t)*. Any fluctuation in intensity profile is caused by the movement of number of particles, *N(t).* Based on intensity fluctuations, the autocorrelation function (ACF) is defined as follows:

$$G(\tau) = \frac{\langle \delta I(t).\delta I(t+\tau)\rangle_t}{\langle I(t)\rangle_t^2} \quad (9)$$

Where $I(t) = \langle I\rangle + \delta I(t)$, $\delta I(t)=I(t)-\langle I(t)\rangle$, ($\langle I(t)\rangle_t = \frac{1}{T}\int_1^T I(t)dt$), $\delta I(t)$ stands for fluctuation in *I(t)* at time *t* and <...> means average over time. For simplicity, some authors set the time *t = 0* and rewrite the formula as:

$$G(\tau) = \frac{\langle \delta I(0).\delta I(\tau)\rangle_t}{\langle I(t)\rangle_t^2} \quad (10)$$

Because $I(t)= \langle I(t)\rangle+\delta I(t)$ and $\langle \delta I\rangle = 0$, one could write the formula as follows:

$$G(\tau) = \frac{\langle I(t).I(t+\tau)\rangle_t}{\langle I(t)\rangle_t^2} - 1 \quad (11)$$

Or in a simple expression:

$$G(\tau) = \frac{\langle I(t).I(t+\tau)\rangle_t}{\langle I(t)\rangle_t^2} \quad (12)$$

So, some groups, instead of using fluctuations on the fluorescence signals, use the fluorescence itself. In the first way, when time is approaching to infinite, correlation decays to 0, while in the second way correlation decays to 1 instead.

In a typical calculation of ACF, *I(t)* is determined by concentration of particles

located at position *r* at the time *t*. With the definition of optical system spatial collection efficiency as *S(r)*, spatial excitation intensity distribution as *P(r)* and brightness of species in focal volume as *ε(t)*, I could write:

$$I(t) = \sum_{i=1}^{n} \int \varepsilon_i(t).C_i(\vec{r},t).P(\vec{r}).S(\vec{r})dV \quad (13)$$

Where *n* is the number of species with a specific brightness. Using this calculation, the correlation function could be re-written.

If I suppose that only there is one species in the sample and the number of particles, *N*, then for amplitude of correlation function at t=0, *G(0)*, I will have:

$$G(0) = \frac{\langle \delta I(t)^2 \rangle}{\langle I \rangle^2} = \frac{\langle I^2 \rangle - \langle I \rangle^2}{\langle I \rangle^2} = \frac{\langle N^2 \rangle - \langle N \rangle^2}{\langle N \rangle^2} = \frac{1}{\langle N \rangle} \quad (14)$$

Therefore *G(0)* is used to determine the average number of particles in the focal volume of recording.

In the 3D Gaussian geometry, it is assumed that the probability of fluorescence emission at the center of the focal volume is higher due to spatial distribution of light intensity. V_{eff} could be calculated by:

$$V_{eff} = \pi^{3/2} r_{xy}^2 r_z \quad (15)$$

Where r_{xy} and r_z are the radial and axial radii, respectively.

1.5.1 Fitting models

According to the characteristic of the environment and target particles, different fitting models are used to extract accurate quantitative results.

1.5.1.1 3D normal diffusion

The simplest model of diffusion is assuming that one species of fluorescent particle

with a constant brightness is diffusing freely in the medium. For finding an appropriate model, first I start from definition of the Fick's Law:

$$\frac{\partial C(\vec{r},t)}{\partial t} = D\nabla^2 C(\vec{r},t) \tag{16}$$

There are some preliminary assumptions; I apply them to elucidate the concentration expression. Assume that particles start their diffusion at *t = 0* from origin in the system without physical barrier. Therefore, the initial condition is *C(r;0)* = <*C*>. *δ(r)* and *C(r;t) = 0*, when *r* is approaching to infinite. Then for concentration, I write:

$$C(\vec{r},t) = \frac{\langle C\rangle}{(4\pi Dt)^{3/2}} e^{-r^2/4Dt} \tag{17}$$

Using this definition, it is more straightforward to introduce a right model for 3D diffusion which is reported for the first time in 1974, (Elson and Magde, 1974).

$$G(\tau) = \frac{1}{\langle C\rangle}\frac{1}{r_0^2\pi^{3/2}r_z}\left(1+\frac{\tau}{\tau_D}\right)^{-1}\left(1+\frac{1}{\gamma^2}\frac{\tau}{\tau_D}\right)^{-1/2}$$

$$G(\tau) = \frac{1}{\langle N\rangle}\left(1+\frac{\tau}{\tau_D}\right)^{-1}\left(1+\frac{1}{\gamma^2}\frac{\tau}{\tau_D}\right)^{-1/2} \tag{18}$$

Where $\tau_D = \frac{r_{xy}^2}{4D}$ is the diffusion time for one-photon excitation, $\tau_D = \frac{r_{xy}^2}{8D}$ is for two-photon excitation, and $\gamma = \frac{r_z}{r_{xy}}$ is called structural parameter.

In FCS records of particles which are moving in two dimensions, any movement in z direction is negligible or in simple expression, γ>>1, then the ACF is written in two dimensions as follows:

$$G(\tau) = \frac{1}{\langle N\rangle}\left(1+\frac{\tau}{\tau_D}\right)^{-1} \tag{19}$$

1.5.1.2 Triplet state, photophysical kinetics

Suppose there are two distinct pools of target particles. The first group is fluorescent and the second group is not, and there is a mechanism between the two groups for intergroup conversions, then the diffusion profile of such a mixture is called diffusion of two-state photophysical system. The mechanism of fluorophores with triplet energy transitions is the most known example for these systems. The intersystem energy crossing between the singlet and triplet energy states causes two separate groups of the off and on fluorophores, which cannot be explained by a simple 3D diffusion interpretation. With assuming a totally dark state for one of the groups, the triplet system correlation function is explained by an additional part as follows:

$$G_{(triplet)}(\tau) = \frac{1-\theta_T+\theta_T.e^{-\tau/\tau_T}}{1-\theta_T} \quad (20)$$

θ_T is the fraction of particles inside the focal volume which are in the triplet state with time constant of τ_T.

According to the two-state diffusion model, for systems with triplet state, an accurate correlation function with a single on-off blinking term will be:

$$G(\tau) = \left(\frac{1-\theta_T+\theta_T.e^{-\tau/\tau_T}}{1-\theta_T}\right)\frac{1}{\langle N\rangle}\left(1+\frac{\tau}{\tau_D}\right)^{-1}\left(1+\frac{1}{\gamma^2}\frac{\tau}{\tau_D}\right)^{-1/2} \quad (21)$$

1.5.1.3 Multi-component models

In more general cases, it is possible that more than one species diffuse in the system. If it is supposed that *n* non-interacting species with different brightness of ε_i and diffusion times of τ_{Di} are diffusing simultaneously, the ACF of system is introduced as:

$$G(\tau) = \frac{\sum_i^n C_i\varepsilon_i^2.G_{Bi}}{V_{eff}(\sum_i C_i\varepsilon_i)^2} \quad (22)$$

Whereas $$G_{Bi} = \left(1 + \frac{\tau}{\tau_{Di}}\right)^{-1} . \left(1 + \frac{\tau}{\gamma^2 \tau_{Di}}\right)^{-1/2} \quad (23)$$

1.5.1.4 Cross-correlation

In cases that binding or dissociation between two differently labeled molecules are investigated, cross-correlation or measuring the correlation between diffusion of two independent fluorescent molecules is used (Schwille et al., 1997). For cross-correlation experiments, two detectors are used. The cross-correlation function is defined as:

$$G_{1,2}(\tau) = \frac{\langle \delta I_1(t) . \delta I_2(t+\tau) \rangle_t}{\langle I_1(t) \rangle \langle I_2(t) \rangle} \quad (24)$$

In addition, to extract information of binding of two molecules, cross-correlation is less suffered from inherent noises caused by detectors due to the intrinsic normalization process than autocorrelation analyses. Such a noise is produced after detection of each photon, which is called afterpulsing noise, and may affect fast diffusions in the 1-5 μs range. Cross-correlation is a well-suited method to investigate the binding between macromolecules.

1.5.1.5 Anomalous diffusion

The anomalous diffusion is a condition that diffusive particles do not obey the rules of free diffusion, and translocation of molecules is not called Brownian motion. In the non-Brownian motions, the Fick's law is not applicable, and obstacles, barriers or confined spaces change the pattern of diffusion. With some modifications in definitions and assumptions, the ACF for anomalous diffusion is written as:

$$G(\tau) = \left(\frac{1-\theta_T+\theta_T . e^{-\tau/\tau_T}}{1-\theta_T}\right) \frac{1}{\langle N \rangle} \left(1 + \left(\frac{\tau}{\tau_D}\right)^{\alpha}\right)^{-1} \left(1 + \frac{1}{\gamma^2} \left(\frac{\tau}{\tau_D}\right)^{\alpha}\right)^{-1/2} \quad (25)$$

In case α=1, diffusion is normal and is calculated as explained before, but if α≠1,

diffusion is anomalous and calculated *D* is called apparent diffusion coefficient (Banks and Fradin, 2005).

1.5.1.6 Used FCS formula in this study

For multiple diffusing species, the ACF of n species with different diffusion times was defined by:

$$G(\tau) = G(0).\sum_{i=1}^{n} \varphi_i.\left(1+\frac{\tau}{\tau_{D,i}}\right)^{-1}.\left(1+\frac{\tau}{\gamma^2\tau_{D,i}}\right)^{-1/2} + G_{\infty} \qquad (26)$$

$$\sum_{i=1}^{n} \varphi_i = 1 \quad and \quad 0 \le \varphi_i \le 1$$

On and off switch of dyes by changing their quantum efficiency was another factor which altered *I(t)* and was taken into account in opting the appropriate autocorrelation equation (Haupts et al., 1998). According to the Stokes-Einstein's equation, if R_h(Eq. 8) is the hydrodynamic radius of particles, to find relation between mass of particles and diffusion coefficient, I assumed the linear relation between volume and mass of molecules. So, for volume and mass, I could write: $V_P = \frac{4}{3}\pi R_h^3 \propto m$, then for *D* and *M* as a molecular mass, I will have:

$$D \propto \frac{1}{\sqrt[3]{M}} \quad , \quad \frac{D_2}{D_1} = \sqrt[3]{\frac{M_1}{M_2}} \qquad (27)$$

Based on Eq (22 and 23), the average fluorescence intensity of the mixture of species will be given by $\langle I_t \rangle = \sum_{i=1}^{n} \langle I_i \rangle$, whereas $\langle I_i \rangle = \mathcal{E}_i.N_i$. With this definition for two-component system, I will have (Chen et al., 2000):

$$\langle I_t \rangle = \varepsilon_1.N_1 + \varepsilon_2.N_2 \qquad (28)$$

$$\langle I_t \rangle = (\varepsilon_1.C_1 + \varepsilon_2.C_2).V_{eff} \qquad (29)$$

$$\varepsilon_1 = \frac{\langle I_t \rangle}{V_{eff}(C_1 + \frac{\varepsilon_2}{\varepsilon_1}.C_2)} \quad (30)$$

By using Eq (22) as a model and extracting fitting parameters such as concentration and brightness ratio, ε_1 or ε_2 are calculated by using Eq (30). For fitting of ACF, τ_T = 0.15 ms was used for all analyses (Eq. 25).

1.6 Two-photon fluorescence correlation spectroscopy

For any FCS experimental setups, illumination of sample, collection of emitted fluorescence and calculation of correlation data are essential. According to the advantages of two-photon FCS setup (Berland et al., 1995), I chose to use two-photon excitation for FCS records based on an acousto optic deflector (AOD)-driven two-photon setup (Shafeghat et al., 2016).

1.6.1 Advantages of two-photon FCS

The two-photon fluorescence correlation spectroscopy uses non-linear two-photon excitation. Because of the low probability of excitation out of the laser focus region, no pinhole before detector is necessary for the two-photon system, while using pinhole is mandatory in the confocal system to get rid of out of focus emissions. In addition, using wavelengths which are roughly two-fold of that used wavelengths in confocal microscopes makes easy separation of excitation and emission light. Less photophysical interactions of light with tissue and less photo damage are other advantages.

1.6.2 Signal to noise ratio

For reliable analysis of FCS records, high signal to noise ratio (S/N) is necessary. Some factors are important for having high S/N. The brightness of target molecules and

the emitted number of photons per molecule from a fluorophore is a crucial factor for S/N. S/N is influenced by the level of scattered light, background optical noise, stability of exciting light source and shot noise of detectors. Using two-photon microscopy and bright fluorophores are two factors which remove most of the noises.

1.6.3 Photobleaching

Photobleaching due to using high light power is not a desirable effect for fluorescence recordings and causes wrong interpretation of molecular events. Therefore, the fluorescence records with non-flat baseline should be considered for correction.

The most efficient way to avoid photobleaching is choosing appropriate laser power. In order to choosing the best power, it is necessary to know the relation between emitted intensity of a specific fluorophore and the power of light. Finding the optimum power to avoid bleaching and in parallel to have enough photon number in order to plot the smooth autocorrelation curve is a critical step to decide.

On the other hand, reducing the recording time is another factor, which reduces the bleaching effect. It is recommended to do record several times with short durations. Recording from one point for longer time and dividing the recorded intensity trace to several time-windows in order to calculate several autocorrelation curves and then averaging them is not recommended. Longer recording times cause more bleaching. Therefore, changing the recording points helps to reduce the bleaching level.

It should be noted that sometimes the bleaching is not avoidable. For example, in recordings from confined spaces such as dendrites, bleaching is more likely than record from soma or nucleus. Therefore, having correction mechanisms in analysis before conversion to autocorrelation curve is mandatory. Using algorithms for linear regression or fitting the baseline with single or double exponential curves and compensation of

bleaching effect is essential.

1.6.4 Acousto-optic modulators and deflectors

To be able to record from any desired single points, it is necessary to steer the laser beam properly. Steering devices such as mechanical galvanometric mirrors or AODs as a scanning system is used to guide the laser beam. I followed the proposed setup of Salome and colleagues, which introduced the AOD driven random-scanning two photon microscope setup. They used two perpendicular AODs in their setup and one acousto optic modulator (AOM) for spatial compensation due to the use of the AODs, which is placed before the AODs. Such a setup is able to record from all the desired points with a jumping time between the points (Salomé et al., 2006).

1.6.5 Recording system and detectors

The emitted light from sample is collected by the objective and guided toward detectors. Based on the experimental design, one or two detectors are used to record from one or two distinct spectra of emitted light. In particular, for the cross-correlation experiments where two labeled target molecules with different dyes are recorded simultaneously, two detectors are used. FCS needs detectors with high sensitivity such as PMTs. In PMTs, each incident photon is converted to an electron and then the PMT enhances the signal by multiplication of produced electrons.

1.6.6 Time-Correlated Single Photon Counting

The time-correlated single photon counting (TCSPC) technique measures the time difference between the excitation pulse from source pulsed laser and the time of photon detection in detector. In this mode, the light sources with high repetition rate of 80 MHz are used for excitation. Emitted photons are detected by APDs or PMTs. Then each

detection is conveyed to a TCSPC module. A TCSPC card starts a ramp signal with the detection of each photon in the detector using a “time to amplitude” converter. Corresponding laser pulse is used to stop the signal. Subsequently, an “analogue to digital” convertor is used to address each voltage start-stop cycle. The “analogue to digital” converter counts the number of cycles accordingly. The dead time between two consecutive incident photons is preferred to be minimum. The TCSPC recording mode has high sensitivity to low number of photons. A limit is detection of only one photon within the time window of two consecutive laser pulses. In this system, extra photons (more than one) in each time window are rejected.

1.6.7 Requirements of intracellular FCS recording

FCS is a method for recording from the steady state systems. The cells as dynamic systems never fulfill this requirement. Therefore, all the intracellular records should be short enough to reduce the impacts of non-equilibrium medium characteristics. Having enough interval between records helps to reduce local bleaching of intracellular media. To avoid bleaching, recording from different points is another alternative. In addition, using bright fluorophores, stable excitation light and fast and sensitive detectors are necessary for acceptable intracellular records (Kim et al., 2007).

1.6.8 Optical system and calibration

The size and shape of focused laser light are the factors which directly determine the quality of FCS records. Well-tuned Gaussian distributed laser light helps to fulfil theoretical assumptions and have ideal correlation curves. In FCS, it is assumed that there is a gradient of intensity from the center of focal volume outward. Structural parameter as a ratio of axial to radial radius of the focal volume should be between 3 to

7. In addition to the ratio, sizes of the two radii should be enough small to keep the volume in the order of femto liter. To have a reliable FCS records, optical setup alignment and calibration are recommended. To know the information of focal volume, calibration is usually done by using a standard dye with known diffusion coefficient. The most well-known dye for calibration is Rhodamine-6G (Rh-6G). Diffusion coefficient of Rh-6G is 280 $\mu m^2/s$ in solution (Kim et al., 2007). By calibration of a setup, appropriate radial and axial radii were estimated according to a known value of *D* of Rh-6G or other dyes.

1.6.9 Multi-point fluorescence correlation spectroscopy

Multi-point fluorescence correlation spectroscopy (MFCS) is one of the extensions for the fluorescence correlation spectroscopy technique that allows simultaneous or consecutive FCS measurement from distinct locations within a field of view. Single-point FCS (SFCS) records are limited to collection of data from one point. MFCS also reduces necessary time for collection of data by parallel recording. The simplest way for MFCS which guarantees spatial and temporal resolution is using several laser beams to irradiate the sample (Brinkmeier et al., 1999; Dittrich and Schwille, 2002; Ohsugi and Kinjo, 2009). The alignment of laser beams besides necessity of using separate detectors for each beam is the difficulty of the method. In this method. To increase the number of recorded points, scanning FCS is another approach. At first all scanning FCS experiments were done in homogeneous samples (Koppel et al., 1994; Petersen, 1986; Weissman et al., 1976). Later the scanning FCS technique was improved to record from a line (Baum et al., 2014; Digman et al., 2005; Ries et al., 2009) or circular scans (Petrásek and Schwille, 2008; Ruan et al., 2004). There are other methods such as using spatial light modulators (SLM) to create several

light points by modulating the phase of the light with high time resolution more than 50 kHz for 5 points (Kloster-Landsberg et al., 2012). The drawback of this method is possible cross talk between light beams. Using spinning disks is also another method which has been used for MFCS (Needleman et al., 2009; Sisan et al., 2006). In this method in addition to difficulty of arrangements in optical setup, temporal resolution is not ideal for recording from biological particles with fast diffusion.

1.7 Diffusion of proteins in living cells

Neurons are complex systems in terms of their shapes and functions. Inside the cells, proteins are responsible for all the cellular reactions including short- and long-term responses. One of the important aspects of their function is their translocations and diffusion patterns. Proteins are responsible for most of the cell functions. Looking to activities of proteins in different compartments helps to understand the function of neurons clearly. CaM and calcium/calmodulin-dependent protein kinase II (CaMKII) proteins are important proteins for the neuron function. They are responsible for regulation of signaling pathways from synaptic inputs. Here I briefly review the CaM and CaMKII diffusion information and beforehand I will go through the information of GFP diffusion.

1.7.1 Green fluorescent protein (GFP)

GFP as a small fluorescent protein, which could be inserted in the sequence of various proteins without affecting their functions, has been widely used in the biological researches. Variations of GFP such as EGFP, yellow fluorescent protein (YFP) and cyan fluorescent protein (CFP) have been introduced with different stabilities and spectra of excitations and emissions.

Diffusion of GFP has been investigated by different groups (Brock et al., 1999; Chen et al., 2002; Haupts et al., 1998; Mullineaux et al., 2006; Nomura et al., 2001). The GFP molecule shows non-emissive states which means that a part of GFP molecules stay in dark state which should be taken into account in time related fluorescence studies such as FCS (Dickson et al., 1997).

Some groups tried to focus on GFP diffusion with the FRAP technique and reported estimated intracellular diffusion coefficient of GFP (Elowitz et al., 1999; Mullineaux et al., 2006; Slade et al., 2009). Slade and colleagues showed that co-expression of GFP and other cytoplasmic proteins such as CaM in Escherichia coli did not cause any effects on the diffusion of GFP using the FRAP technique (Slade et al., 2009). Terada and colleagues showed that there were two separate populations of GFP diffusion in HeLa cells using FCS. The first group diffused faster, and the second group was much slower both in cytoplasm and nucleus (Terada et al., 2005). Such a distinction between the faster and slower diffusion of GFP has been reported by others (Nomura et al., 2001; Sanabria et al., 2008).

1.7.2 CaM and CaMKII diffusion

The molecular diffusion is a key element determining the activity of cytosolic signaling molecules such as CaM and CaMKII through governing the molecular association rate. Diffusion properties of CaM and CaMKIIα have been studied using techniques such as FRAP (Khan et al., 2012; Lin and Redmond, 2009; Luby-Phelps et al., 1985, p. 3), FCS (Kim et al., 2004; Lee et al., 2009; Sanabria et al., 2009, 2008; Sanabria and Waxham, 2010), image correlation spectroscopy (ICS) (Johnson and Harms, 2016; Sanabria et al., 2008), single molecule tracking (SPT) (Johnson and Harms, 2016), photoactivated localization microscopy (PALM) (Lu et al., 2014),

FCS-FRET (Lee et al., 2009; Price et al., 2011, 2010) and fluorescence polarization and fluctuation analysis (FPFA) (Nguyen et al., 2015). These studies were performed in cell free media or non-neuronal cells. There has been no comprehensive study on diffusion of CaM and CaMKII in neurons.

1.8 Hippocampal neurons

Hippocampus is located in the medial temporal lobe of the brain. The hippocampal neurons are acting to form, organize and store the memory. They encode the memory and help to recall it.

1.8.1 Calmodulin

Calmodulin is the center integrator for synaptic plasticity. Its diverse potential to interact with different substrate proteins makes it a unique regulatory protein for signal transduction (Kursula, 2014; Tidow and Nissen, 2013; Xia and Storm, 2005). CaM mediates the activation of several signaling pathways in a Ca^{2+} concentration dependent manner. Four Ca^{2+} bind to CaM, which induce conformational changes in the CaM structure and increase its affinity to other proteins. Two Ca^{2+} bind to the C-terminus and two Ca^{2+} bind to the N-terminus of the protein to open up the structure of the protein. Two EF hands in the C and N lobes can bind Ca^{2+}. After binding of Ca^{2+}, the hydrophobic domain of CaM is exposed to its substrates (Kursula, 2014). In a Ca^{2+} free state, while the N-terminus of protein is closed but the C-terminus is in a semi-open state, and CaM binds other proteins via the C-terminus at rest (Chin and Means, 2000; Gabelli et al., 2015). Partners of CaM recognize CaM in the Ca^{2+} -bound form or the Ca^{2+} -free from (Hoeflich and Ikura, 2002; Kortvely and Gulya, 2004). Influx of Ca^{2+} first opens the N-terminus which has more affinity to Ca^{2+} than the C-terminus (Chin

and Means, 2000). Such a Ca^{2+} concentration dependent behavior lets CaM be the best candidate for integration of signals. Interaction with more than 100 substrate proteins shows how flexible the CaM structure is. This conformational plasticity of CaM allows for diverse protein targeting (Simon et al., 2015; Xia and Storm, 2005). CaM enhances activation or inactivation of other proteins (Tidow and Nissen, 2013). One of the most important substrate proteins for CaM is CaMKII which is activated by the Ca^{2+}/CaM complex. Binding of Ca^{2+}/CaM promotes phosphorylation of CaMKII which is essential for translocation and function of the protein in the learning and memory system (Xia and Storm, 2005).

1.8.2 CaMKII family proteins

CaMKII proteins are one of the most important regulators in synaptic plasticity with their unique functions (Fink and Meyer, 2002; Kerchner and Nicoll, 2008; Lee et al., 2009; Lisman et al., 2012, 2002). In mammals four distinct CaMKII proteins, α, β, γ and δ, are encoded in different genes of high homology (Schulman and Hanson, 1993) and more than 30 isoforms are produced by alternative splicing (Brocke et al., 1999; Hudmon and Schulman, 2002a; Lantsman and Tombes, 2005; Rostas and Dunkley, 1992; Takeuchi et al., 2000, 2002). All the four subtypes are expressed in the brain (Hudmon and Schulman, 2002b), whereas the α and β subtypes are the most abundant in the brain, richly found in neurons. CaMKIIα transduces Ca^{2+} concentration changes to downstream signals (De Koninck and Schulman, 1998; Hell, 2014; Lisman et al., 2002), while CaMKIIβ is well known by its ability to bind F-actin (Sanabria et al., 2009). CaMKIIβ is also responsible for taking CaMKIIα to the postsynaptic site after Ca^{2+} influx (Shen et al., 1998).

1.8.2.1 Structure of CaMKII proteins

The structure of CaMKII proteins consists of three main domains. The N-terminal catalytic domain with kinase activity is followed by the regulatory domain containing an autoinhibitory and a CaM binding sites. A variable linker follows the regulatory domain, in which nuclear translocation signal (NLS) is found in some isoforms. By linkage between the C-terminal association domains (Fink and Meyer, 2002), CaMKII proteins form a dodecameric structure, holoenzyme, consisting of 6-12 homo- or heteromeric subunits (Hoelz et al., 2003; Kanaseki et al., 1991; Kolodziej et al., 2000; Lantsman and Tombes, 2005). This dodecameric holoenzyme is one of the largest cytosolic proteins of 600 - 660 kDa, approximately 15-35 nm in diameter. According to electron microscopy results, the association domains make a stable central hub structure after polymerization, while the catalytic domains are more flexible. Based on the position of catalytic domains, two major conformational modes are defined. The compact mode of 15 nm diameter is the state that all catalytic domains are tightly attached to the core of holoenzyme. In the extended state in which the diameter of molecule increases to 35 nm, the molecule is more available for cooperative activations (Kanaseki et al., 1991; Kolb et al., 1998; Myers et al., 2017).

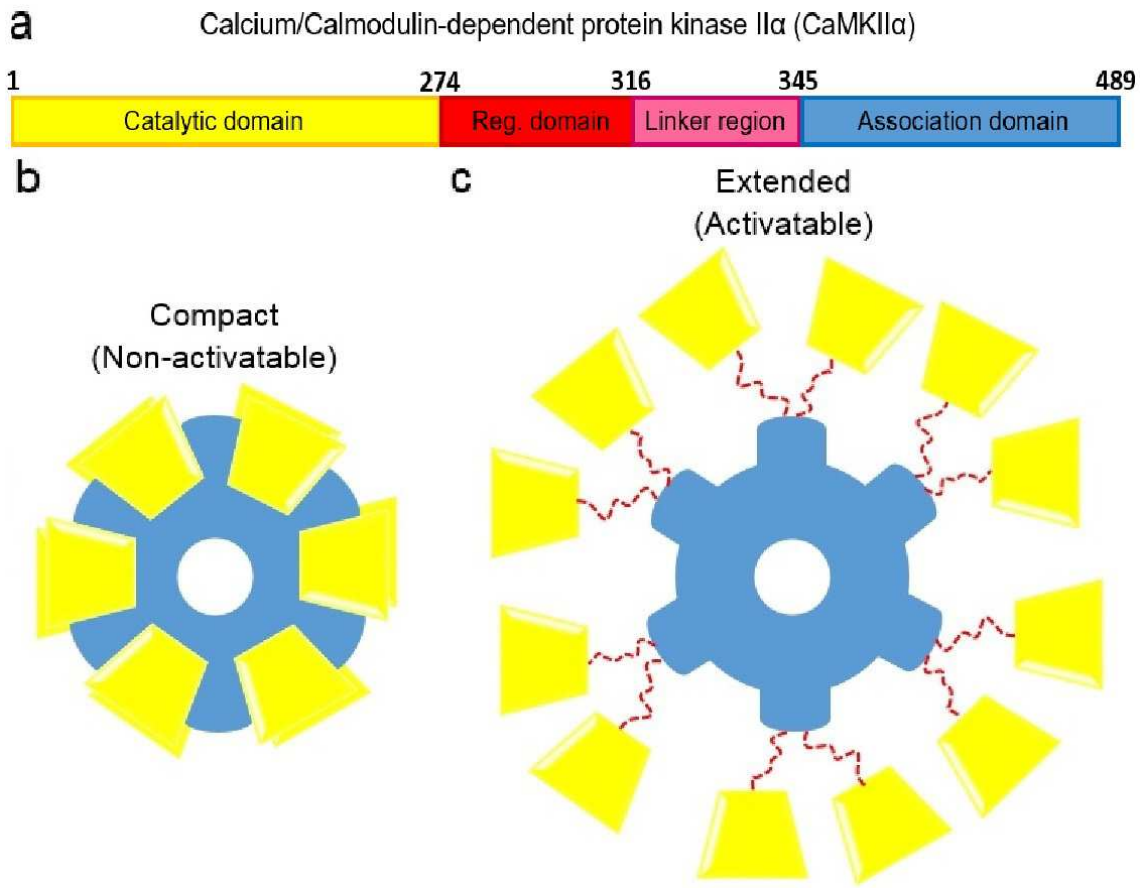

Figure 1-4. CaMKIIα conformational modes.
(a) Order of domains in CaMKIIα structure. The catalytic domain with kinase activity is followed by the regulatory (Reg) domain. A variable linker and the association domain follow the regulatory domain. (b) CaMKIIα in its compact form. (c) CaMKIIα in its extended form. The catalytic domains are flexible to change the mode of protein from the non-activatable state to the activatable mode. The diameter of protein changes between 15 to 35 nm according to the position of catalytic domains.

Forming this structure induces inter-subunit autophosphorylation at Thr^{286} of CaMKIIα or Thr^{287} of CaMKIIβ upon Ca^{2+}/CaM binding, which keeps partial CaMKII activity in Ca^{2+}-independent manner long after the initial Ca^{2+} increase event (De Koninck and Schulman, 1998; Hudmon and Schulman, 2002a, 2002b).

1.8.2.2 CaMKII as a memory protein

The holoenzyme formation is thought to be a necessary step for the function of

protein (Shen and Meyer, 1998), and the existence and function of the monomeric form of CaMKII has been rarely discussed. Lisman hypothesized that CaMKII holoenzyme could transmit and propagate the activated holoenzyme state to not activated ones, which was postulated as a "molecular memory" mechanism, through subunit exchange between activated and not activated holoenzymes (Lisman, 1994), and Stratton et al. demonstrated the subunit exchange between CaMKIIα holoenzymes in *in vitro* experiments (Stratton et al., 2014). In doing so, CaMKII could stay in active state long after stimulation of neuron and regulate the synaptic activity dynamics.

1.8.2.3 CaMKII as a regulator for gene expression

Although the CaMKII proteins have been implicated in transmitting signal from plasma membrane to nucleus to control gene expression, or in the neuron from the synapse to the nucleus (Coultrap et al., 2011; Ma et al., 2015), the detail is not clear. CaMKII isoforms containing NLS, e.g. α_β, γ_A, δ_7 and δ_B, localize in the nucleus (Colbran, 2004; Takeuchi et al., 2002). Phosphorylation of serine residues immediately after the NLS sequence (Heist et al., 1998; Heist and Schulman, 1998) or phosphorylation of Thr^{286} are implied in the regulation of nuclear targeting of these CaMKII species (Bayer and Schulman, 2001). Combination of different subunits with or without NLS in a holoenzyme also determines nuclear localization (Srinivasan et al., 1994). Ma et al. proposed that CaMKIIγ with an NLS in the variable region serves as a synapse-nuclear messenger by translocating to nucleus upon phosphorylation by CaMKIIα and phosphorylating transcription factors and DNA binding proteins, while CaMKIIα and β, which lack NLS, play roles in the cytosol (Heist and Schulman, 1998; Ma et al., 2015).

1.8.3 Stimulation of neurons

Elevation in intracellular Ca^{2+} level is the main trigger for activation of neurons. Influx from extracellular medium or release from internal sources are the two possible ways for such an elevation. Various receptors and channels are involved in the stimulation of neurons. They are responsible for ion exchange between extra and intracellular medium. Types of involved receptors and channels depend on types of stimuli. Combination of L-glutamate (Glu) and glycine (Gly) is one of common stimuli. Both of these neurotransmitters bind to the N-methyl-D-aspartate (NMDA) receptor and let Ca^{2+} enter the cell. Intracellular elevation in Ca^{2+} level is followed by activation of signaling proteins such as CaM and CaMKII. Stimulation of neurons causes increase in number and size of spines and cascades of molecular signals.

1.8.3.1 Molecular mechanism of stimulation by glutamate/glycine

NMDA receptors are non-selective cation channels that interact with glycine and glutamate via the NR1 and NR2 subunits, respectively (Dolino et al., 2016). While binding of glutamate or aspartate leads to activation of the receptor, co-agonist binding of glycine helps for efficient opening. Ca^{2+} influx through the NMDA receptor is one of the major triggers for synaptic plasticity. Mg^{2+} or Zn^{2+} binds to the receptor and blocks the passage of other ions through the channel.

1.8.3.2 Hyper-stimulation

If the amount of stimuli is excessive or duration of exposure to stimuli is long, neurons will be hyper-stimulated. It resembles the ischemia condition in neurons which is under continuous stimulation. Neurons show different responses to hyper-stimulation.

It has been shown that 40% of neurons die after 4 hour exposure to 200 μM glutamate/20 μM glycine while others live normally (Ashpole and Hudmon, 2011). It has been shown that one of the reasons for this difference is the CaMKII activity levels in neurons upon activation.

1.8.3.3 Proteolytic activity after stimulation

In addition to activation of kinases and phosphatases upon elevation of intracellular Ca^{2+} level in neurons, Ca^{2+} might act as a trigger to activate proteolytic activity (Baudry et al., 2015; Goll et al., 2003; Kim et al., 2002; Liu et al., 2006). A number of calcium-mediated proteolytic signaling mechanisms have been discussed (Olofsson et al., 2008). The calpains, calcium dependent neutral cysteine proteases, consist of 15 isoforms (Vosler et al., 2008). The calpains cleave and activate substrates for instance some caspases which are involved in the apoptosis process. On the other hand, it has been shown that the LTP phenomenon needs calpain. Activation and inhibition of calpain by leupeptin prevents LTP formation (Baudry et al., 2015, 2013). The CaMKII and calpain are key proteins for LTP formation and in glutamate mediated excitotoxicity, inhibition of both CaMKII and calpain results in appearance of varicosities on axons (Hou et al., 2009). It has been shown that CaMKII itself is a substrate of calpain and is cleaved by activated calpain in stimulated cerebrocortical neurons (Hajimohammadreza et al., 1997). If CaMKII proteins are cleaved by calpain after autophosphorylation, they will stay in the active state in a Ca^{2+} independent manner, while any cleavage before autophosphorylation leads to production of inactive subunits (Yoshimura et al., 1996).

1.9 Main aim of this study

In this study, I monitored the molecular behavior of GFP, CaM, CaMKIIα and

CaMKIIβ proteins with the FCS technique in HEK293 cells and in hippocampal neurons by comparing cytosol and nucleus. There was no comprehensive information of diffusion of these proteins in neurons. Therefore, first I performed experiments in HEK293 cells and compared my results with results of other groups in non-neuronal cells with FCS or other techniques. Then I focused on diffusion of the mentioned proteins in neurons. I recorded from different compartments of neurons to characterize patterns of diffusion. I stimulated the neurons by means of L-glutamate and glycine and monitored the response of proteins to the stimulation. It revealed faster diffusion of CaM and CaMKII proteins due to stimulation. CaMKII proteins showed significant increase in diffusion kinetics by neuron stimulation, implying that drastic changes in protein structure took place upon neuronal activation. These results demonstrated feasibility of multipoint FCS in protein dynamics measurement in neurons, as well as complex regulation mechanisms of diffusion properties of CaM and CaMKII during neuronal activations.

Most of the results of this dissertation have been published (Heidarinejad et al., in press).

2 Materials and Methods

2.1 Animal care

All animal care was in accordance with guidelines outlined by the Institutional Animal Care and Use Committee of Waseda University. All experiments were done under the protocol which was approved by the Committee on the Ethics of Animal experiments of Waseda University (2011-A068), and all efforts were made to minimize the number of animals used and their suffering during the experiments.

2.2 HEK293 cells culture and transfection

HEK293 cells were grown in the Dulbecco's modified Eagle medium (DMEM, Nacalai tesque, Kyoto, Japan) supplemented with 10% fetal bovine serum (FBS) and 0.05% penicillin/streptomycin (Wako chemical industries, Japan). Cover slips (12 mm in diameter, 121001, Matsunami, Tokyo, Japan) were coated with Matrigel (Corning, MA, USA) for 1 hour and washed with DMEM containing FBS 3 times. Then passaged cells were plated on the coverslips in 24-well tissue culture plates (TPP, Trasadingen, Switzerland). The cells were transfected by Lipofectamine 2000 (Thermo Fisher Scientific, Tokyo, Japan) by the method described by the manufacturer. Medium of transfected HEK293 cells was changed 1 hour after the transfection to fresh medium. 6-15 hours after the transfection, the cells were used for FCS records. HEPES-buffered saline (HBS: 20 mM HEPES, 115 mM NaCl, 5.4 mM KCl, 1 mM $MgCl_2$, 2 mM $CaCl_2$, 10 mM glucose, pH 7.4) was used as a recording solution at room temperature.

2.3 Neuron primary culture

Primary culture from Wistar rat hippocampi was prepared according to a standard method (Bannai et al., 2009). In brief, Hippocampal neurons were isolated from embryos on day 18 (E18) of either sex. Cells were seeded on coated cover slips

(Matsunami). Cover slips were washed with 1% nitric acid by shaking overnight and rinsed for 3 hours. To facilitate adhesion of neurons to the cover slips, glass surfaces were coated with 0.04% Polyethylenimine (p-3134, PEI, Sigma-Aldrich Japan, Tokyo, Japan). Cover slips were placed in 24 multi-well dishes and 60 µl of PEI (0.04%, diluted by MilliQ) were dropped on each cover glass. After overnight incubation at RT the cover slips were washed 3 times with sterilized water and kept dry. After seeding the cells, 500 µl/well attachment media (MEM (Nacalai tesque) supplemented with 2 mM L-Glutamine, 1 mM Sodium Pyruvate (Gibco, NY, USA), and 10% horse serum) was used as culture medium for 3 days, and later 300 µl of attachment medium was replaced by 350 µl of maintenance medium (Neurobasal-A (1X) (Gibco), 2% B27 (Gibco), 2 mM L-Glutamine, 0.05% penicillin/streptomycin (Wako)) every 3 days. Neurons were transfected with Lipofectamine 2000 at 7–14 days *in vitro* (DIV) and recorded 12–18 hours after transfection in HBS medium at room temperature.

2.4 Stimulation and drug application

By bath application, neurons were stimulated with 100 µM L-glutamate (Nacalai tesque) and 10 µM glycine (Nacalai tesque) as final concentration in the HBS medium. The stock was kept at -20°C. For stimulation of neurons, two separate protocols were applied. In some experiments, stimuli were bath applied and exposed to cells during all recording time, while in other experiments, stimuli were washed out by 5 min circulation of normal HBS 20 min after the onset of stimulation.

2.5 Molecular modifications and new constructs design

EGFP with the A207K point mutation known as monomeric GFP (mGFP) is used in this study to avoid dimerization of GFP (Yang et al., 1996; Zacharias et al., 2002). All

proteins were tagged with mGFP. To have low level of protein expression, truncated versions of promoter were used in all the plasmids (Watanabe and Mitchison, 2002). To produce appropriate truncated promoters, the CMV promoter sequence (576 bp) of pEGFP-N1 (Takara Bio USA, Mountain View, CA, USA) was internally cut with *Aat*II and digested with nuclease *BAL*31 for 5, 7.5 and 10 minutes. Based on digestion time, 361, 430 and 500 bp of CMV promoter was deleted, respectively. Rate of expression was compared among the three versions of promoters, and the 500 bp deleted version was used. mGFP vectors, mGFP-N1 and mGFP-C3, were constructed by inserting double digested mGFP (*Age*I/*Bsr*GI) from mGFP-CaMKIIα (α isoform of rat CaMKIIα, a gift from Dr. Paul De Koninck, Laval University, Quebec, Canada) (Hudmon et al., 2005) into pEGFP-N1 and pEGFP-C3 (Takara Bio, USA), respectively. mGFP-CaM was constructed by subcloning a CaM sequence from pDEST 12.2-CaM (a gift from Dr. Takeo Saneyoshi, RIKEN institute, Wako, Japan) (Goshima et al., 2008) into mGFP-C3 at the *Bam*HI/*Sac*I site. mGFP-CaMKIIβ was constructed with double digestion (*Age*I/*Hind*III) of GFP-C1-CaMKIIβ (β isoform of rat CaMKIIβ, addgene plasmid # 21227) and replacing EGFP by mGFP. Monomeric CaMKIIα (mCaMKIIα) was designed by changing the Gly^{316} of CaMKIIα sequence to a TGA stop codon (Kolb et al., 1998) by polymerase chain reaction (PCR). For site-directed mutagenesis using PCR, forward and reverse primers were designed. In addition to mCaMKIIα, four other mutants of CaMKIIα (I205K, T286A, A302R, T305/306A) were generated. Ile^{205} was replaced with Lys using a forward primer of 5´-CTGTATAAGTTGCTGGTTGGGTATCCC-3´. Thr286Ala and Ala302Arg were mutated using 5´-CAGGAGGCCGTGGACTGCCTGAAGAAG-3´ and 5´-AAGGGACGCATCCTCACCACTATGCTG-3´, respectively, and in the same way, the

last mutant was generated by double point mutagenesis, Thr305/306Ala, using 5´-ATCCTCGCCGCCATGCTGGCCACCAG-3´. All PCR results were verified by sequencing.

2.6 Two-photon FCS optical setup

The FCS measurements were carried out using a random access two-photon optical setup explained in detail previously (Shafeghat et al., 2016). In brief a custom-made two-photon microscope was equipped with a femtosecond pulsed Ti:Sapphire laser (Tsunami 3941, Spectra-Physics, Santa Clara, USA) at 900 nm pumped by a diode solid laser (Millennia VIII, Spectra-Physics). An upright microscope (BX-51W, Olympus, Tokyo, Japan) with a 20x water immersion lens (XLUMPlan FL, N.A. 1.0, Olympus) was used for FCS records. We adopted the optical design of the AOD-driven scanning system that was developed by the L. Bourdieu group (Salomé et al., 2006). The laser beam was deflected by two orthogonal AODs (DTSXY-400-850.950, AA, Opto-Electronic, Orsay, France) to scan the field of view and jumped among the chosen points. The AODs allowed to access to any point within 11 µs with an adequate spatial precision. This access time was spent for deflection change. So for the multi-point recordings ((11+x)*n) µs was the calculated dwell time for recording from n points with x µs as an exposure time for each point. The emitted fluorescence collected with the same lens of excitation and recorded by photomultiplier tubes (PMTs, H7422PA-40, Hamamatsu Photonics, Hamamatsu, Japan). The collected photons were analyzed with a time-correlated single photon counting module (SPC-150, Becker and Hickl, Berlin, Germany) (Becker, 2013), based on timing of detection of photons.

2.7 Optical setup calibration

As it was mentioned, two perpendicular AODs were used as a scanning system. An AOM (MTS144-B47A15-720.950, A.A Sa) was used right before the AODs with 45 degree angle to compensate the spatial distortion of AODs. Temporal broadening of the laser pulses in the AODs was pre-compensated by inserting a pair of prisms in the light pass to make a double pass for the laser light. In order to calibrate the optical setup, the laser beam was guided through the of all lenses and optical devices with minimum reduction of its power. Displacement in laser orientation was occurring weeks by weeks. After adjusting hitting points of light on the surface of all the lenses and mirrors, the power of light was measured after AOM. Then the light beam radius was adjusted by the lenses to backfill the entrance aperture of objective.

2.8 Calibration of laser focal volume

Before each experiment, it was necessary to tune the laser shape and orientation on the sample. For this purpose, two methods were tested.

In the first approach, the point spread function (PSF) was measured. Fluorescent beads of 100 μm diameter were dried on a surface of cover glass at low concentration, and then isolated round shapes of single beads were selected. The selected beads were scanned in z direction with 1 μm steps with piezo-driven objective scanner (P-725 PIFOC, Physik instrumente, PI, Karlsruhe, Germany) and the 3D structure was constructed. Then the 3D intensity profile was analyzed. r_x, r_y and r_z were defined as a distance of points from the center in three dimensions where their intensity is 1/e of the intensity of the center.

The second method was the calibration with a standard dye. Rhodamine 6G (Rh-6G, Tokyo chemical industry, TCI, Tokyo, Japan) is widely used for calibration of

FCS setups because of its known diffusion coefficient of 280 μm²/s at room temperature (Kim et al., 2007). Stock solution was prepared by dissolving Rh-6G in methanol at concentration of 10 mM. 0.05% Tween 20 was added to avoid aggregation, and the solution was kept at 4°C. The solution was diluted in phosphate buffered saline (PBS) (D5652, Sigma-Aldrich Japan) on the day of calibration with final concentration of 10 nM and autocorrelation graph of its diffusion was fitted with a one component model with the known *D* value. Based on the fitting parameters, axial and radial dimensions were estimated for the focal volume. For my setup, the estimated values for the laser focal volume were 0.35 ± 0.01 and 3.02 ± 0.03 μm for radial and axial radii, respectively.

In some experiments, Sulforhodamine101 (SR101, Santa Cruz Biotechnology, Dallas, USA) was used as a standard fluorescent dye. SR101 powder was dissolved in methanol with 0.05% Tween 20 at 10 mM, and the stock solution was kept at 4°C. The solution was diluted with PBS with final concentration of 10 nM.

2.9 Single- and Multi-point FCS

The laser power was adjusted at 10-15 mW before the objective by the AOD transmission. Cells with too high expression of fluorescence proteins were photobleached with high laser power (30 mW before objective) for 30 to 60 seconds prior to FCS measurements.

For cell free experiments in solution, purified EGFP was used. Subcloned EGFP in a His-tag plasmid vector was expressed in E. Coli, sonicated, purified with a Ni-NTA resin column in PBS buffer, and eluted with imidazole. The purified EGFP was dissolved in PBS at 10 nM and used for FCS.

For multi-point FCS, after raster scanning 93 × 93 μm area, recording points were

chosen inside the cells by opting the best z plane controlled by the piezo-driven objective scanner with 1 μm steps. 7-15 consecutive records lasting for 15 sec each with 10-15 sec intervals were carried out. The same power and recording duration was used for both single and multi-point recordings. In multi-point records, consecutive records among the points were done with a 11 μs jumping time. A bleach correction algorithm was applied to remove bleaching effects, if existed. Later on, the recorded photons of each point was integrated and the ACF of each point was made.

Then all records from each compartment were converted to ACF. ACFs of a single cell were averaged and fitted to a single or two component model of Eq (22) by a Levenberg-Marquardt algorithm (Wohland et al., 2001).

Calculation of absolute ε_1 and ε_2 was done using Eq (30). C_1, C_2 and $\varepsilon_{2/}\varepsilon_1$ were obtained by fitting to a two component model of Eq (22). $\langle I_i \rangle$ was obtained from recorded results, and ε_1 was calculated by Eq (30). The ε_i value was inherently affected by the laser power which was changing weeks by weeks. To compare the ε_i values of different molecular species, I conducted a set of experiments in which laser power was adjusted to a constant value (10 mW) before objective.

In this paper diffusion coefficient (D), which is calculated from τ_D and r_{xy}, $D = \frac{r_{xy}^2}{8\tau_D}$ (Kim et al., 2004), is indicated as D_{fast} and D_{slow} for the faster and slower components of a two component model.

2.10 Confocal setup

A confocal microscope (FV 300, Olympus, Tokyo, Japan) equipped with a 488 nm Argon laser (IMA 10X, Argon-ion laser, Melles Griot, NY, USA) was used for time-lapse imaging of transfected HEK293 cells and hippocampal neurons. A water

immersion 60x objective (UPlanSApo, N.A. 1.2, Olympus) was used.

2.11 Software for analysis

All online recordings were performed using TI Workbench, in-house software written by Prof. Takafumi Inoue running on a Mac computer. All offline analyses were performed using TI Workbench in combination with Igor Pro (Wave metrics, Lake Oswego, OR, USA) and Microsoft Excel (Microsoft Japan, Tokyo, Japan). All indicated data are given as average ± SEM. The statistical difference between groups was determined using Student's t-test when a significant result at the level of 95% was found.

3 Results (GFP and CaM)

3.1 Intensity-laser power

As an initial step, the relation between the laser power and intensity of emitted fluorescence was plotted. In the two-photon excitation system, the intensity (I) is proportional to square of the laser power (P). The plot shows the relation between the light power and the intensity and helps to determine the saturation condition of a specific dye.

$$\log I \propto 2 \log P$$

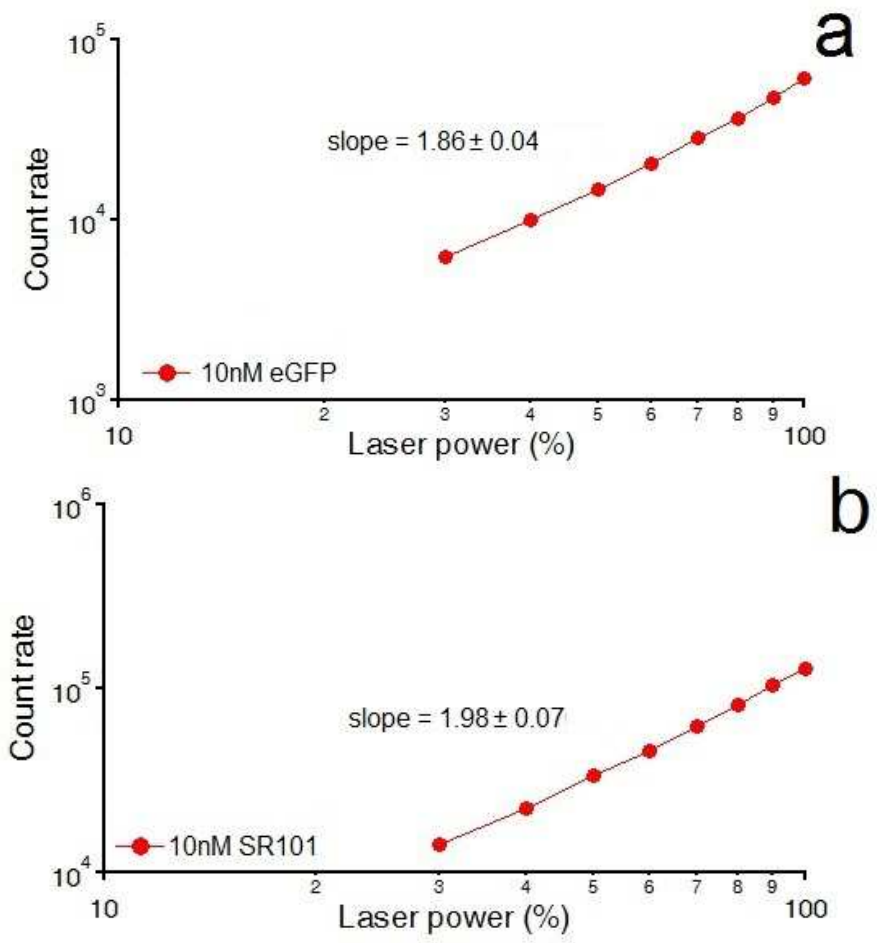

Figure 3-1. Intensity-laser power relationship.
Relation between intensity and laser power for EGFP (a) and Sulforodamine101 (b) in two-photon system. Slope of graphs are 1.86 and 1.98 for EGFP and SR101, respectively.

In the ideal two photon excitation, the expected slope value of logarithmic graph is

two. Fig. 3-1 shows intensity-laser power relation of the Sulforhodamine101 (SR101) and EGFP dyes, which were in accordance with theoretical expectations.

According to the plots, the SR101 and EGFP dyes were not saturated within the range of laser power which I used in our system. I adjusted the laser power at 10-15 mW to minimize bleaching and photodamage while the maximum power was around 30-35 mW before objective.

3.2 Point spread function and laser light calibration

For finding the size of focal volume, two methods were used. As the first method, point spread functions of fluorescent beads were measured with two photon microscope according to the protocol explained in the materials and methods section (Fig. 3-2). In each calibration step, five beads were imaged and averaged. This method had limitations. The major limitation was the comparable size of pixels of image with the radial radius of focal volume. Therefore, the extracted values for the radial radius were not enough precise even with averaging of several records. I found out that the dimensions revealed by the point spread function method ($r_x = r_y = 0.3 \pm 0.01$ and $r_z = 1.3 \pm 0.05$ μm) were not showing the appropriate values for calculation of *D* even in case of the standard dyes because of the comparable sizes of image pixels and focal volume radial radius.

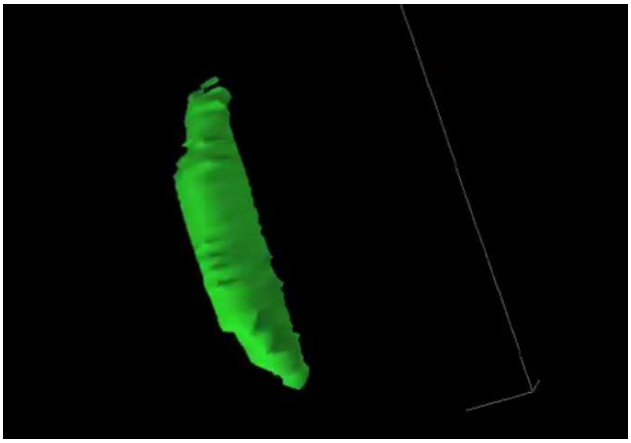

Figure 3-2. Intensity profile of fluorescent beads.
Fluorescent beads were scanned and the 3D intensity pattern of them was constructed.

The second method was using ACF of Rh-6G or other standard dyes such as SR101 in PBS. One component model was used for analyzing of Rh-6G ACFs. Records from 10 nM solution were done for 70-90 s, and the autocorrelation curves were fitted with a one component model. For each calibration, 5-10 records were done, and extracted values for radial and axial radii were averaged and used in analysis of other FCS records.

3.3 Triplet transitions and photobleaching

Knowing that the GFP fluorophore has molecular dark states, I tried to characterize the GFP behavior by fitting the autocorrelation of EGFP in PBS by using appropriate autocorrelation formula (Eq. 21). According to residual of fitting and diffusion value of EGFP, I found that 0.15 ms as a triplet time constant was an appropriate value.

3.4 Diffusion of EGFP in solution

For FCS records, collected photons were represented as a fluorescence trace (Fig. 3-3). A bleach correction method was used to remove the bleaching effect from traces, if existed. It was done by fitting the traces with a double exponential function. Therefore,

all records had a flat base line before conversion to ACF.

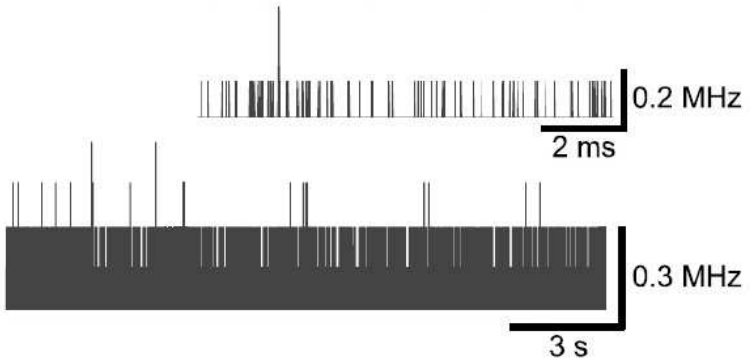

Figure 3-3. Fluorescence trace of recorded photons from a single point.
Fluorescence trace of EGFP in PBS recorded for 15 s from single point. Inset, An expanded view.

For FCS experiments, I recorded intensity fluctuations of EGFP proteins in PBS solution. For all records, the laser power was adjusted to 10-15 mW before objective to avoid bleaching. I found that the diffusion coefficient of 10 nM EGFP in the PBS buffer was 77 $\mu m^2/s$, which was in accordance with previous reports recorded with two-photon FCS, which were 78 and 83 $\mu m^2/s$ (Chen et al., 2002; Sanabria et al., 2008).

.

3.5 Diffusion of mGFP and CaM proteins in HEK293 cells and in neurons

I started intracellular FCS measurements with mGFP and CaM proteins. HEK293 cells were transfected with mGFP and mGFP-tagged CaM (mGFP-CaM) encoding plasmids using a lipofection method. Promoter of plasmids were truncated (see Materials & Methods) to reduce amount of expressed proteins. There was a clear difference in amount of expressed proteins between normal and truncated plasmids (Fig. 3-4). The cells were recorded 6-15 hours after transfection. As Fig. 3-5 shows that mGFP and CaM were homogeneously distributed in all cell regions of HEK293 cells.

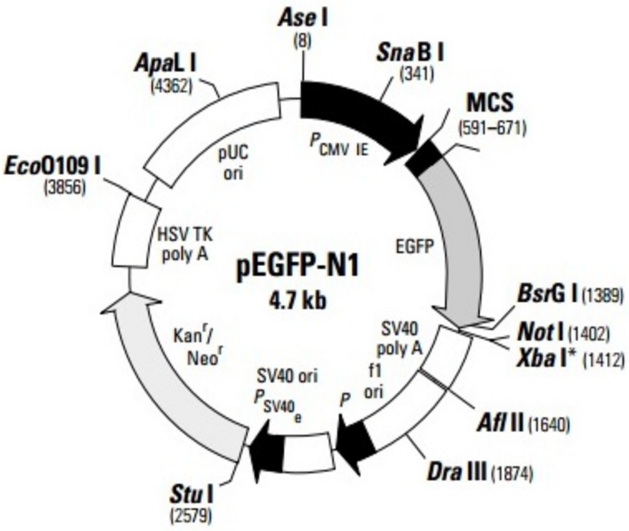

Truncated plasmid Normal pEGFP-N1

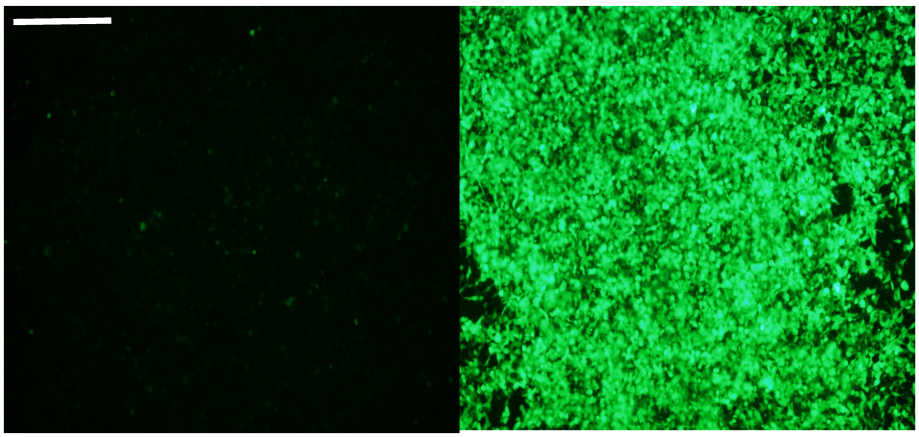

Figure 3-4. Efficiency of HEK293 cells transfection with truncated and normal pEGFP-N1 plasmids.

(Top) Normal pEGFP-N1 plasmid with a full length of CMV promoter. (Bottom) Transfected HEK293 cells with a truncated pEGFP-N1 plasmid (left) and normal pEGFP-N1 plasmid (right) 24 hours after transfection. There was a clear difference in amount of EGFP expression between the two groups. Scale bar: 500 µm.

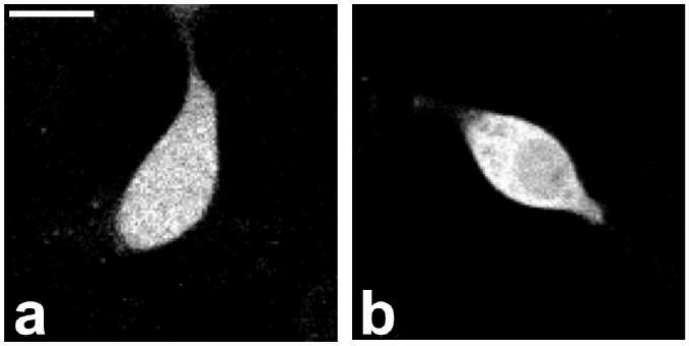

Figure 3-5. Expression of mGFP and mGFP-tagged CaM in the HEK293 cells.
Fluorescence images of HEK293 cells transfected with mGFP (a) and mGFP-CaM (b). Scale bar: 10 μm (Heidarinejad et al., in press).

For FCS analysis, 7-15 consecutive records were performed from nucleus and cytosol. Fig. 3-6 shows overlapped graphs of ACFs recorded from the cytoplasm of a HEK293 cell expressing mGFP-CaM. Then all the ACFs were averaged and used for further analyses.

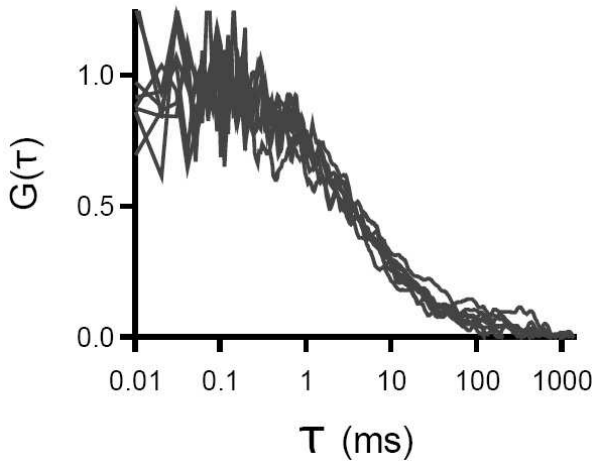

Figure 3-6. Overlapped ACFs.
Recorded 7 consecutive autocorrelation curves from cytosol of the HEK293 cells transfected with mGFP-CaM. The graphs were averaged before fitting (Heidarinejad et al., in press).

For quantitative analyses, one component and two component fit models were tested. The two component model had a clear merit for fitting the graphs while one component model, which failed to show acceptable residual on fitting. As Fig. 3-7 shows, two component fit had less deviation from ACF than one component model.

Thus, in this study, the two component model was used for analyses of intracellular FCS records. Fitting with a two component model is a common way in intracellular FCS studies (Michelman-Ribeiro et al., 2009; Mikuni et al., 2007; Renz and Langowski, 2008; Sanabria et al., 2008).

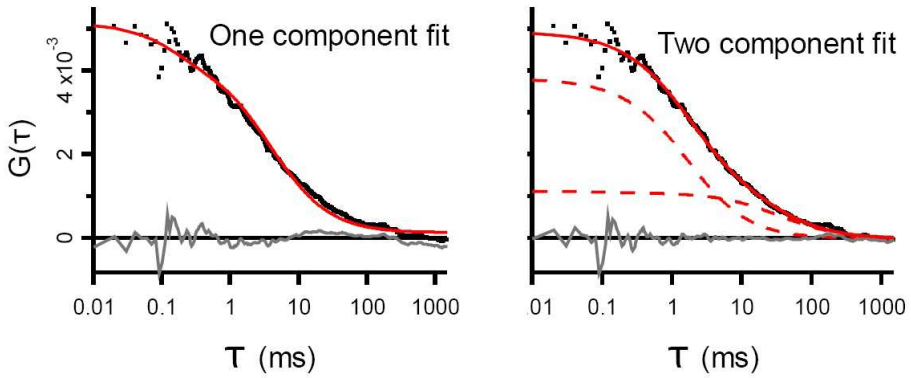

Figure 3-7. One and two component fit model for the recorded ACFs.
Quality of fit by one and two component 3D free diffusion models for the graphs which are shown in Fig. 3-6. The two component model showed better fit than the one component model (Heidarinejad et al., in press).

I also checked the concentration of expressed proteins. All were between 10-1000 nM in HEK293 cells. In addition, I did not find any effect of concentration on extracted parameters such as diffusion coefficient within the above range of concentration in FCS records (Fig. 3-8).

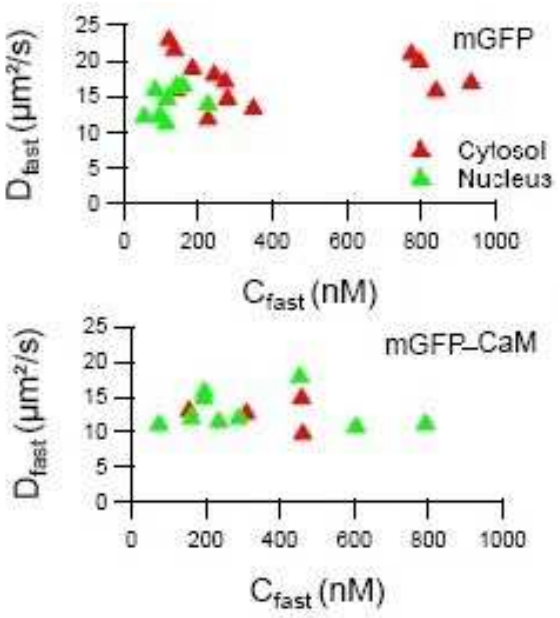

Figure 3-8. Relation between concentration of expressed proteins and diffusion coefficient.

Recorded D_{fast} values versus concentration of mGFP, mGFP-CaM in HEK293 cells. It seems that there was no dependency between D value and concentration of the faster component.

As Fig. 3-9 shows, ACFs of mGFP and CaM were all similar in the cytosol and nucleus of HEK293 cells.

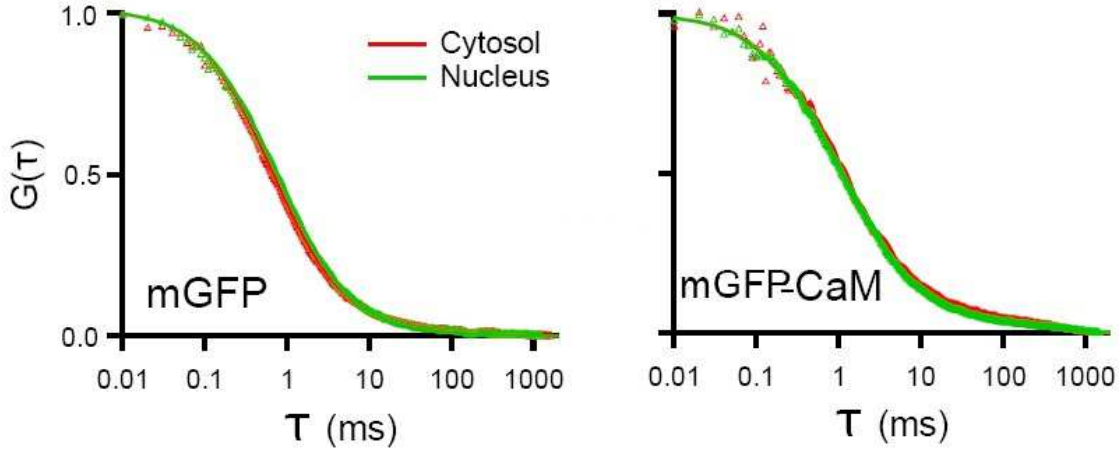

Figure 3-9. ACF of the mGFP and mGFP-CaM proteins in the cytosol and nucleus of HEK293 cells.

Normalized averaged ACFs of mGFP and mGFP-CaM in the cytosol (red) and nucleus (green) of HEK293 cells. ACFs of records in a single cell were averaged first, and then the averages of all cells were averaged and indicated. mGFP and CaM diffused similarly in the cytosol and nucleus (Heidarinejad et al., in press).

mGFP and CaM diffused in the nucleus and cytosol with similar distribution pattern.

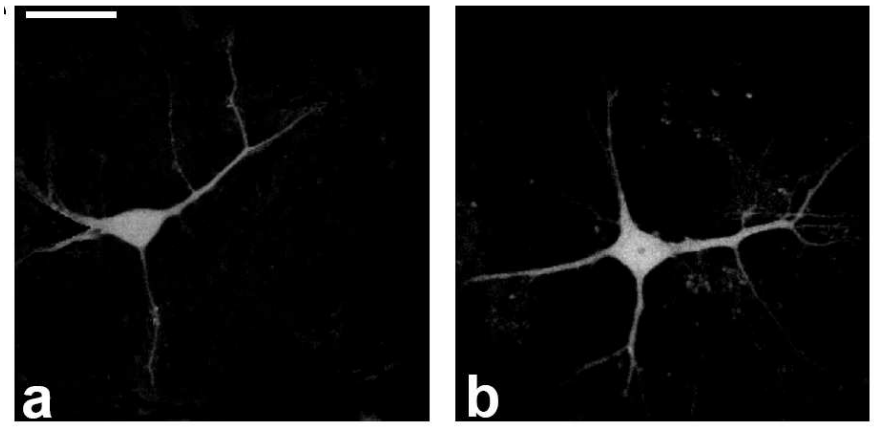

Figure 3-10. Expression of mGFP and mGFP-CaM in hippocampal neurons.
Fluorescence images of neurons transfected with mGFP(a) and mGFP-CaM (b). Scale bar: 20 μm (Heidarinejad et al., in press).

I expressed above-mentioned proteins in hippocampal neurons. Neurons at DIV 7-14 were transfected by a lipofection method, and used for FCS records within 12-18 hours after transfection. Similar to the HEK293 cells, mGFP and mGFP-CaM were distributed evenly in all compartments of the neurons (Fig. 3-10).

FCS was performed in the soma, nucleus and dendrite (Fig. 3-11). There was no apparent difference in the diffusion of mGFP in different compartments of neurons.

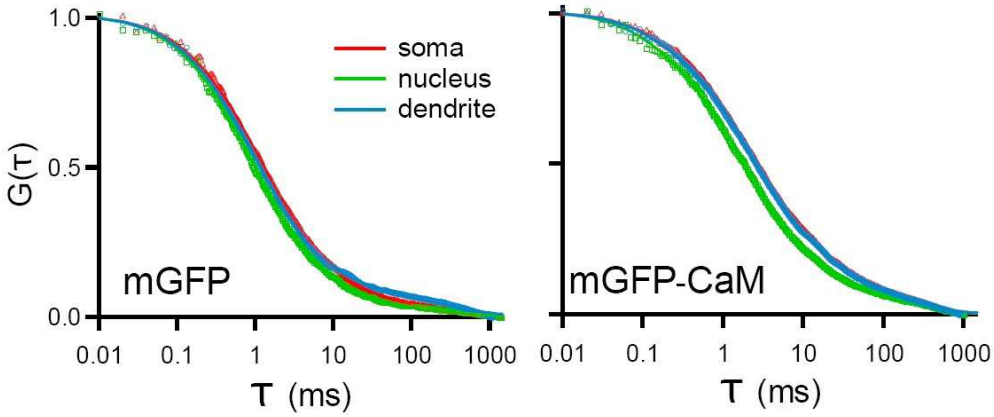

Figure 3-11. ACF of mGFP and mGFP-CaM in hippocampal neurons.
Normalized averaged ACFs from soma (red), nucleus (green) and dendrite (blue) of mGFP and mGFP-CaM. ACFs in a single cell were averaged first, and then the averages of all cells were averaged and indicated. CaM showed faster diffusion in the nucleus than in the soma and dendrite (Heidarinejad et al., in press).

It has been shown that GFP is diffusing freely in the cell (Slade et al., 2009). mGFP diffusion in HEK293 cells was 4-5 times slower than EGFP in PBS. Diffusion coefficient of mGFP was 17.0 ± 0.7 and 14.4 ± 0.6 μm²/s in the cytosol and nucleus of HEK293 cells, respectively (Fig. 3-12 and Table 3-1). The subunit distribution ratio of the faster component to the entire components (Φ_{fast}/Φ_{total}) for mGFP was 92% in the cytosol, i.e., 92% of photons were emitted from molecules diffusing as the faster component, confirming that mGFP has minimum association with intracellular milieus. Molecular masses of mGFP and CaM are 27 and 14 kDa, respectively (Sanabria et al., 2008). Therefore, molecular mass of mGFP-CaM will be 41 kDa. In my results, tendency of the mGFP-CaM protein to have slower diffusion than mGFP was clear. Diffusion coefficient of CaM was 12.9 ± 0.9 and 12.9 ± 0.8 μm²/s in the cytosol and nucleus, respectively. Φ_{fast}/Φ_{total} of CaM in the cytosol was 93%, suggesting that most of the CaM molecules were freely diffusing as mGFP did in HEK293 cells (Fig. 3-12).

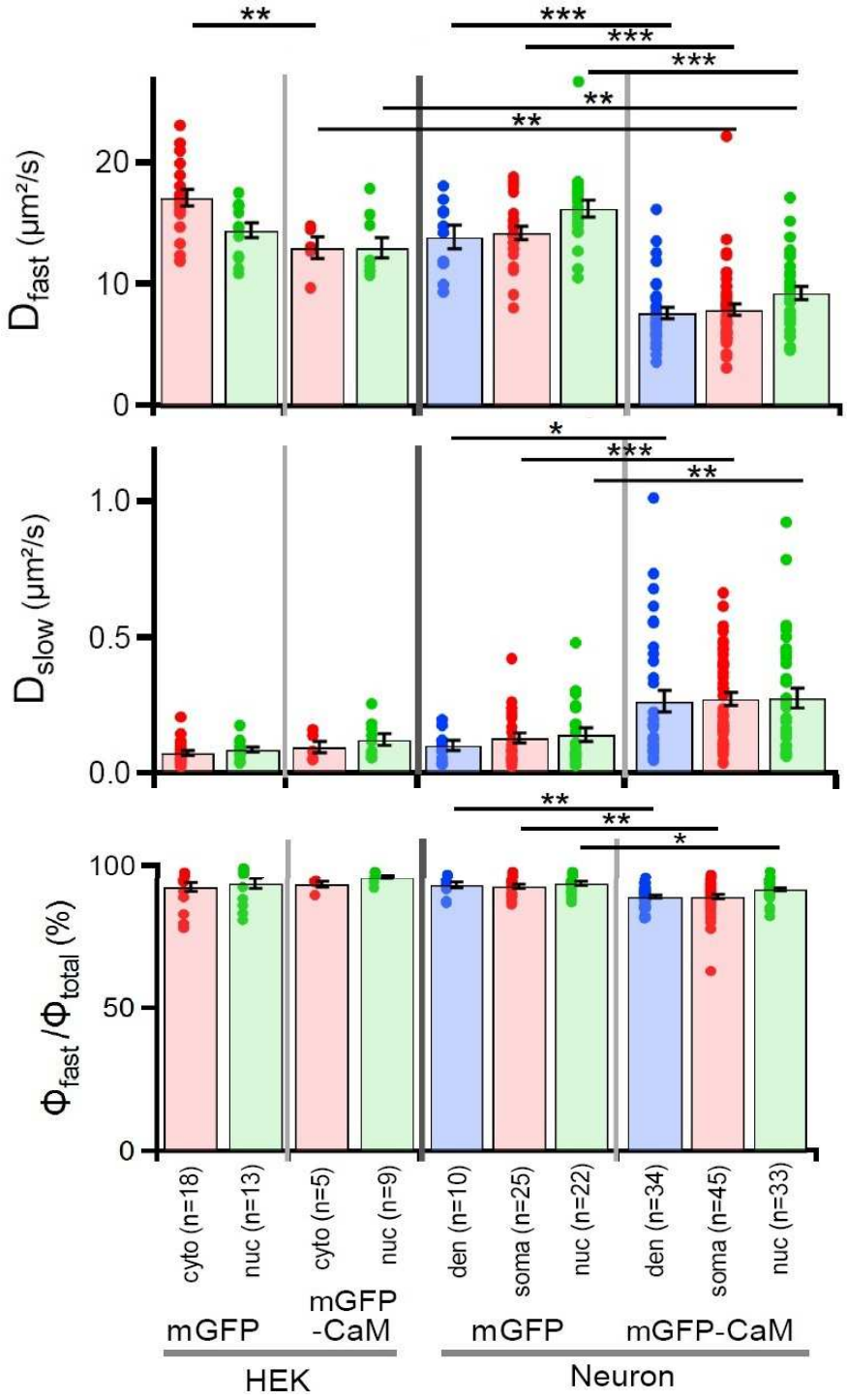

Figure 3-12. Quantitative results of FCS analyses of mGFP and mGFP-CaM in the HEK293 cells and in the hippocampal neurons.

Diffusion coefficient of the faster (D_{fast}) and slower (D_{slow}) diffusion components, fraction of molecular distribution of the faster diffusion component (Φ_{fast}/Φ_{total}) in the cytosol (cyto) and nucleus (nuc) of the HEK293 cells and in the soma, nucleus and dendrite (den) of the hippocampal neurons. In this figure each result of a single cell is indicated by a dot, and averages and S.E.Ms are indicated by bars and error bars, respectively (*p < 0.05, **p < 0.01, ***p < 0.001, Student's test) (Heidarinejad et al., in press).

Results in the dendrite were basically similar to those in the soma unless otherwise indicated. There was no apparent difference in D_{fast} of mGFP among the cellular compartments (13.8 ± 0.9, 14.2 ± 0.5 and 16.2 ± 0.7 μm²/s in the dendrite, soma, nucleus, respectively (Fig. 3-12 and Table 3-1), but mGFP-CaM had tendency to diffuse faster in the nucleus (9.2 ± 0.5 μm²/s) than in the cytosol (soma: D_{fast} = 7.6 ± 0.5 and dendrite: D_{fast} = 7.8 ± 0.5 μm²/s, respectively). CaM diffused slower in neurons than in HEK293 cells. It may reflect intracellular interactions for CaM in neurons.

Table 3-1. D_{fast}, D_{slow}, Φ_{fast}/Φ_{total} and ε_{fast} of mGFP, mGFP-CaM proteins in the cytosol and nucleus of HEK293 cells and in dendrite, soma and nucleus of hippocampal neurons.

cell	Protein	n (cell)	D_{fast} ($\mu m^2/s$)	D_{slow} ($\mu m^2/s$)	Φ_{fast}/Φ_{total} (%)	ε_{fast} (a.u.)
HEK293	mGFP					
	Cytosol	18	17.0 ± 0.7	0.07 ± 0.01	92.4 ± 1.4	86 ± 13 (n=5)
	Nucleus	13	14.4 ± 0.6	0.08 ± 0.01	93.5 ± 1.8	95 ± 14 (n=5)
	mGFP-CaM					
	Cytosol	5	12.9 ± 0.9	0.10 ± 0.02	93.4 ± 1.0	
	Nucleus	9	12.9 ± 0.8	0.12 ± 0.02	95.8 ± 0.6	
Neuron	mGFP					
	Dendrite	10	13.8 ± 0.9	0.10 ± 0.02	93.0 ± 1.1	
	Soma	25	14.2 ± 0.5	0.12 ± 0.02	92.5 ± 0.7	69 ± 4 (n=7)
	Nucleus	22	16.2 ± 0.7	0.14 ± 0.02	93.7 ± 0.7	69 ± 3 (n=7)
	mGFP-CaM					
	Dendrite	34	7.6 ± 0.5	0.27 ± 0.04	88.9 ± 0.6	
	Soma	45	7.8 ± 0.5	0.27 ± 0.02	89.0 ± 0.7	75 ± 4 (n=4)
	Nucleus	33	9.2 ± 0.5	0.28 ± 0.04	91.7 ± 0.6	75 ± 3 (n=4)

The values were calculated by fitting the autocorrelation curves to a two-component diffusion model. Laser power was adjusted to the same level in the experiments measuring the ε values. Results of single cell were calculated and averaged. Average ± S.E.M is indicated (Heidarinejad et al., in press).

3.6 Multi-point recording from Neurons

Number of collected photons in simultaneous multi-point records was less than that of single-point records. ACFs of Multi-point records had less smoothness than

single-point records. To reduce the noise of ACFs, I examined three methods. The first method was increment in duration of records for multi-point records. Based on 15s recording time for single-point records, for two and three-point records, I applied 60 and 90s recording durations, respectively. The longer recording time caused right shift change for ACFs (Fig. 3-13).The second method was increase of the laser power. The higher laser power resulted left shift for ACFs due to increase in number of bleached target proteins. The third method was increase in the number of records. The result was very similar to behavior of single-point records. Therefore, the same value of laser power and recording duration were used in this study for all single- and multi-point records, and just more number of records was performed for MFCS.

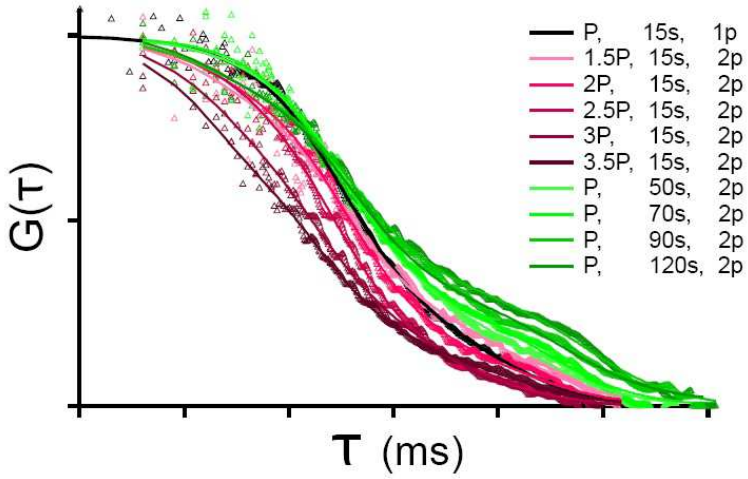

Figure 3-13. Effect of laser power and recording duration on ACFs of multi-point records in compared to single-point FCS.
Single-point FCS (1p) was performed by recording from soma of hippocampal neuron transfected with mGFP-CaM using laser light with power of P for 15s as a duration of record (Black line). To compare, series of two-point records (2p) with different powers and durations were done from the same cell. ACFs with longer record durations (gradient of green colors) and with higher laser power (gradient in purple colors) were plotted. Increase in duration and power made right and left shift changes for ACFs of MFCS records compared to SFCS records, respectively.

In doing so, I recorded from two and three points of transfected neurons with mGFP-CaM. Two-point records were performed from soma and nucleus and for three-point records, dendrite was also recorded. Fig. 3-14 shows result of records from

one cell.

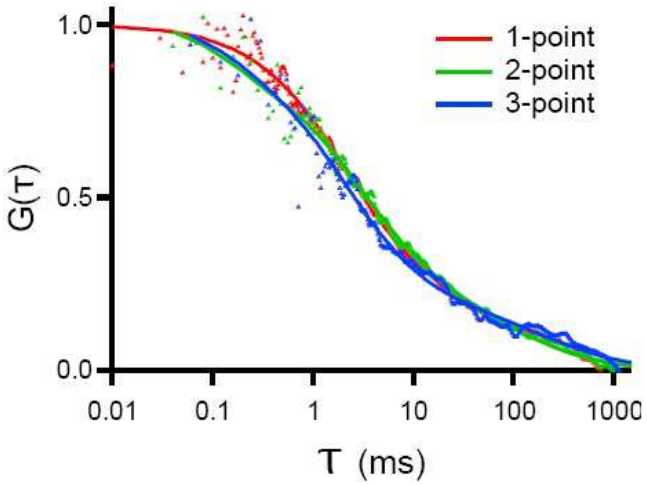

Figure 3-14. Normalized ACFs of one-, two- and three-point records from soma of neuron transfected with mGFP-CaM.
The transfected neuron was recorded with single and multi-point FCS. Then the all records from soma were averaged and represented here. Normalized ACFs shows that there is a reasonable similarity between single-point (red), two-point (green) and three-point (blue) records (Heidarinejad et al., in press).

Averages of all the two- and three-point records from different cells show the same behavior as the one-point records (Fig. 3-15).

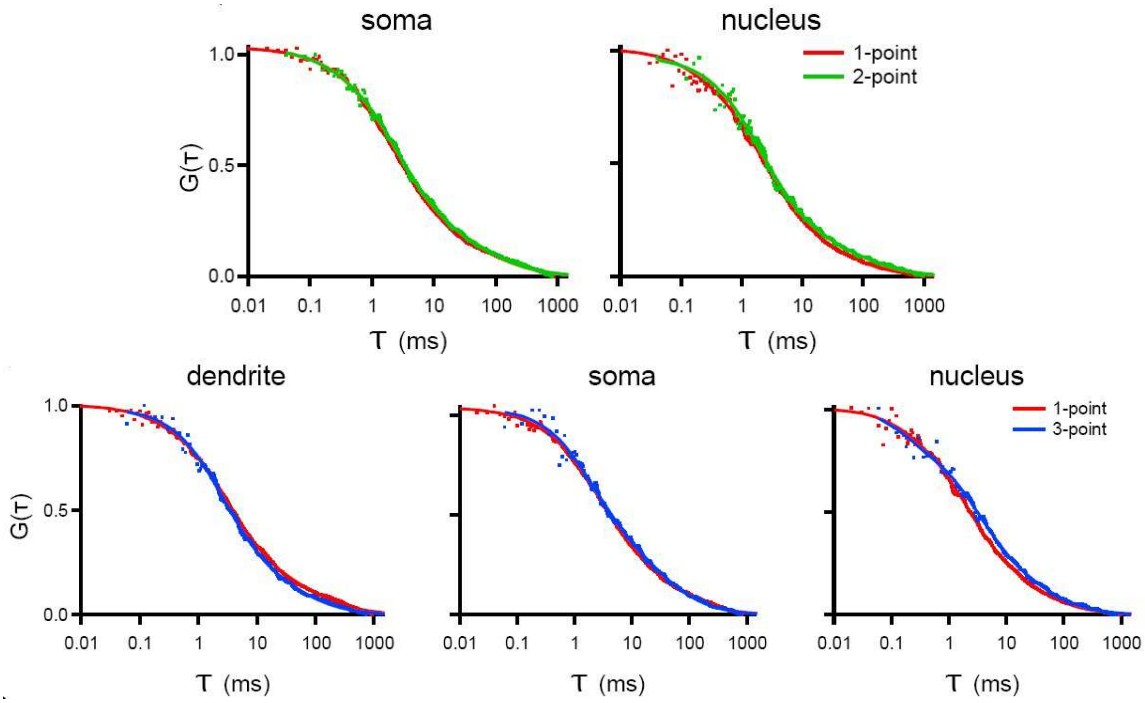

Figure 3-15. Normalized ACFs of one-, two- and three-point records from different compartments of hippocampal neurons.
Two and three-point FCS measurements were recorded from soma, nucleus and dendrite of neurons transfected with mGFP-CaM. ACFs of all records from one cell were averaged first and average of all cells is represented here. Results show that multi-point ACFs from soma, nucleus and dendrite are reasonably similar to that of single-point records (Heidarinejad et al., in press).

For further analysis, all averages were fitted by the two-component model and result of single- and multi-point records were compared. The D_{fast} and D_{slow} values for single- and multi-point records were in the same range and there was no significant difference between the single- and multi-point records. Therefore, my proposed method for multi-point recording was a trustable method to use especially in recording from cells such as neurons with high diversity of function among the compartments (Figs. 3-16 and 3-17).

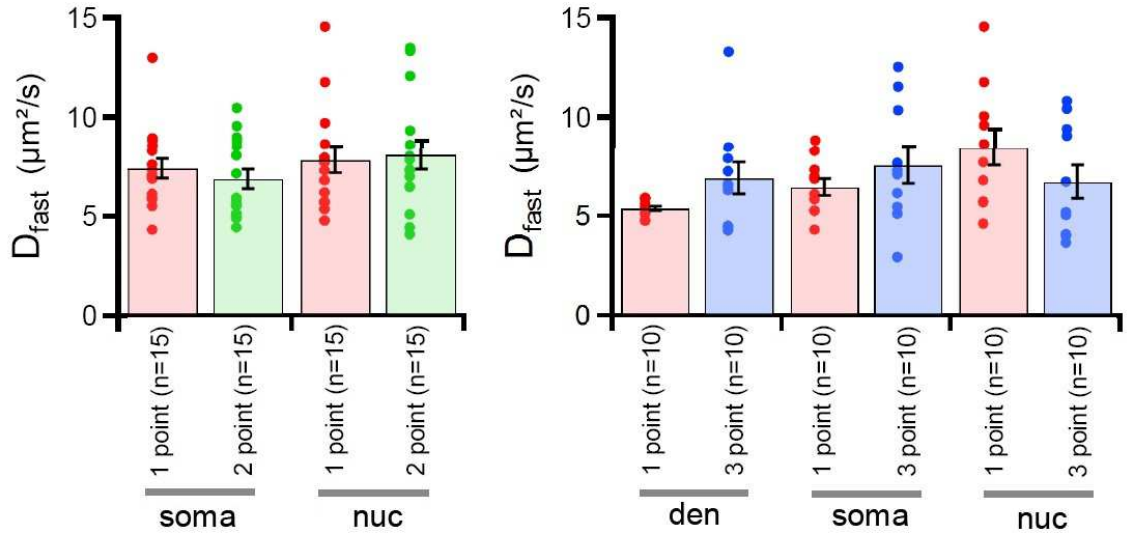

Figure 3-16. *D_{fast}* of single- and multi-point FCS analyses of mGFP-CaM recorded from neurons.

Diffusion coefficient of the faster diffusion component in the soma, nucleus (nuc) and dendrite (den) recorded by one, two and three-point FCS. In this figure, each result of a single cell is indicated by a dot, and averages and S.E.Ms are indicated by bars and error bars, respectively (Heidarinejad et al., in press).

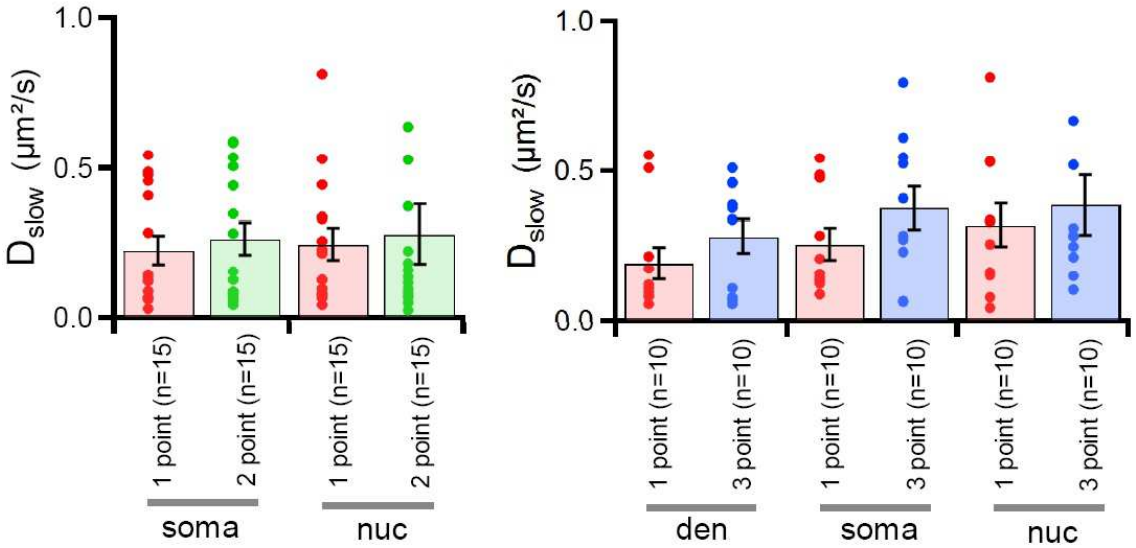

Figure 3-17. *D_{slow}* of single- and multi-point FCS analyses of mGFP-CaM recorded from neurons.

Diffusion coefficient of the slower diffusion component in the soma, nucleus (nuc) and dendrite (den) recorded by one, two and three-point FCS. In this figure, each result of a single cell is indicated by a dot, and averages and S.E.Ms are indicated by bars and error bars, respectively (Heidarinejad et al., in press).

3.7 Diffusion of mGFP and CaM Proteins in stimulated neurons

I stimulated neurons with 100 µM Glu/ 10 µM Gly in the HBS medium. CaM did not show any noticeable changes in its distribution upon stimulation (Fig. 3-18).

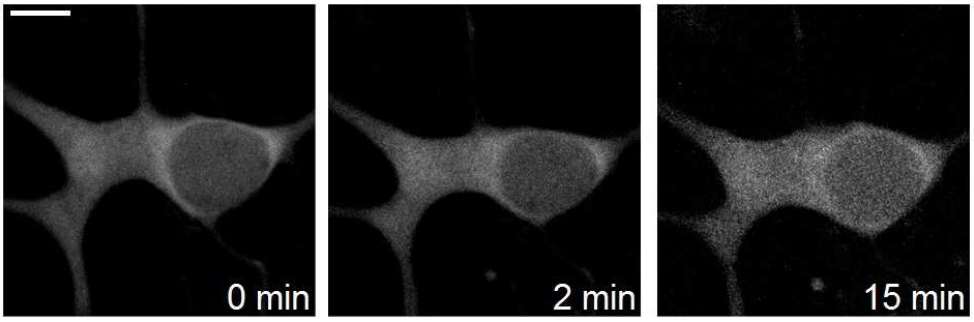

Figure 3-18. Stimulation of hippocampal neurons transfected with mGFP-CaM.
Fluorescence images of a neuron transfected with mGFP-CaM before (0 min) and 2 and 15 min after stimulation with 100 µM Glu/10 µM Gly. No change on distribution of CaM was detected. Scale bar: 4 µm.

I also recorded from mGFP in different compartments of neurons before and 15-25 min after stimulation. FCS results showed that diffusion of mGFP and CaM is influenced by stimulation (Fig. 3-19). CaM showed faster diffusion after stimulation in all compartments of the neurons.

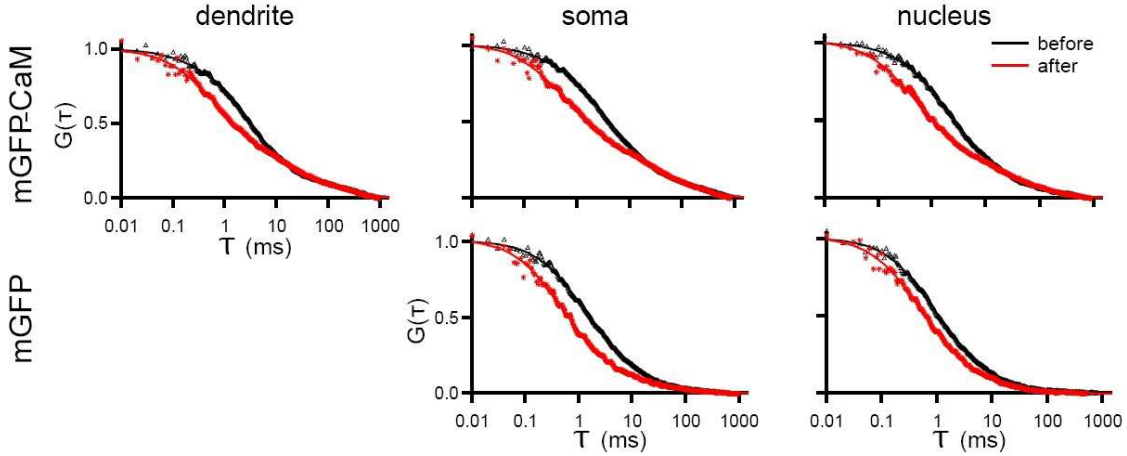

Figure 3-19. FCS results recorded from hippocampal neurons before and after stimulation.
Normalized ACFs of mGFP and mGFP-CaM before (black) and after (red) stimulation in the dendrite, soma and nucleus of hippocampal neurons. ACFs in the cells were averaged first, and then the averages of all cells were averaged. ACFs of mGFP and CaM showed left shifts after stimulation (Heidarinejad et al., in press).

ACFs taken before and after stimulation were fitted. Φ_{fast}/Φ_{total} of CaM in the dendrite, soma and nucleus (91, 90 and 92%) and of mGFP in the soma and nucleus (91 and 94%) before stimulation was changed to 83, 87 and 88% for CaM and 95 and 95% for mGFP after stimulation (Fig. 3-20). It shows transition of CaM proteins from the faster component to the slower component. Such a transition did not happen for mGFP.

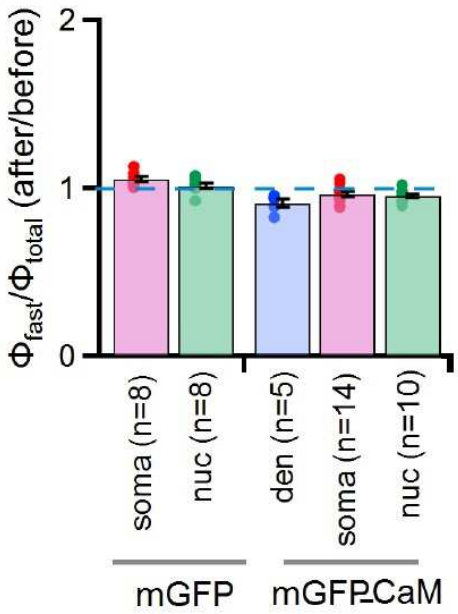

Figure 3-20. Changes in Φ_{fast}/Φ_{total} of FCS parameters of mGFP and mGFP-CaM before and after the Glu/Gly stimulation in the soma, nucleus (nuc) and dendrite (den) of hippocampal neurons.

Ratio of Φ_{fast}/Φ_{total} after stimulation to those before stimulation is shown. The data of after stimulation were taken between 15 to 25 min after the stimulation. Φ_{fast}/Φ_{total} of mGFP-CaM decreased after stimulation. Each result of a single cell is indicated by a dot, and averages and S.E.Ms are indicated by bars and error bars, respectively (Heidarinejad et al., in press).

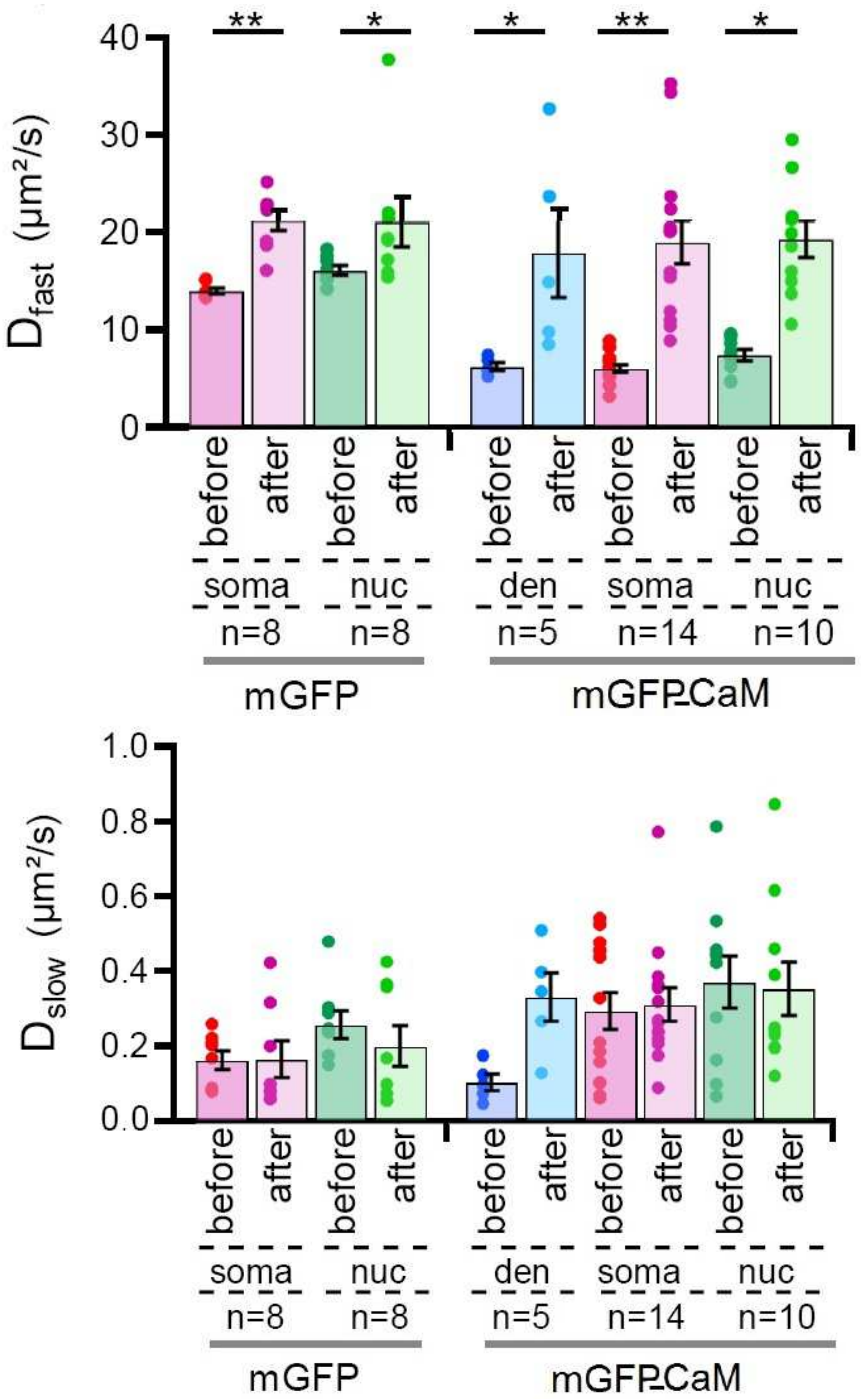

Figure 3-21. Changes in D_{fast} and D_{slow} of FCS parameters of mGFP and mGFP-CaM before and after the Glu/Gly stimulation in the soma, nucleus (nuc) and dendrite (den) of hippocampal neurons.

D_{fast} and D_{slow} before and after stimulation is shown. The data of after stimulation were taken between 15 to 25 min after the stimulation. mGFP and mGFP-CaM proteins diffused faster after stimulation. Each result of a single cell is indicated by a dot, and averages and S.E.Ms are indicated by bars and error bars, respectively (*$p < 0.05$, **$p < 0.01$, Student's paired t-test) (Heidarinejad et al., in press).

D_{fast} of CaM was increased in all the compartments (Fig. 3-21). The increase in D_{fast} of CaM was almost more than twice of that of mGFP.

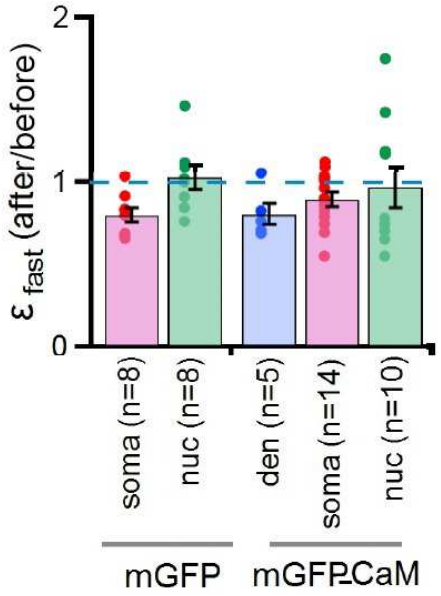

Figure 3-22. Changes in ε_{fast} of mGFP and mGFP-CaM before and after the Glu/Gly stimulation in the soma, nucleus (nuc) and dendrite (den) of hippocampal neurons.

Ratio of ε_{fast} after and before stimulation is shown. The data of after stimulation were taken between 15 to 25 min after the stimulation. The ε_{fast} values of mGFP and mGFP-CaM were not changed during the stimulation. Each dot indicates average values of records from each cell. Each result of a single cell is indicated by a dot, and averages and S.E.Ms are indicated by bars and error bars, respectively (Heidarinejad et al., in press).

According to Fig. 3-22, there were no significant change on the brightness of mGFP and CaM before and after stimulation.

To check long-term effects of stimulation, I performed series of FCS records of mGFP and CaM. Transfected neurons were stimulated with Glu/Gly as before, and the stimulation solution was changed to the normal HBS by 5 minutes circulation 20 min after the onset of Glu/Gly application. Records were continued for 40 min after the wash of stimuli. As Fig. 3-23 shows, mGFP and mGFP-CaM represented left-shift in ACF during 10 to 20 min after stimulation, and the diffusion profile was recovered after the wash of stimuli.

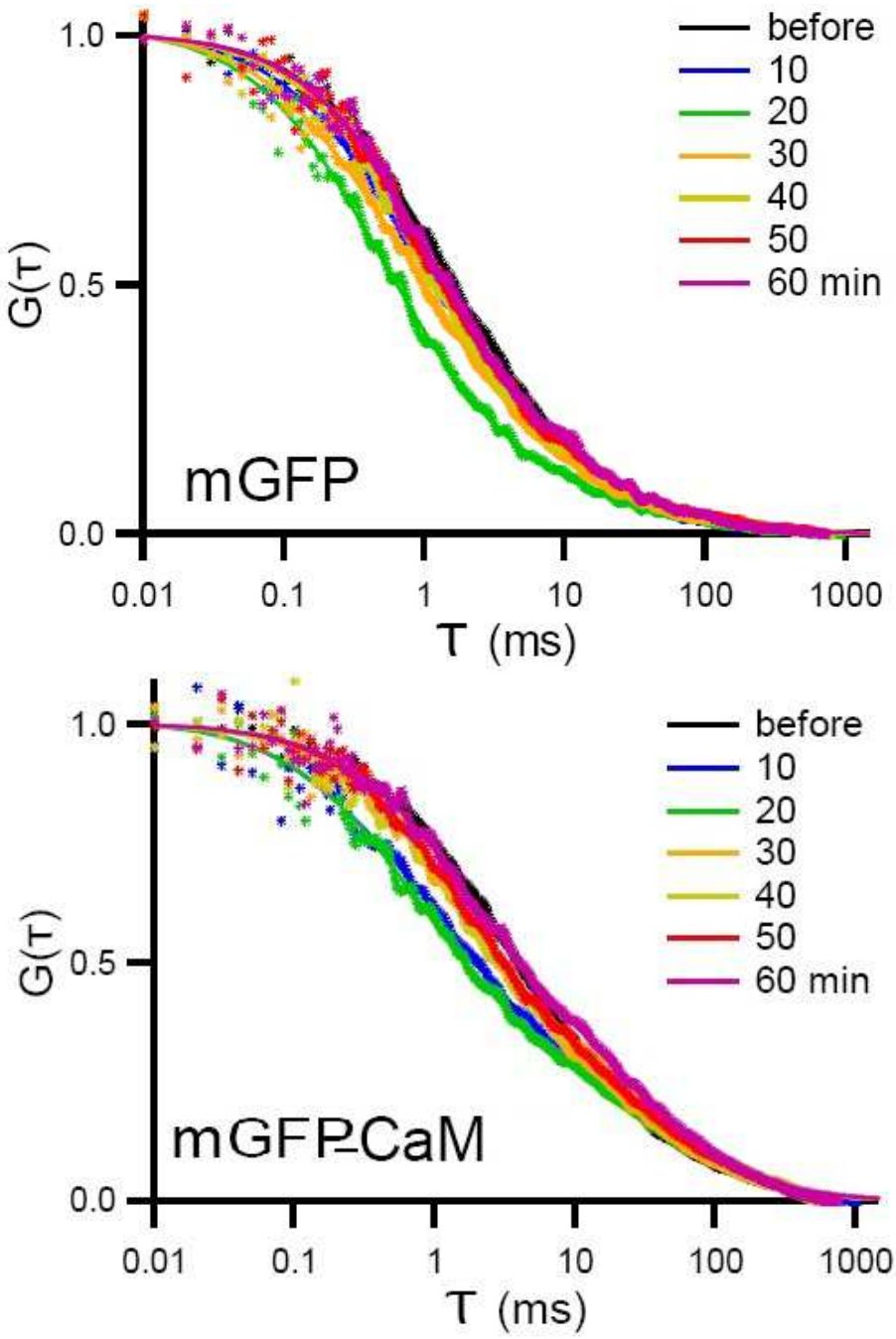

Figure 3-23. Time course of ACF of mGFP and mGFP-CaM in somata of single neurons upon stimulation with 100 *μ*M Glu/10 *μ*M Gly.

Transfected neurons with mGFP (n=8) and mGFP-CaM (n=7) were stimulated with 100 μM Glu/10 μM Gly for 20 min and then the recording solution was replaced by normal HBS via 5 min circulation. FCS records continued for 40 min after wash. The left shift of ACF started 10 min after the onset of Glu/Gly application and recovered after washout of stimuli. ACFs of cells at each time point were averaged and represented here. Dots indicate ACFs at indicated time points, and lines show fitting results (Heidarinejad et al., in press).

D_{fast} of mGFP and CaM was increased after stimulation 10 to 20 min after the

onset of stimulation until washout of stimuli. After removing Glu/Gly, D_{fast} of mGFP and CaM was decreased (Fig. 3-24).

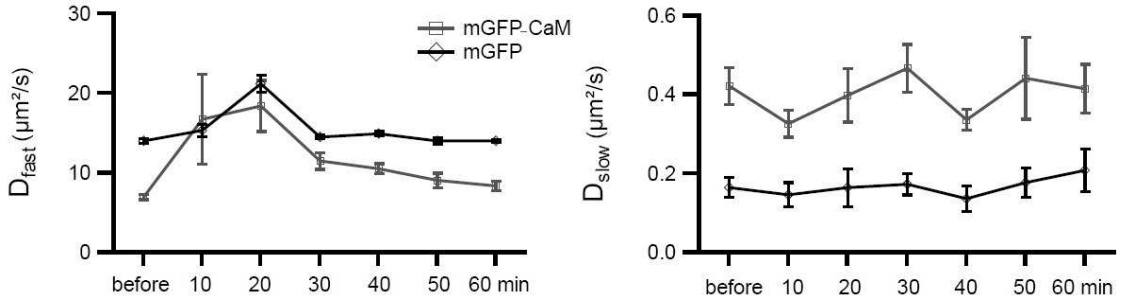

Figure 3-24. Changes in D_{fast} and D_{slow} of time course FCS parameters before, after stimulation and after washout of stimuli in somata of hippocampal neurons.
D_{fast} and D_{slow} of mGFP (n=8) and mGFP-CaM (n=7) proteins before, after stimulations and after washout of stimuli are shown. The data were collected every 10 min and the stimulation solution was washed out 20 min after the onset of stimulation by 5 min circulation of normal HBS. The increase in D_{fast} of mGFP and mGFP-CaM suggests dissociation of protein from substrates besides changes in viscosity of intracellular medium. Averages and S.E.Ms are indicated by bars and error bars, respectively (Heidarinejad et al., in press).

D_{slow} did not show clear change upon stimulation. Stimulation of neurons caused faster diffusion for CaM. The change in diffusion of CaM was not accompanied by change in brightness. So, the possibility of dissociation of aggregated forms after stimulation or any aggregation is low (Fig. 3-25).

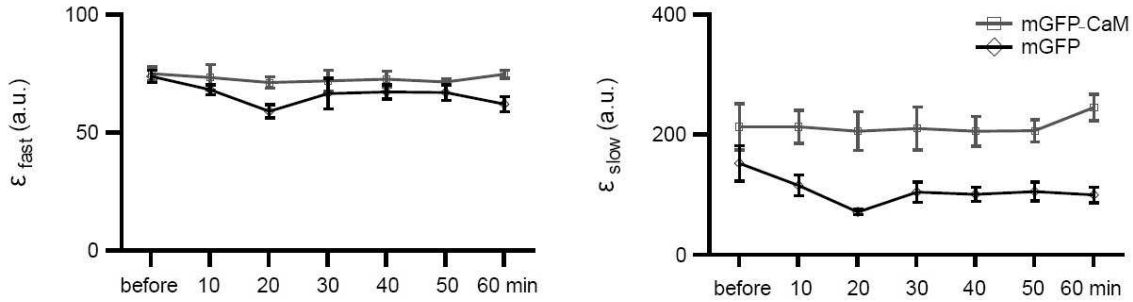

Figure 3-25. Changes in ε_{fast} and ε_{slow} of time course FCS parameters before, after stimulation and after washout of stimuli in somata of hippocampal neurons.
ε_{fast} and ε_{slow} of mGFP (n=8) and mGFP-CaM (n=7) proteins before, after stimulations and after washout of stimuli are shown. The data were collected every 10 min and the recording solution was washed out 20 min after the onset of stimulation by 5 min circulation of normal HBS. The mGFP-CaM protein does not show any change on its brightness upon stimulation. Averages and S.E.Ms are indicated by bars and error bars, respectively (Heidarinejad et al., in press).

4 Results (CaMKII)

4.1 Diffusion of CaMKII proteins in HEK293 cells and in neurons

After investigation of intracellular diffusion of CaM, I focused on behavior of CaMKII proteins in particular the CaMKIIα and CaMKIIβ types in HEK293 cells and neurons.

I transfected HEK293 cells with monomeric CaMKIIα (mGFP-mCaMKIIα), CaMKIIα (mGFP-CaMKIIα and CaMKIIα- mGFP) and CaMKIIβ (mGFP-CaMKIIβ) plasmids using the lipofection method. mCaMKIIα lacks the C-terminal association domain and thus devoid of forming holoenzyme (Kolb et al., 1998). Similar to behavior of mGFP and CaM, mCaMKIIα was homogeneously distributed in all cell regions (Fig. 4-1). In contrast, cells transfected with CaMKIIα and CaMKIIβ had dimmer nucleus than cytosol. The difference in the nuclear localization patterns of CaMKIIα, β and mCaMKIIα can be explained by the difference in molecular mass: the molecular mass of mGFP-mCaMKIIα is around 60 kDa, which permits free nuclear pore passage, while the molecular masses of holoenzymes of CaMKIIα and β (599 and 633 kDa, respectively (Kanaseki et al., 1991; Kolb et al., 1998; Silver, 1991)) are too large for passive translocation to the nucleus without having an NLS sequence (Ma et al., 2015; Srinivasan et al., 1994).

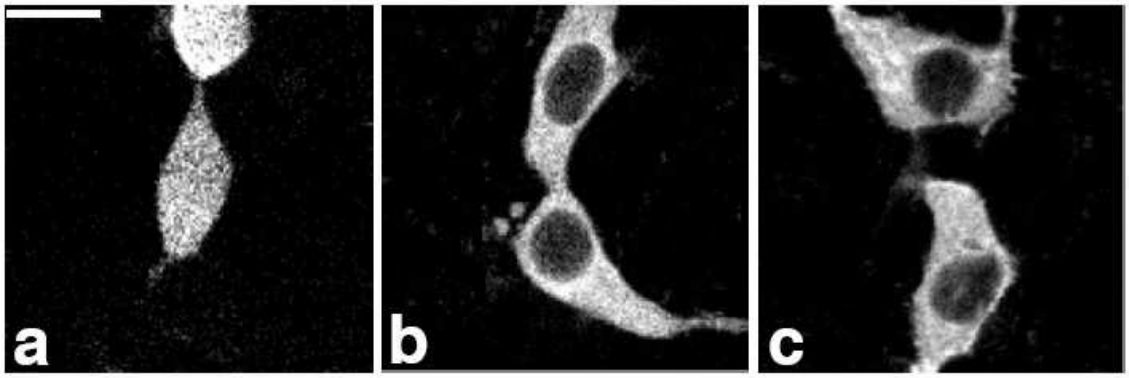

Figure 4-1. Expression of mGFP-CaMKII proteins in the HEK293 cells.
Fluorescence images of HEK293 cells transfected with mGFP-mCaMKIIα (a), mGFP-CaMKIIα (b) and mGFP-CaMKIIβ (c). Scale bar: 10 μm. CaMKIIα and β showed nuclear escape patterns (Heidarinejad et al., in press).

I expressed all above-mentioned proteins in HEK293 cells (Fig. 4-1) and in the hippocampal neurons (Fig. 4-2). Neurons at DIV 7-14 were transfected, and used for FCS records within 12-18 hours after transfection.

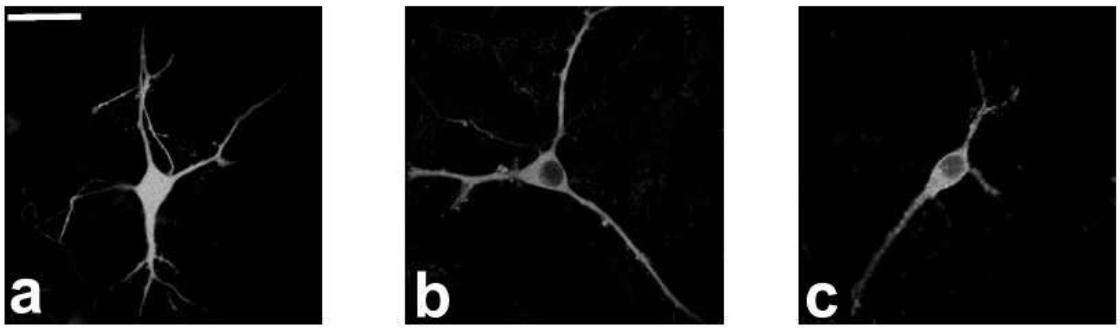

Figure 4-2. Expression of mGFP-CaMKII proteins in hippocampal neurons.
Fluorescence images of neurons transfected with mGFP-mCaMKIIα (a), mGFP-CaMKIIα (b) and mGFP-CaMKIIβ (c). Scale bar: 20 μm. CaMKIIα and β showed nuclear escape patterns (Heidarinejad et al., in press).

Similar to the HEK293 cells, mCaMKIIα was distributed evenly in all compartments of the neurons, and CaMKIIα and β were distributed much less in the nucleus. FCS was performed in the soma, nucleus and dendrite. There was no impact by intracellular concentration (C_{fast}) within the range of measured concentrations of transfected proteins on D_{fast} value (Fig. 4-3).

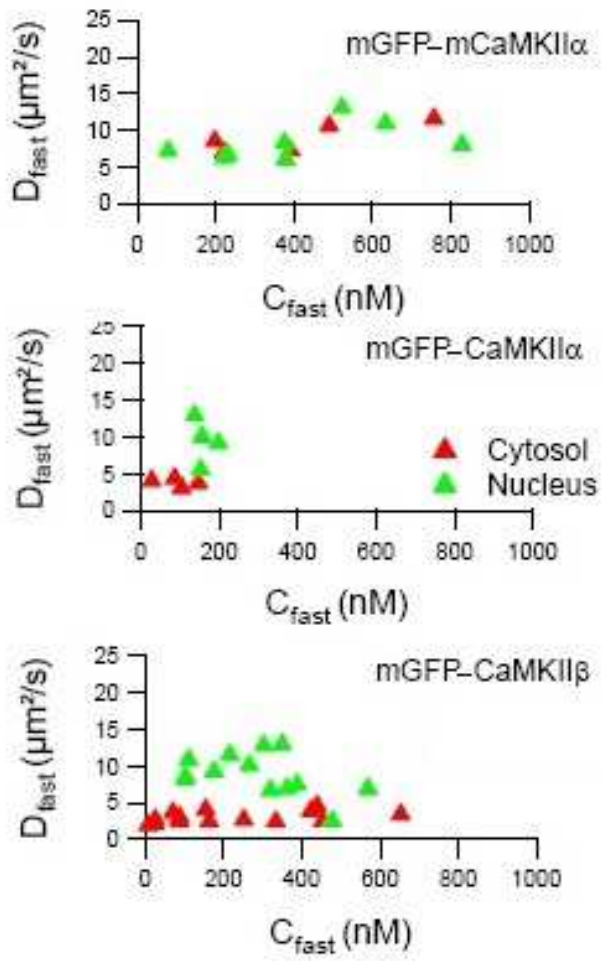

Figure 4-3. Relation between concentration of expressed proteins and diffusion coefficient of fast component.
D_{fast} values versus fast component concentration of mCaMKIIα, CaMKIIα and CaMKIIβ in HEK293 cells. It seemed that there was no impact by intracellular concentration on *D* value.

According to ACFs of Fig. 4-4, there were no apparent difference in the diffusion of mCaMKIIα in different compartments of HEK293 cells, which was confirmed by statistical analyses of quantitative results (Fig. 4-5). However, mCaMKIIα was diffusing faster in the nucleus than in the soma and dendrite in neurons. Such a difference in diffusion of CaM and mCaMKIIα between cytosol and nucleus in neurons was not seen in the HEK293 cells.

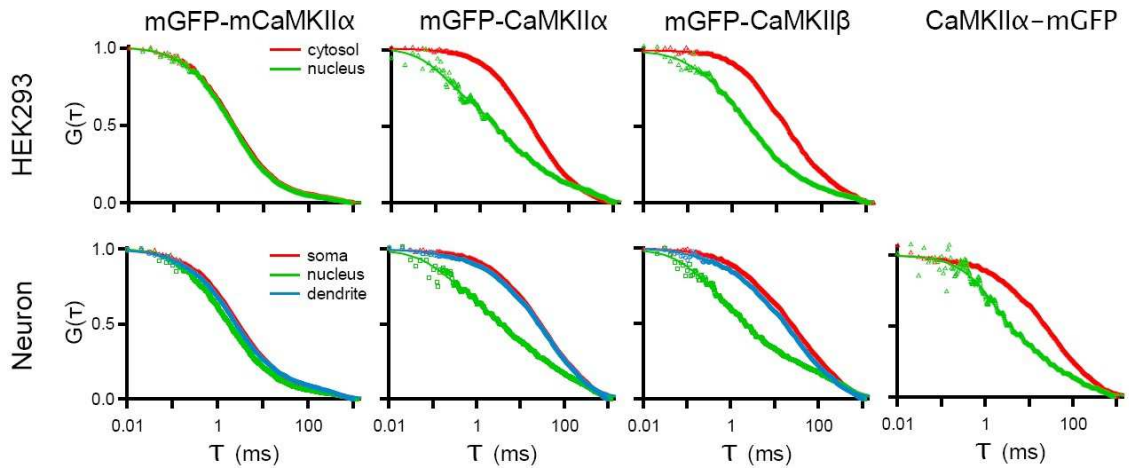

Figure 4-4. ACFs of proteins in cytosol and nucleus of HEK293 cells and neurons. Normalized averaged ACFs of mGFP-mCaMKIIα, mGFP-CaMKIIα, mGFP-CaMKIIβ and CaMKIIα-mGFP in the cytosol (red) and nucleus (green) of HEK293 cells and in the soma (red), nucleus (green) and dendrite (blue) of neurons. ACFs in a single cell were averaged first, and then the averages of all cells were averaged and indicated. CaMKIIα and β showed apparently faster diffusion in the nucleus than in the cytosol (Heidarinejad et al., in press).

As Fig. 4-4 shows, diffusion profiles of mCaMKIIα were all similar in the cytosol and nucleus of HEK293 cells. On the contrary, diffusion pattern of the CaMKIIα and β proteins showed faster diffusion in the nucleus than the cytosol.

D_{fast} of mCaMKIIα in HEK293 cells was 8.2 ± 0.6 and 8.8 ± 0.9 μm²/s, in the cytosol and nucleus, respectively, which was significantly slower than those of mGFP and CaM (Fig. 4-5).

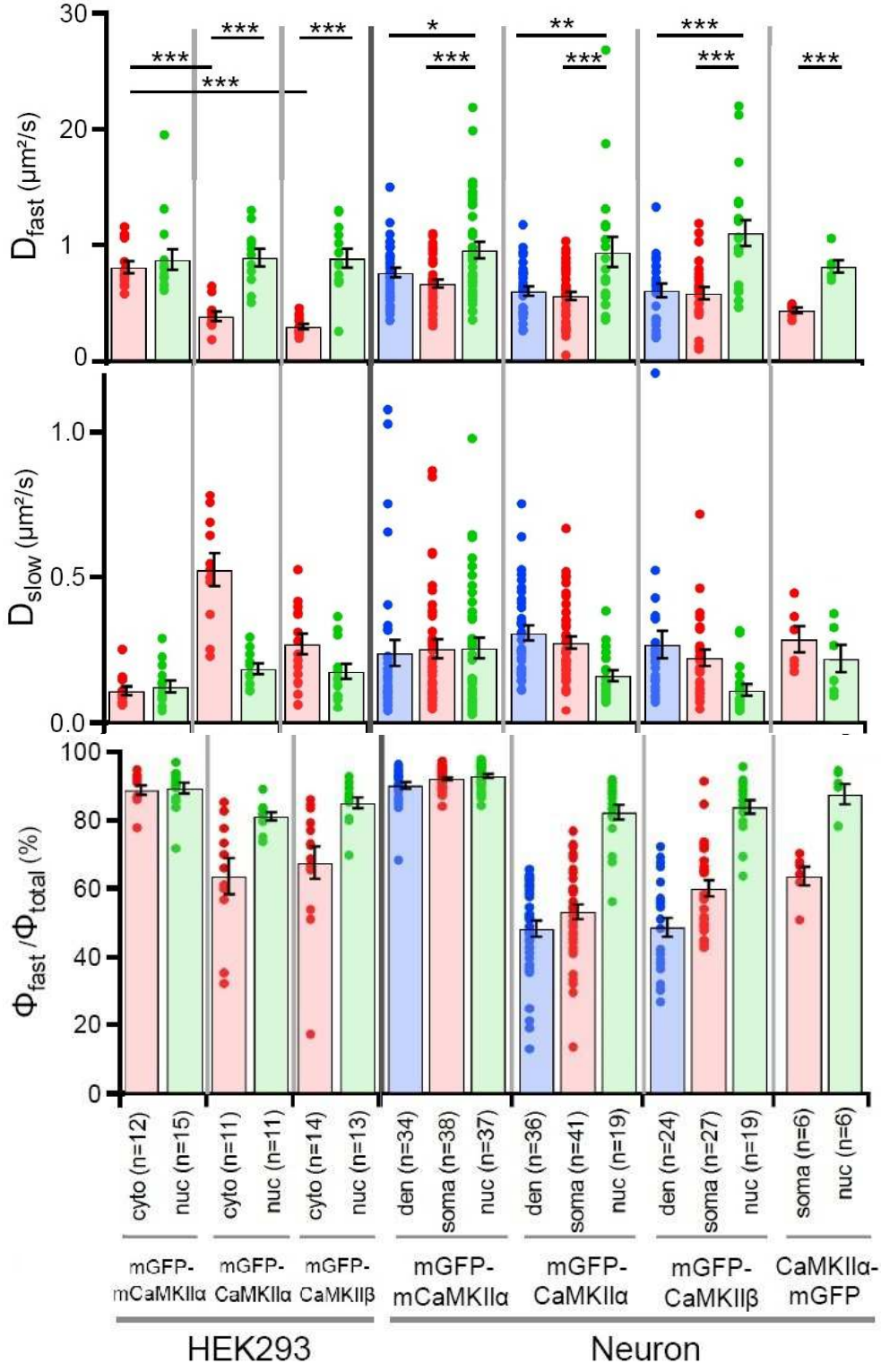

Figure 4-5. Quantitative results of FCS analyses of mGFP-mCaMKIIα, mGFP-CaMKIIα, mGFP-CaMKIIβ and CaMKIIα- mGFP in the HEK293 cells and neurons.

D_{fast} and D_{slow} and Φ_{fast}/Φ_{total} in the cytosol (cyto) and nucleus (nuc) of HEK293 and soma, nucleus and dendrite (den) of neurons. In this figure each result of a single cell is indicated by a dot, and averages and S.E.Ms are indicated by bars and error bars, respectively (*p < 0.05, **p < 0.01, ***p < 0.001, Student's test) (Heidarinejad et al., in press).

CaMKIIα and CaMKIIβ showed totally different diffusion properties both in the cytosol and nucleus from mCaMKIIα. The values of D_{fast} of CaMKIIα and CaMKIIβ in the cytosol of HEK293 cells (3.9 ± 0.4 and 3.0 ± 0.2 μm²/s, respectively) were much smaller than those in the nucleus (9.0 ± 0.8 and 8.9 ± 0.8 μm²/s, $p < 0.001$, respectively) and those of mCaMKIIα (8.2 ± 0.6 μm²/s, $p < 0.001$) in the cytosol. On the other hands, the values of D_{fast} of CaMKIIα and CaMKIIβ in the nucleus of HEK293 cells (9.0 ± 0.8, 8.9 ± 0.8 μm²/s, respectively) were within a similar range with that of mCaMKIIα (8.8 ± 0.9 μm²/s). The values of D_{slow} of CaMKIIα and CaMKIIβ in the cytosol (0.53 ± 0.06 and 0.27 ± 0.04 μm²/s, respectively) were larger than those of mGFP, CaM and mCaMKIIα (0.07 ± 0.01, $p < 0.01$, 0.10 ± 0.02, $p < 0.01$ and 0.11 ± 0.02 μm²/s, $p < 0.01$, respectively, Table 3-1 and 4-1).

In neurons, mCaMKIIα diffused faster in the nucleus (9.4 ± 0.7 μm²/s) than in the cytosol (soma: D_{fast} = 6.6 ± 0.3 μm²/s, $p < 0.001$, dendrite: D_{fast} = 7.5 ± 0.4 μm²/s, $p < 0.05$).

Φ_{fast}/Φ_{total} of mGFP-mCaMKIIα in the soma was 90.1 ± 0.5%, indicating that about 90% of the mutant CaMKIIα were diffusing as the faster component. D_{fast} of CaMKIIα and β in the nucleus (9.2 ± 1.3 and 10.8 ± 1.1 μm²/s, respectively) was indeed larger than that in the soma (5.6 ± 0.4, $p < 0.001$ and 5.7 ± 0.5 μm²/s, $p < 0.001$, respectively) and in the dendrite (5.9 ± 0.4, $p < 0.05$ and 5.9 ± 0.6 μm²/s, $p < 0.001$, respectively).

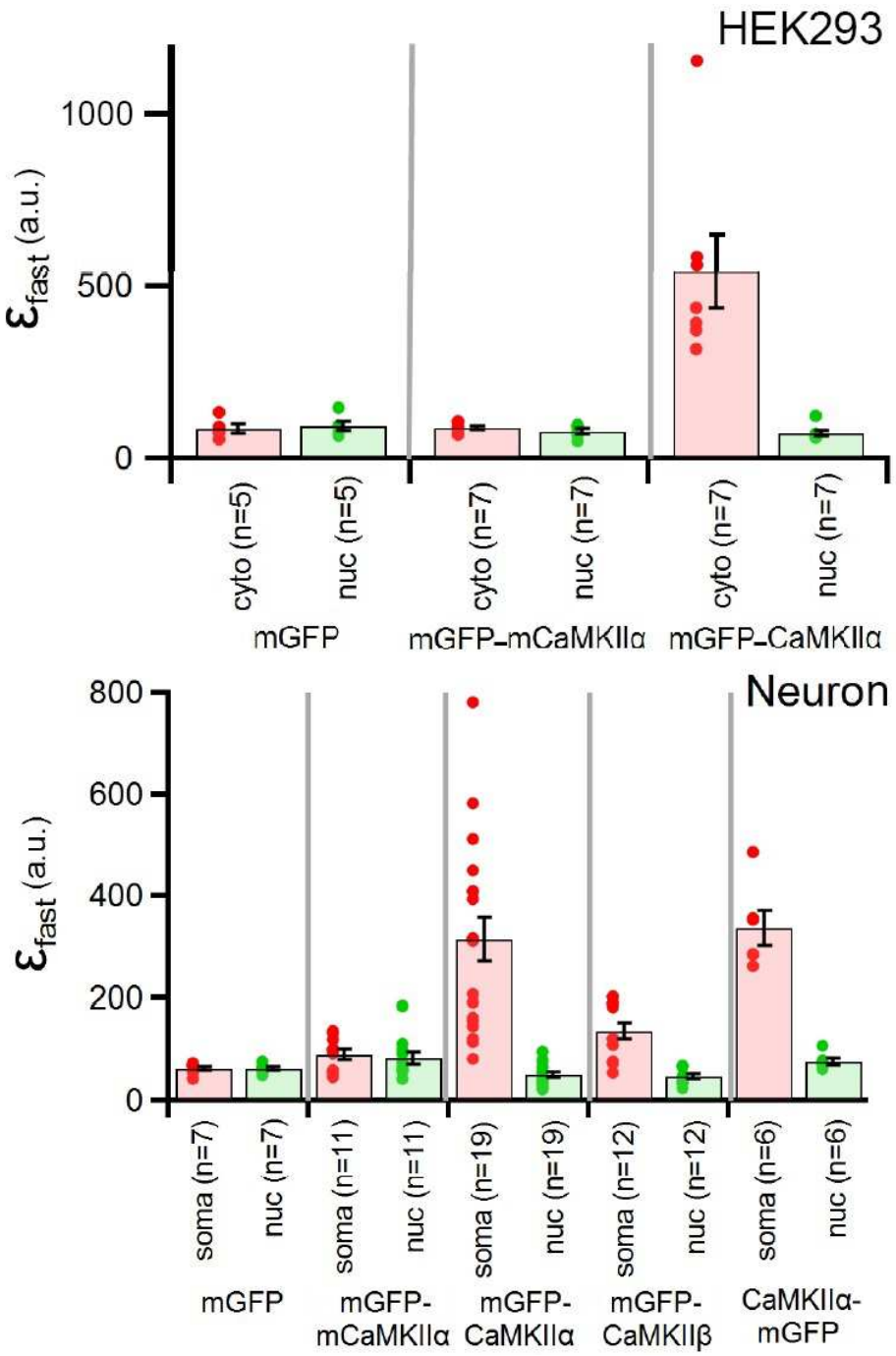

Figure 4-6. ε_{fast} in the cytosol and nucleus of HEK293 cells and neurons.
Particle brightness of the faster (ε_{fast}) diffusion component in the cytosol (cyto) and nucleus (nuc) of mGFP, mGFP-mCaMKIIα and mGFP-CaMKIIα of transfected HEK293 cells and in the soma and nucleus of mGFP, mGFP-mCaMKIIα, mGFP-CaMKIIα, mGFP-CaMKIIβ and CaMKIIα-mGFP of transfected neurons. The ε_{fast} values of CaMKIIα in the cytosol were much larger than that in the nucleus and those of mGFP and mGFP-mCaMKIIα. Laser power was adjusted to the same level in the experiments to compare ε value among experiments. In this figure each result of a single cell is indicated by a dot, and averages and S.E.Ms are indicated by bars and error bars, respectively (Heidarinejad et al., in press).

In HEK293 cells, brightness analyses of the faster component (Eq. 30) revealed that the brightness of mCaMKIIα in the cytosol was similar to that in the nucleus (Fig. 4-6), while CaMKIIα was 7.2 ± 0.7 times brighter in the cytosol than in the nucleus, which means that CaMKIIα exists as holoenzyme composing of at least 7-8 subunits in the cytosol, as is well established, but it exists as a monomer or just fragments of protein in the nucleus. CaMKIIβ showed a similar level of ε_{fast} in the nucleus of HEK293 cells to that of mGFP and about 7 times brighter in the cytosol than in the nucleus (data not shown), though the laser power was not rigidly adjusted in the case for CaMKIIβ.

In neurons, ε_{fast} of mCaMKIIα was 1.7 and 1.5 times larger than that of mGFP in the soma and nucleus, respectively, suggesting that the mCaMKIIα proteins were diffusing in the forms of monomer or dimer (Fig. 4-6). The intensity of nucleus in transfected neurons with CaMKIIα was lower than in soma. Existence of small fragments of protein or difference on number of subunits of CaMKIIα in the soma and nucleus are the possible reasons. CaMKIIα and CaMKIIβ showed similar ε_{fast} values in the nucleus to that of mGFP and about 6 and 3 times brighter in the cytosol than in the nucleus, respectively. All of these results suggest that the CaMKIIα and CaMKIIβ proteins exist as holoenzyme in the neuronal cytosol.

Φ_{total} as an index of the total number of mGFP tagged subunits of CaMKIIα and CaMKIIβ was 2.9 and 4 times higher in the soma than the dendrite, respectively. It is indicating that the lower number of CaMKII proteins localize in the dendrite than in soma. While Φ_{total} was in the same order for mGFP and CaM in the soma and dendrite, almost two-fold difference for mCaMKIIα in the soma and dendrite was a sign that

mCaMKIIα diffusion mechanisms was different than both of mGFP and CaM.

The ratio of ε_{slow} and ε_{fast} of mGFP, CaM and mCaMKIIα in the soma was almost two in average (1.9 ± 0.1, 2.3 ± 0.1 and 2.1 ± 0.1, respectively, Fig. 4-7). On the contrary, the ratio of ε_{slow} to ε_{fast} of CaMKIIα and CaMKIIβ in the soma was almost five-fold (5.4 ± 0.3 and 4.9 ± 0.4, respectively), which can be interpreted as an aggregation of holoenzymes. In simpler words, CaMKII proteins in soma are diffusing in form of single holoenzymes or are aggregation of roughly five holoenzymes with a 10 times slower diffusion rate.

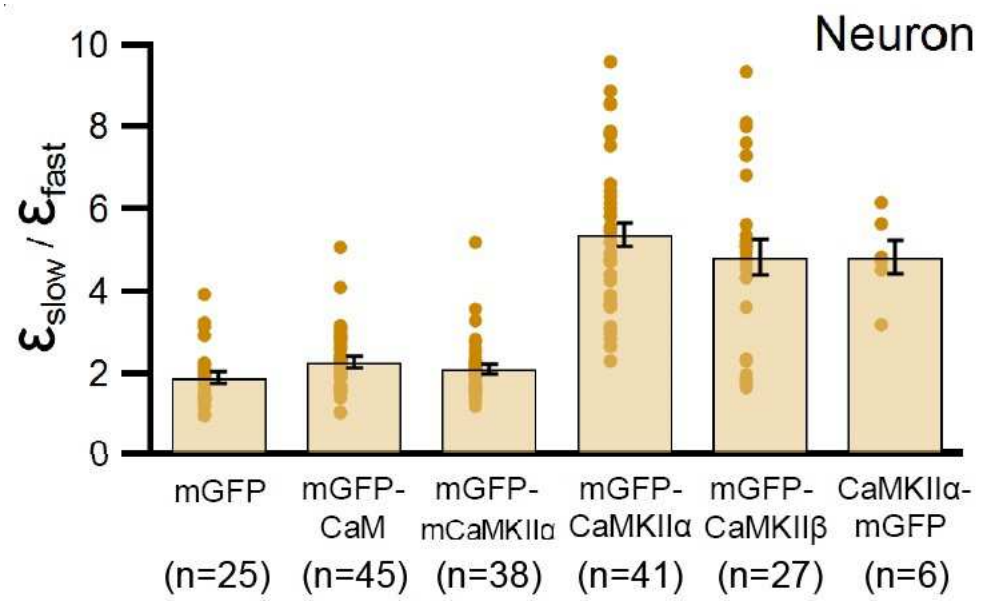

Figure 4-7. $\varepsilon_{slow}/\varepsilon_{fast}$ in the soma of neurons.
Slower components of mGFP, mGFP-CaM, mGFP-mCaMKIIα, mGFP-CaMKIIα, mGFP-CaMKIIβ and CaMKIIα-mGFP were brighter than the faster component, indicating that the proteins in the slower component formed aggregated superstructures of proteins in the faster component (Heidarinejad et al., in press).

Table 4-1. D_{fast}, D_{slow}, Φ_{fast}/Φ_{total} and ε_{fast} of mGFP-mCaMKIIα, mGFP-CaMKIIα, CaMKIIα- mGFP and mGFP-CaMKIIβ proteins in the cytosol and nucleus of HEK293 cells and in dendrite, soma and nucleus of hippocampal neurons.

cell	Protein	n (cell)	D_{fast} ($\mu m^2/s$)	D_{slow} ($\mu m^2/s$)	Φ_{fast}/Φ_{total} (%)	ε_{fast} (a.u.)
HEK 293	mGFP-mCaMKIIα					
	Cytosol	12	8.2 ± 0.6	0.11 ± 0.02	89.1 ± 1.4	90 ± 5 (n=7)
	Nucleus	15	8.8 ± 0.9	0.13 ± 0.02	89.5 ± 1.5	78 ± 7 (n=7)
	mGFP-CaMKIIα					
	Cytosol	11	3.9 ± 0.4	0.53 ± 0.06	63.8 ± 5.3	545 ± 108 (n=7)
	Nucleus	11	9.0 ± 0.8	0.19 ± 0.02	81.2 ± 1.3	73 ± 8 (n=7)
	mGFP-CaMKIIβ					
	Cytosol	14	3.0 ± 0.2	0.27 ± 0.04	67.7 ± 4.8	
	Nucleus	13	8.9 ± 0.8	0.18 ± 0.03	85.3 ± 1.6	
Neuron	mGFP-mCaMKIIα					
	Dendrite	34	7.5 ± 0.4	0.24 ± 0.04	88.1 ± 0.9	
	Soma	38	6.6 ± 0.3	0.25 ± 0.03	90.1 ± 0.5	90 ± 10 (n=11)
	Nucleus	37	9.4 ± 0.7	0.25 ± 0.04	90.8 ± 0.5	83 ± 12 (n=11)
	mGFP-CaMKIIα					
	Dendrite	36	5.9 ± 0.4	0.30 ± 0.03	47.2 ± 2.2	
	Soma	41	5.6 ± 0.4	0.27 ± 0.02	52.0 ± 2.0	315 ± 40 (n=19)
	Nucleus	19	9.2 ± 1.3	0.16 ± 0.02	80.3 ± 2.1	52 ± 5 (n=19)
	CaMKIIα-mGFP					
	Soma	6	4.3 ± 0.2	0.28 ± 0.04	62.2 ± 2.7	338 ± 34 n=6)
	Nucleus	6	8.0 ± 0.5	0.22 ± 0.05	85.5 ± 2.9	78 ± 7 (n=6)
	mGFP-CaMKIIβ					
	Dendrite	24	5.9 ± 0.6	0.26 ± 0.05	47.6 ± 2.7	
	Soma	27	5.7 ± 0.5	0.22 ± 0.03	58.7 ± 2.4	136 ± 16 (n=12)
	Nucleus	19	10.8 ± 1.1	0.11 ± 0.02	82.0 ± 1.9	48 ± 5 (n=12)

The values were calculated by fitting the autocorrelation curves to a two-component diffusion model. Laser power was adjusted to the same level in the experiments measuring the ε values. Results of single cell were calculated and averaged. Average ± S.E.M is indicated (Heidarinejad et al., in press).

4.2 Diffusion of CaMKII proteins in stimulated neurons

I stimulated neurons with 100 μM Glu/ 10 μM Gly in the HBS medium. Fast redistribution of CaMKIIα and CaMKIIβ proteins was detected (Fig. 4-8), as has been

reported by other groups (Dosemeci et al., 2000; Grant et al., 2008; Hudmon et al., 2005, 1996; Shen and Meyer, 1999; Tao-Cheng et al., 2001).

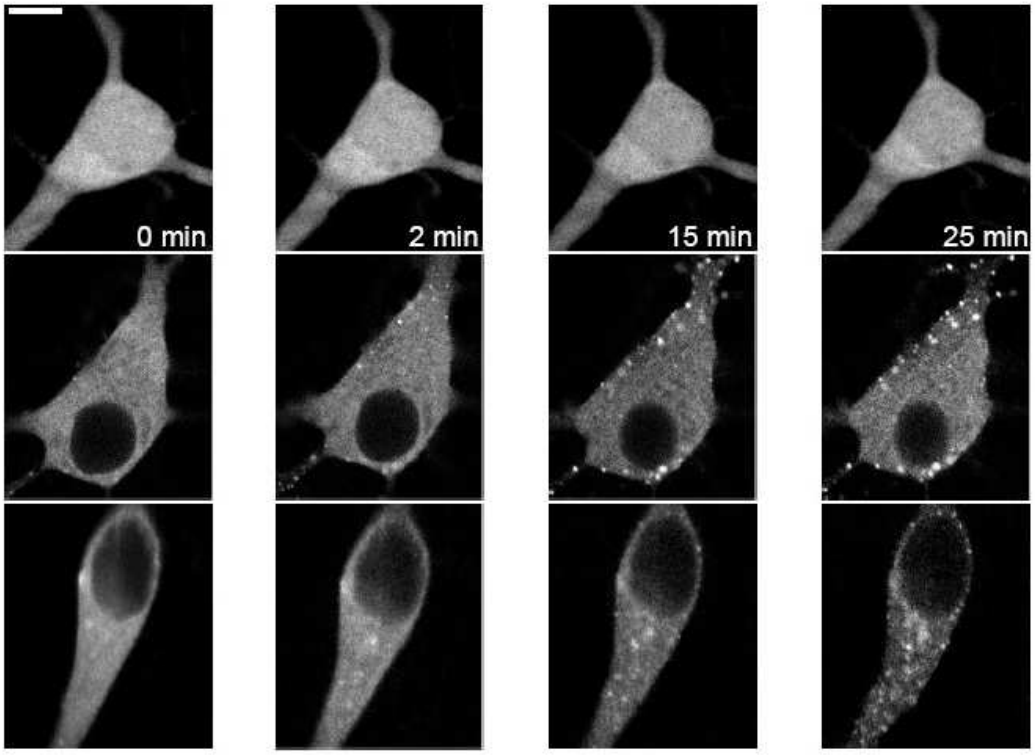

Figure 4-8. Stimulation of hippocampal neurons.
Fluorescence images of neurons transfected with mGFP-mCaMKIIα (top), mGFP-CaMKIIα (middle) and mGFP-CaMKIIβ (down) before (0 min) and 2, 15 and 25 min after stimulation with 100 μM Glu/10 μM Gly. Speckle patterns appeared at 2 min, which became more obvious at 15 min for CaMKIIα and CaMKIIβ proteins. Scale bar, 4 μm (Heidarinejad et al., in press).

For CaMKIIα, speckle patterns were formed within 1 min after the onset of stimulation and lasted until the end of observation. The bright spots were distributed in dendrite and soma but not in nucleus. They were stable for 1 hour and images did not show any disappearance of spots or new formations. The mCaMKIIα proteins did not show any noticeable cluster formation or redistribution.

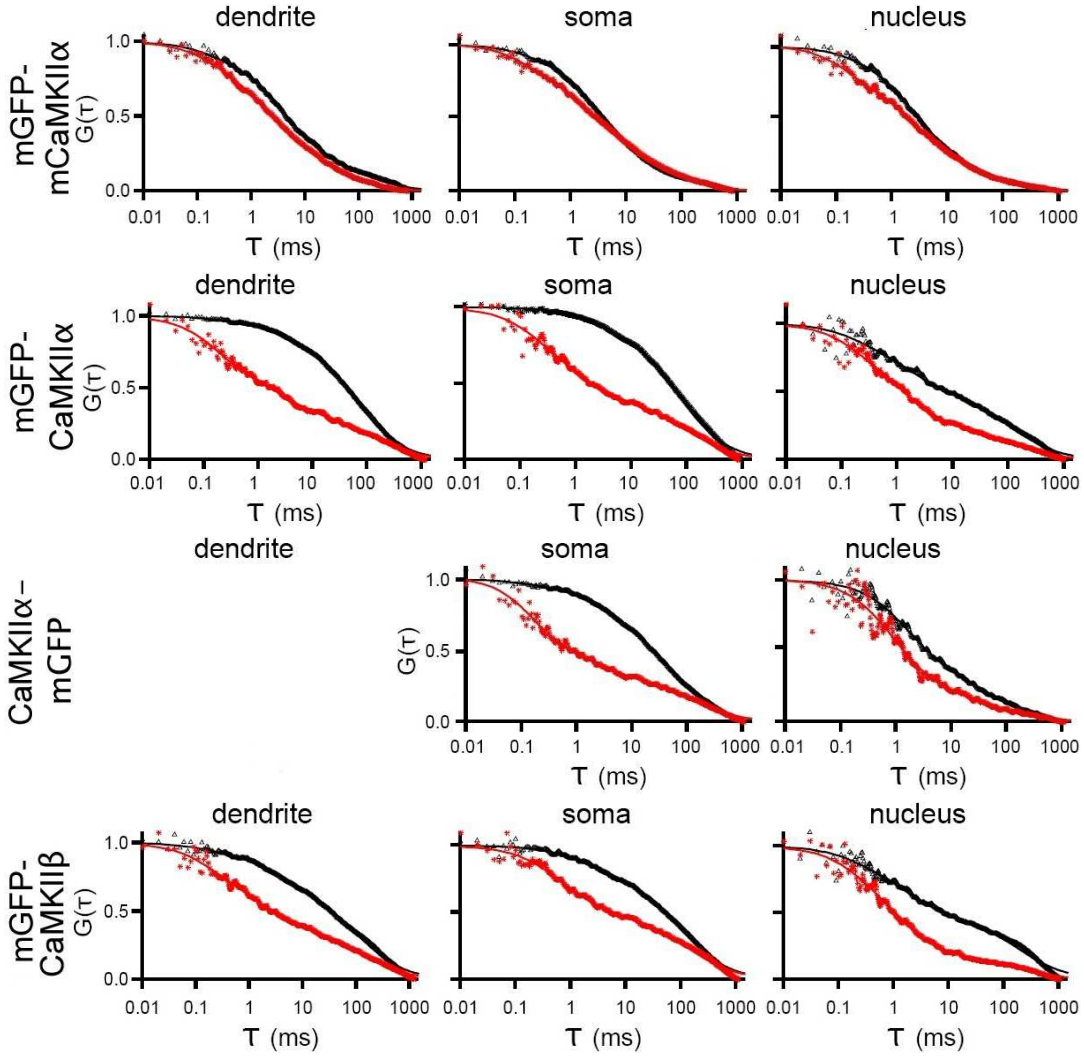

Figure 4-9. FCS results of hippocampal neurons before and after stimulation. Normalized ACFs of mGFP-mCaMKIIα, mGFP-CaMKIIα, CaMKIIα-mGFP and mGFP-CaMKIIβ before (black) and after (red) stimulation in the dendrite, soma and nucleus of hippocampal neurons. ACFs in the cells were averaged first, and then the averages of all cells were averaged. ACFs of all proteins showed left shifts after stimulation (Heidarinejad et al., in press).

FCS results showed that diffusion of mCaMKIIα, CaMKIIα and CaMKIIβ was influenced by stimulation (Fig. 4-9). mCaMKIIα showed left-shift change on ACF in the same way as mGFP and CaM showed, but CaMKIIα and CaMKIIβ showed robustly faster diffusion after stimulation in the soma and dendrite.

4.3 CaMKII mutants

To investigate the relationship between the speckle pattern formation and the changes in the diffusion pattern of CaMKIIα, mutants of CaMKIIα, T286A, I205K, T305/306A and A302R, were expressed in neurons. T286A lacks the kinase activity upon Ca^{2+}/CaM binding. A302R is unable to bind to Ca^{2+}/CaM and does not form clusters by neuronal stimulation (Barcomb et al., 2015; Nguyen et al., 2015; Shen and Meyer, 1999). The I205K mutation is devoid of any interaction at the T-site of the N-terminal catalytic domain with the regulatory domain of other CaMKIIα subunits or the NR2B subunit of NMDA receptor, thus it lacks aggregation of holoenzyme or association with postsynaptic density proteins (Bayer et al., 2001). The T305/306A mutation prevents the enzyme from secondary phosphorylation at a.a. 305 and 306 and therefore lets the protein bind to Ca^{2+}/CaM again after dissociation from CaM (Griffith et al., 2003). The T286A and T305/306A mutants showed the speckle distribution pattern after stimulation with the Glu/Gly, while the other two mutants did not change their even distribution pattern (Fig. 4-10). However, ACFs of all of these mutants were changed similarly to those of wild type by the stimulation. These results indicate that these mutations had no effect on the holoenzyme dissociation or digestion upon stimulation. This phenotypic change in the structure of the holoenzyme and the speckle formation suggests that the speckle formation of CaMKIIα and β by neuron activation may not directly be related to the degradation of the protein.

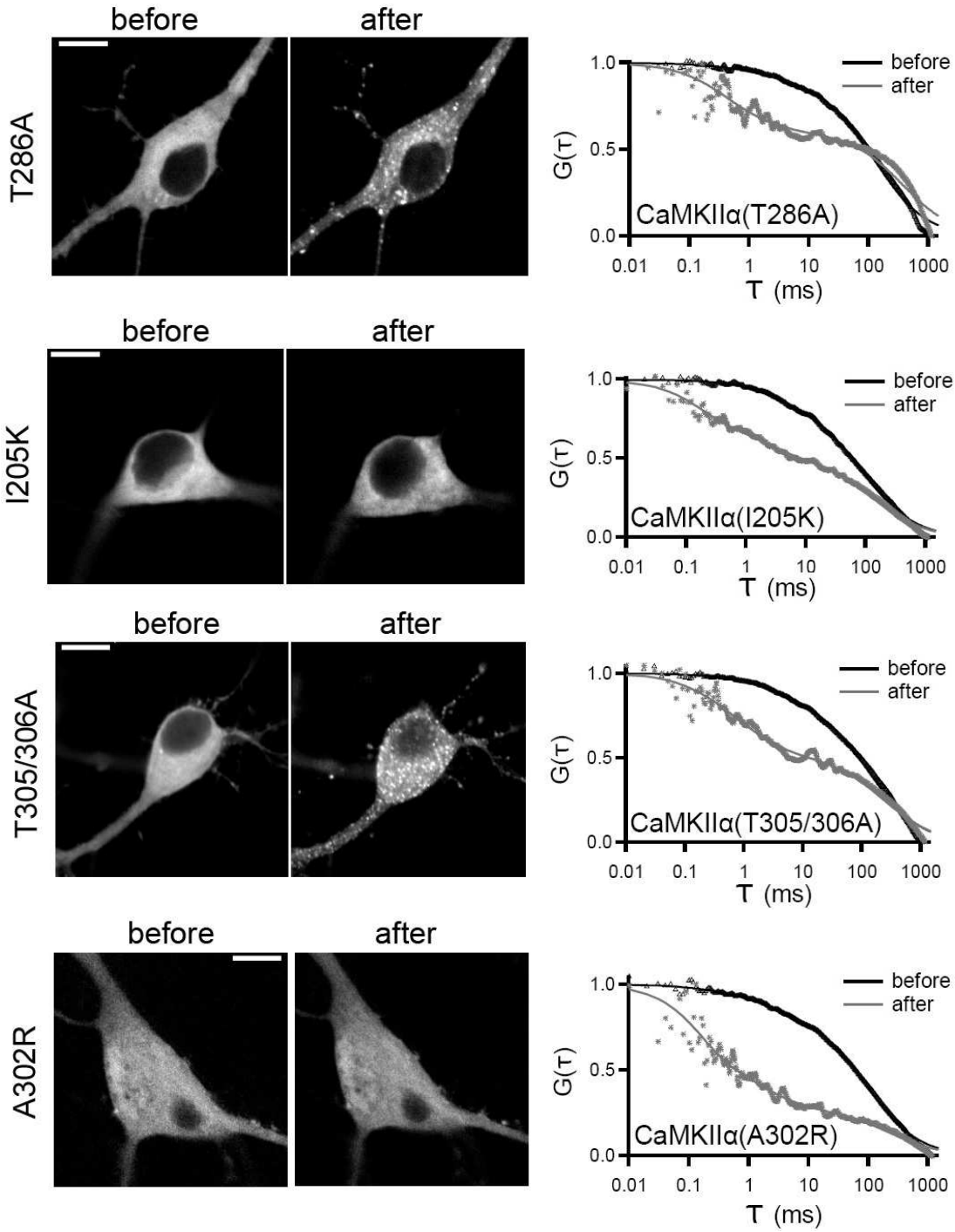

Figure 4-10. Changes on distribution patterns and ACFs of CaMKIIα mutants by Glu/Gly stimulation

mGFP-tagged CaMKIIα mutants, T286A, T305/306A, I205K and A302R, were expressed in hippocampal neurons and stimulated with 100 μM Glu/10 μM Gly (n=3, for T286A, T305/306A and A302R , n=9 for the I205K). Fluorescence images indicate appearance of speckled patterns in neurons expressing the T286A and T305/306A mutants by the stimulation, but not in neurons expressing the I205K and A302R mutants. But ACFs of all these mutants in the soma shifted to the left. ACFs of records in a single cell were averaged first, then the averages of all cells were averaged and indicated. Scale bar, 10 μm (Heidarinejad et al., in press).

After stimulation by Glu/Gly, Φ_{fast}/Φ_{total} of not mCaMKIIα but CaMKIIα and CaMKIIβ was changed (Fig. 4-11). In contrast with mCaMKIIα, Φ_{fast}/Φ_{total} of CaMKIIα and CaMKIIβ (α: 38, 42 and 76% and β: 41, 59 and 75% in the dendrite, soma and nucleus, respectively) was increased in all the compartments (α: 68, 65 and 85% and β: 63, 78 and 89%, respectively). The increases of Φ_{fast}/Φ_{total} of CaMKIIα and β suggest that CaMKIIα and β were liberated from the particles included in the slower diffusing fraction by the stimulation. As Fig. 4-11 shows, Φ_{total} of CaMKIIα and CaMKIIβ was reduced after stimulation. It is explained by the appearance of clusters. Part of the proteins aggregated and made the clusters after stimulation.

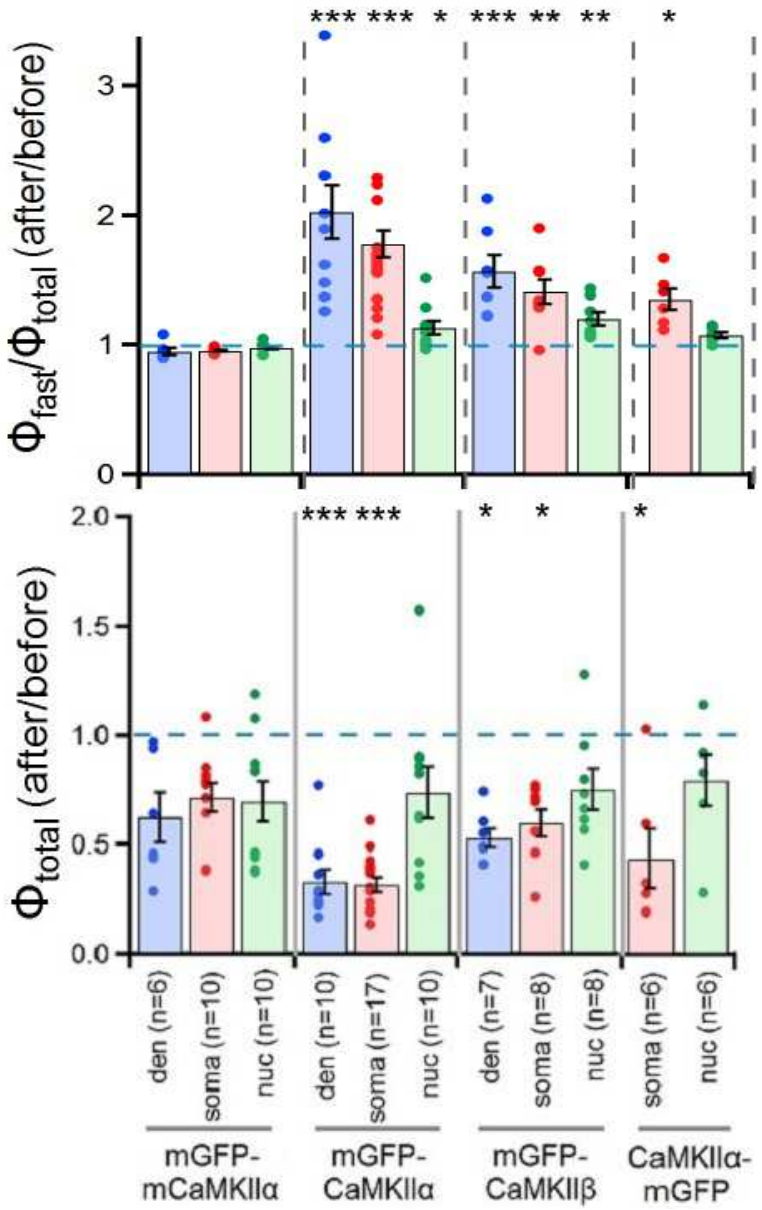

Figure 4-11. Changes in Φ_{fast}/Φ_{total} and Φ_{total} of mGFP-mCaMKIIα, mGFP-CaMKIIα, mGFP-CaMKIIβ and CaMKIIα-mGFP before and after the Glu/Gly stimulation in the soma, nucleus (nuc) and dendrite (den) of hippocampal neurons.

Ratios of Φ_{fast}/Φ_{total} and Φ_{total} before and after stimulation are shown. The data of after stimulation were taken between 15 to 25 min after the stimulation. Each result of a single cell is indicated by a dot, and averages and S.E.Ms are indicated by bars and error bars, respectively (*p < 0.05, **p < 0.01, ***p < 0.001, Student's paired t-test) (Heidarinejad et al., in press).

D_{fast} of mCaMKIIα, CaMKIIα and CaMKIIβ was increased upon stimulation (Fig. 4-12).

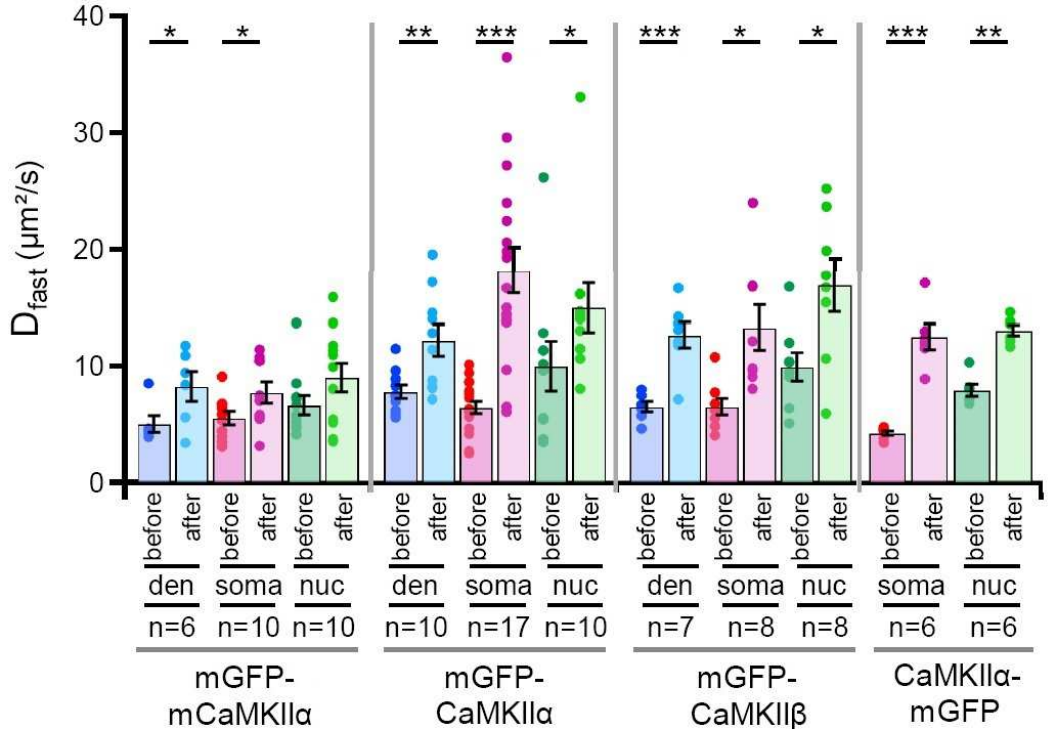

Figure 4-12. Changes in D_{fast} of mGFP-mCaMKIIα, mGFP-CaMKIIα, mGFP-CaMKIIβ and CaMKIIα-mGFP before and after the Glu/Gly stimulation in the soma, nucleus (nuc) and dendrite (den) of hippocampal neurons.

D_{fast} before and after stimulation is shown. The data were taken between 15 to 25 min after the stimulation. The mCaMKIIα, CaMKIIα and CaMKIIβ proteins diffused faster after stimulation. Each result of a single cell is indicated by a dot, and averages and S.E.Ms are indicated by bars and error bars, respectively (*p < 0.05, **p < 0.01, ***p < 0.001, Student's paired t-test) (Heidarinejad et al., in press).

The concentration of proteins was also subjected to change by the stimulation. C_{fast} of CaMKIIα and β was decreased in the nucleus, while that of CaMKIIα in the soma was increased. The stimulation also decreased C_{slow} of CaMKIIα and β in the soma and nucleus (Fig. 4-13).

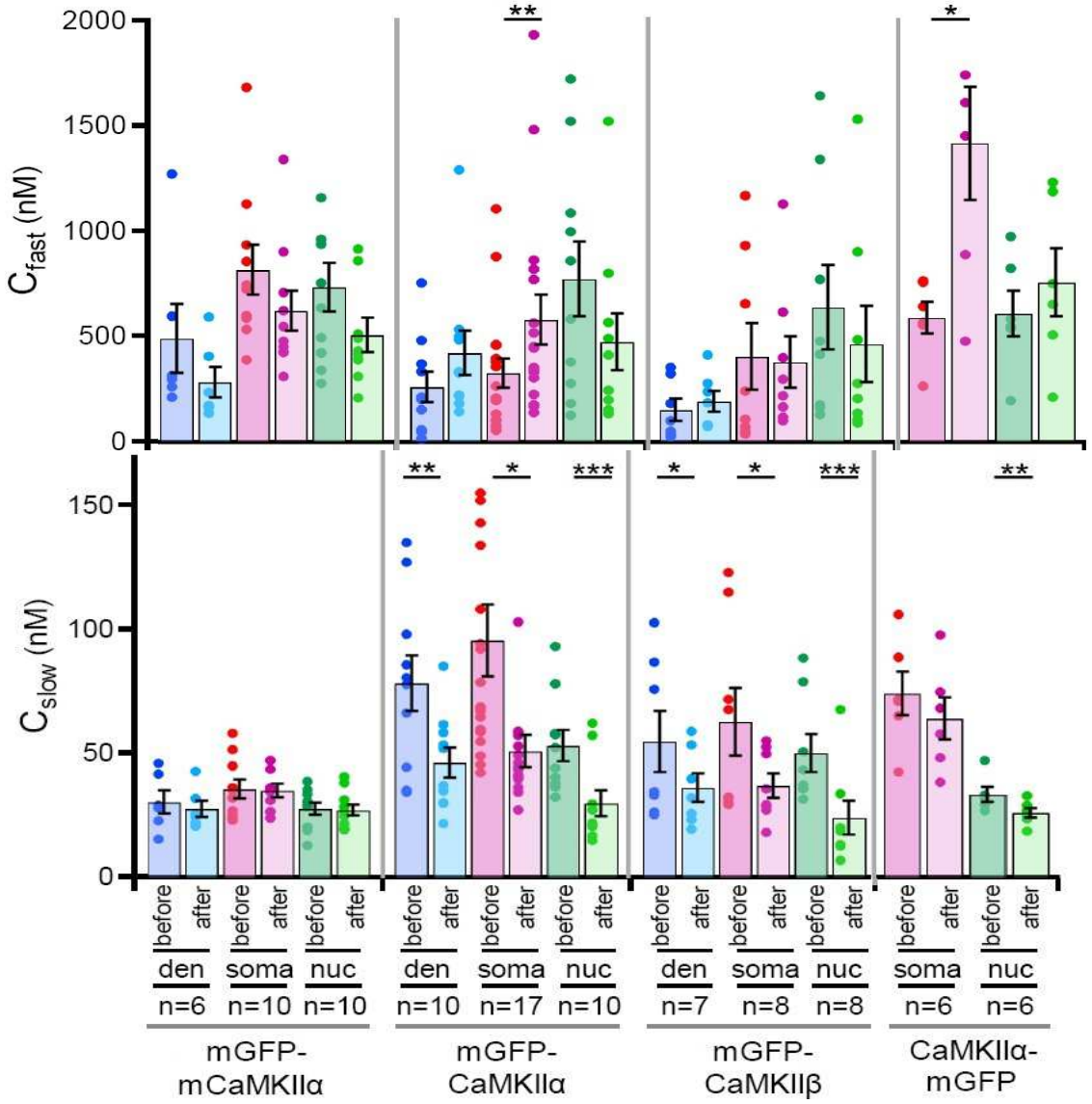

Figure 4-13. Changes in C_{fast} and C_{slow} of FCS parameters of mGFP-mCaMKIIα, mGFP-CaMKIIα, mGFP-CaMKIIβ and CaMKIIα-mGFP before and after the Glu/Gly stimulation in the soma, nucleus (nuc) and dendrite (den) of hippocampal neurons.

C_{fast} and C_{slow} before and after stimulation are shown. The data of after stimulation were taken between 15 to 25 min after the stimulation. C_{fast} of CaMKIIα increased in the soma, and C_{slow} for CaMKIIα and β decreased in the soma and nucleus. Each result of a single cell is indicated by a dot, and averages and S.E.Ms are indicated by bars and error bars, respectively (*p < 0.05, **p < 0.01, ***p < 0.001, Student's paired t-test) (Heidarinejad et al., in press).

To address what is the mechanism for such a change in the diffusion patterns of CaMKII proteins, I looked at the brightness of the faster component before and after stimulation. The brightness of mCaMKIIα did not show noticeable change after

stimulation, but the brightness of faster component of CaMKIIα and CaMKIIβ decreased drastically. ε_{fast} of CaMKIIα and CaMKIIβ decreased 3.1 and 1.6 times in the soma (Fig. 4-14). These results indicate structural changes of CaMKIIα and CaMKIIβ holoenzyme, supporting the idea that the holoenzyme of CaMKIIα and CaMKIIβ in the soma were broken down into smaller pieces upon neuron activation.

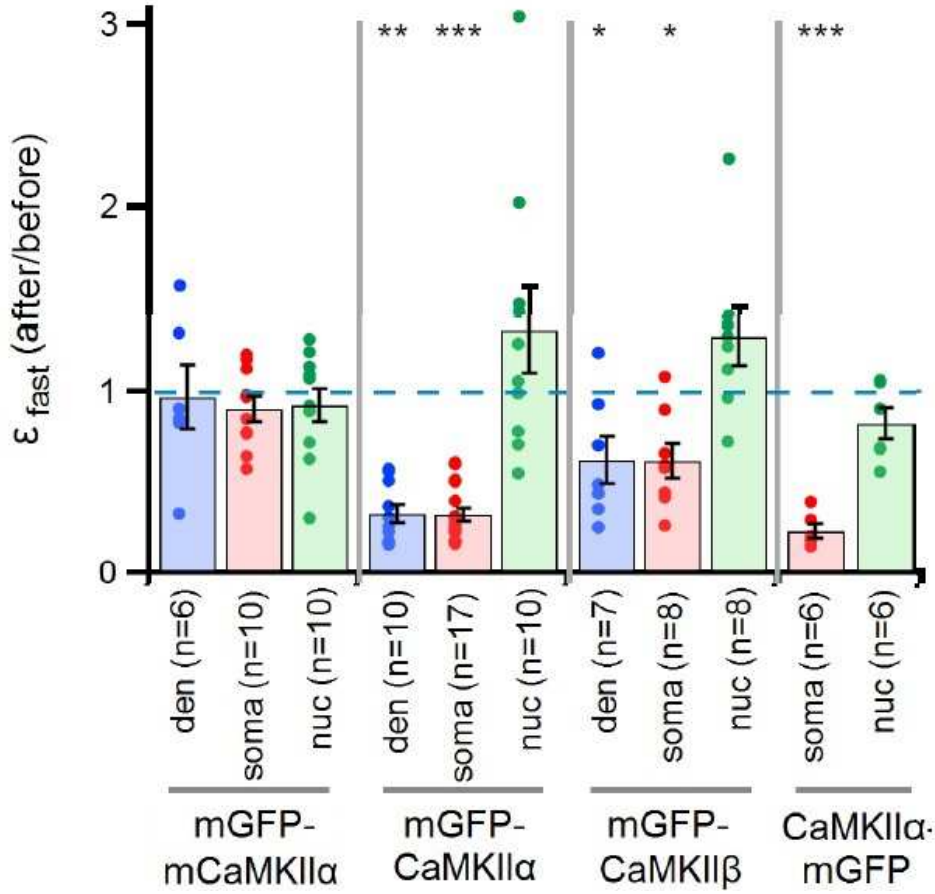

Figure 4-14. Changes in ε_{fast} of mGFP-mCaMKIIα, mGFP-CaMKIIα, mGFP-CaMKIIβ and CaMKIIα-mGFP before and after the Glu/Gly stimulation in the soma, nucleus (nuc) and dendrite (den) of hippocampal neurons.

Ratio of ε_{fast} after and before stimulation is shown. The data of after stimulation were taken between 15 to 25 min after the stimulation. ε_{fast} of CaMKIIα and β in the soma dropped drastically by the stimulation, which became closer to the ε_{fast} values of CaM and mCaMKIIα and those of CaMKIIα and β in the nucleus. Each dot indicates average values of records from each cell. (*p < 0.05, **p < 0.01, ***p < 0.001, Student's paired t-test) (Heidarinejad et al., in press).

To check the long-term effects of stimulation on CaMKIIα, I performed series of FCS records with normal, I205K mutant of CaMKIIα and mCaMKIIα. I205K was chosen because of the lack of speckle formation. Transfected neurons were stimulated with Glu/Gly, and recording solution was changed to normal HBS 20 min after the onset of Glu/Gly application. Records were continued for 40 min after the washout the stimuli. As Fig. 4-15 shows, proteins represented left-shift of ACF during 10 to 20 min and the diffusion profile did not recover even 40 min after washing the stimuli. It shows that the changes in the protein structure were irreversible.

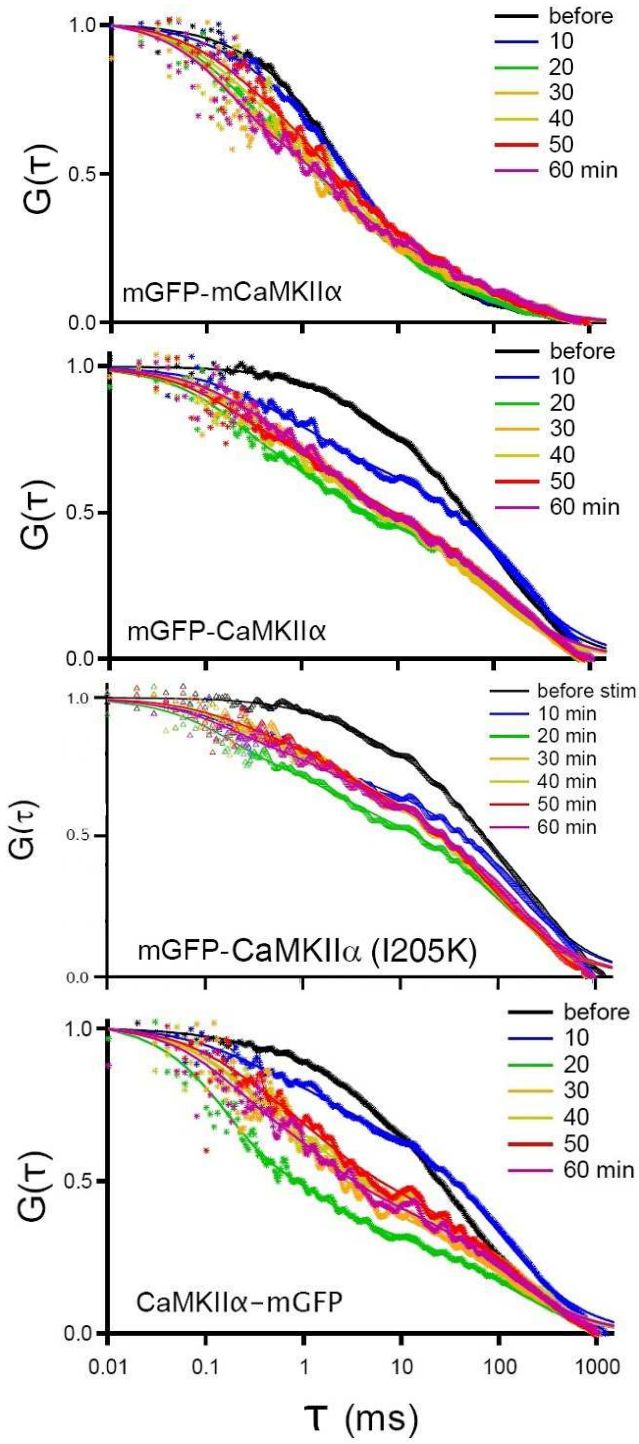

Figure 4-15. Time course of ACFs of mCaMKIIα, CaMKIIα and CaMKIIα mutant (I205K) in somata of neurons upon stimulation with 100 μM Glu/10 μM Gly.
Transfected neurons with mGFP-mCaMKIIα (n=7), mGFP-CaMKIIα (n=7), CaMKIIα-mGFP (n=6) and mGFP-CaMKIIα mutant (I205K) (n=6) cells were stimulated with 100 μM Glu/10 μM Gly for 20 min and then the recording solution was replaced by normal HBS via 5 min circulation. The FCS records continued for 40 min after the washout. The left shift of ACF started after 10 min and did not recovered even after the washout. Dots indicate ACFs at time points, and lines show fitting results. ACFs of records in each time point were averaged (Heidarinejad et al., in press).

D_{fast} of both wild type and mutant CaMKIIα was increased to the same level of D_{fast} of mGFP and CaM, while D_{slow} did not show any change (Fig. 4-16). The increases in D_{fast} of CaMKIIα and CaMKIIα (I205K) suggest dissociation of holoenzyme or digestion of the proteins 10-20 min after the stimulation. The similarity of the results of normal and mutant CaMKIIα indicates that the dissociation or digestion process is independent of the cluster formation.

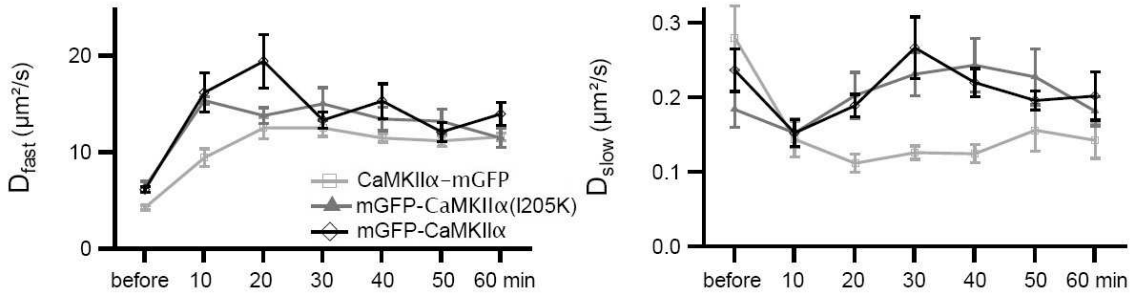

Figure 4-16. Changes in D_{fast} and D_{slow} before, after stimulation and after washout of stimuli in somata of hippocampal neurons.

D_{fast} and D_{slow} of mGFP-CaMKIIα (n=7), CaMKIIα-mGFP (n=6) and mGFP-CaMKIIα (I205K) (n=6) proteins before, after stimulations and after washout of stimuli are shown. The data were collected every 10 min and the recording solution was washed out 20 min after the onset of stimulation by 5 min circulation of normal HBS. Averages and S.E.Ms are indicated by bars and error bars, respectively (Heidarinejad et al., in press).

$\varepsilon_{\text{fast}}$ were decreased without any tendency of recovery even after washout of stimuli (Fig. 4-17). The decreases of $\varepsilon_{\text{fast}}$ suggest digestion or dissociation of proteins 10-20 min after stimulation, and the increases of $\Phi_{\text{fast}}/\ \Phi_{\text{total}}$ suggests that dissociated or degraded forms of CaMKIIα were liberated from the particles included in the slower diffusing fraction by the stimulation.

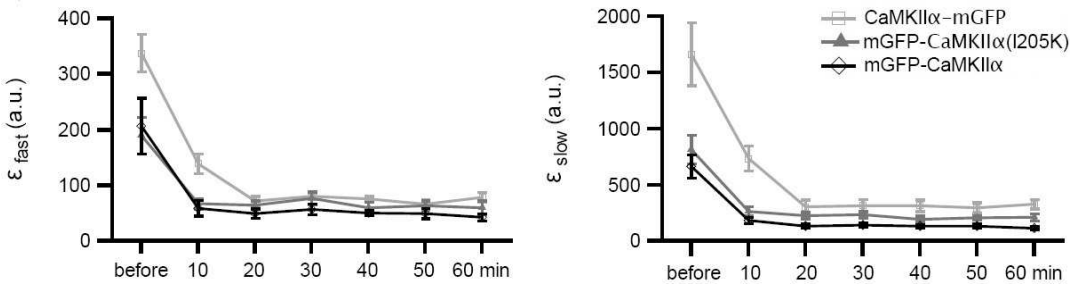

Figure 4-17. Changes in ε_{fast}, ε_{slow} before, after stimulation and after washout of stimuli in somata of hippocampal neurons.

ε_{fast}, ε_{slow} of mGFP-CaMKIIα (n=7), CaMKIIα-mGFP (n=6) and mGFP-CaMKIIα (I205K) (n=6) proteins before, after stimulations and after washout of stimuli is shown. The data was collected every 10 min and the recording solution was washed out 20 min after the onset of stimulation by 5 min circulation of fresh HBS. Averages and S.E.Ms are indicated by bars and error bars, respectively (Heidarinejad et al., in press).

All the quantitative analyses support the possibility of irreversible liberation of subunits or digestion of the CaMKIIα protein and its I205K mutant.

5 Discussion

I reported here diffusion patterns of mGFP, CaM, CaMKIIα and CaMKIIβ in HEK293 cells and hippocampal neurons. The CaM and CaMKII family proteins are regulating important signaling pathways in the neuron where knowledge about their spatial dynamics, translocations, interactions and structures are necessary to understand their function. Using advantages of the two-photon fluorescence correlation spectroscopy with low level background noise and low-level expression of proteins using plasmids with truncated promoters, I recorded from different compartments of the neurons. I also introduced a new approach for multi-point FCS recording which is beneficial for collecting data in neurons. In this study, diffusion coefficients of the mGFP, CaM, CaMKIIα and CaMKIIβ proteins were revealed in HEK293 cells, which were in accordance with previous reports (Johnson and Harms, 2016; Khan et al., 2012; Kim et al., 2004; Luby-Phelps et al., 1985; Sanabria et al., 2008) and in neurons for the first time. Molecular masses of mGFP, CaMKIIα and β holoenzyme are 27 and 559 and 633 kDa, respectively (Kanaseki et al., 1991; Kolb et al., 1998). According to Stokes-Einstein's law (Eq. 8), diffusion coefficient (D_{fast}) for CaMKII should be 2.7 times smaller than mGFP, which was 2.5 in this study.

5.1 Diffusion of CaM in HEK293 cells and in neurons

The results in this study suggest that the function of CaM in neurons is different from HEK293 cells in terms of its slower diffusion due to its possible interactions with substrate proteins (Sanabria et al., 2007; Thorogate and Török, 2004; Zhou et al., 2008). It was previously reported that the diffusion coefficient of CaM in HEK293 cells reduced from 10 to 7 μm²/s when it was co-expressed with CaMKIIα (Sanabria et al., 2008). In neurons, amount of available CaM is regulated by binding with

proteins such as neurogranin and neuromodulin (Xia and Storm, 2005). Existence of these binding partners may explain the difference between the diffusion coefficient rate of CaM in HEK293 cells and neurons.

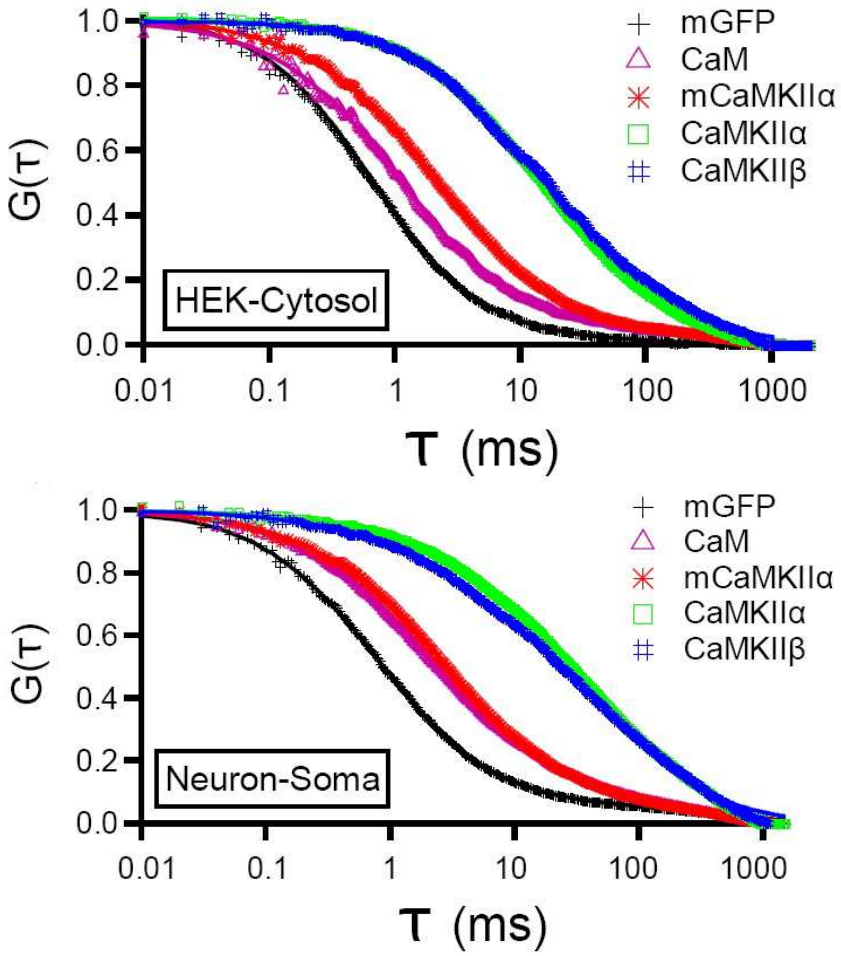

Figure 5-1. Comparison of ACFs in cytosol of HEK293 cells and in soma of neurons.
ACFs of mGFP, mGFP-CaM, mGFP-mCaMKIIα, mGFP-CaMKIIα and mGFP-CaMKIIβ in the cytosol of HEK293 cells and soma of neurons are displayed. The displayed graphs are the same as graphs in Figs. 3-11 and 4-4.

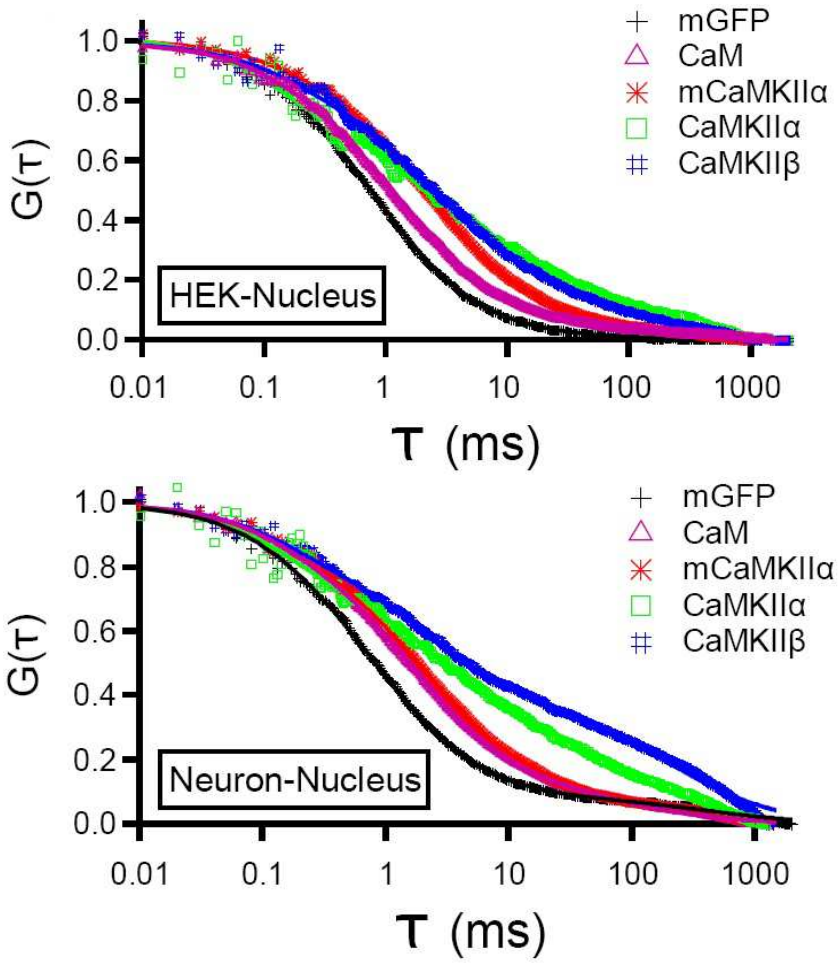

Figure 5-2. Comparison of ACFs in nucleus of HEK293 cells and neurons.
ACFs of mGFP, mGFP-CaM, mGFP-mCaMKIIα, mGFP-CaMKIIα and mGFP-CaMKIIβ in the nucleus of HEK293 cells and neurons were displayed. The displayed graphs are the same as graphs in Figs. 3-11 and 4-4.

Figs. 5-1 and 5-2 showed that in HEK293 cells the diffusion of CaM protein was slower than mGFP but faster than mCaMKIIα. In neurons, diffusion profile of CaM was much similar to that of mCaMKIIα. It means that diffusion coefficient of CaM was reduced due to the intracellular interaction of CaM in neurons.

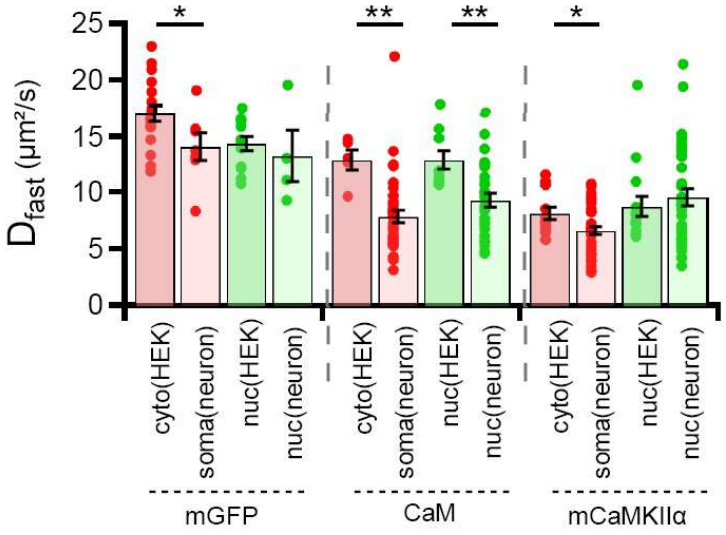

Figure 5-3. Comparison of the diffusion coefficients between HEK293 cells and neurons.

Comparison of D_{fast} of mGFP, mGFP-CaM and mGFP-mCaMKIIα in the cytosol (cyto) and nucleus (nuc) of HEK293 cells to those in the soma and nucleus of the hippocampal neurons. Data in Figs. 3-12 and 4-5 are used. In this figure each result of a single cell is indicated by a dot, and averages and S.E.Ms are indicated by bars and error bars, respectively (*p < 0.05, **p < 0.01, Student's t-test) (Heidarinejad et al., in press).

Furthermore, CaM started to diffuse faster after the Glu/Gly stimulation in the cytosol and nucleus of neurons (Figs. 3-19 and 3-21), suggesting that a population of CaM were detached from their binding partners upon activation and started to diffuse in the cytosol and nucleus, as was demonstrated (Luby-Phelps et al., 1995). During the stimulation, brightness of CaM was not changed. In resting neurons, most of the CaMs are bound with some proteins such as regulator of CaM signaling (RCS), neurogranin and neuromodulin as a member of a protein family called calpacitins. The affinity of CaM to interact with other proteins increase by influx of Ca^{2+}, it was shown that binding of above mentioned proteins decreases by Ca^{2+} (Gerendasy, 1999; Gerendasy and Sutcliffe, 1997; Xia and Storm, 2005). Therefore, these proteins serve as regulating proteins for controlling the free intracellular CaM level. In this study, the slow CaM diffusion in the neuronal compartments following Glu/Gly stimulation was as fast as

CaM in HEK293 cells. Although CaMKII proteins are abundantly expressed in neurons, CaM may bind to different partners that have higher CaM affinities at rest than in stimulated states. The two-fold larger diffusion coefficient of CaM upon stimulation than at rest suggested that the CaM binding partners had a several times larger molecular mass than CaM in the neuron. Because of the higher affinity between the calpacitins and CaM following stimulation, the relatively small molecular sizes of neurogranin (15 kDa) (Watson et al., 1992) and neuromodulin (77 kDa) (Cimler et al., 1985) do not support a simple one-to-one binding of calpacitin proteins to CaM. It is possible that unknown large proteins with a high affinity to Ca^{2+}-free CaM and/or a protein complex containing calpacitins were present.

The RCS protein is a small 9.6-kDa protein which is postulated to serve as a CaM inhibitor via sequestration at high Ca^{2+} (Rakhilin et al., 2004). Because the expression level of RCS is low in the hippocampus (Ouimet et al., 1989), small proteins with a high affinity to CaM at high Ca^{2+} concentrations could play a role similar to RCS in the hippocampus. Thus, it remains to be shown whether naked CaM proteins freely diffuse or whether CaM proteins masked by small inhibiting proteins diffuse as fast as naked forms during neuronal stimulation. In experiments with the washout of stimuli after 20 min, the recovery of CaM diffusion was clear (Figs. 3-23 and 3-24). The possibility of degradation of CaM during stimulation and alteration of the diffusion coefficient is rejected by the reversible changes in D values of CaM during stimulation and wash. Despite the report that CaM translocates to nucleus after activation of neuron via two Ca^{2+}-dependent and independent mechanisms (Deisseroth et al., 1998; Thorogate and Török, 2004), I did not see that pattern of translocation in this study and concentration of CaM did not change in the nucleus upon stimulation. A change in diffusion pattern

upon stimulation was also seen for mGFP, but it was much smaller than that of CaM. So, part of the changes in diffusion coefficient could be due to possible changes in viscosity of intracellular media.

5.2 Diffusion of CaMKII in HEK293 cells and in neurons

CaMKIIα and CaMKIIβ in the dodecameric state are big macromolecules with more than 600 kDa molecular weight. My FCS records in cytosol of HEK293 cells and neurons confirmed the multi subunit structure of these proteins by revealing diffusion coefficient and particle brightness.

Upon stimulation with Glu/Gly, CaMKIIα and CaMKIIβ showed drastic changes in their diffusion profile. mGFP tagged CaMKII proteins diffused faster comparable with cytosolic diffusion of mGFP and mGFP-CaM. A possibility that only the mGFP-tag was cleaved and CaMKIIα proteins were left intact without fluorescence is unlikely, because both N- and C-terminal tagged CaMKIIα proteins showed irreversible increase in D_{fast} by the stimulation. It has been shown that calpain, a calcium-dependent neutral cysteine protease, could cleave the CaMKIIα and β proteins in exposure to excessive NMDA (Hajimohammadreza et al., 1997). Calpain cleaves CaMKIIγ in the nucleus of cerebellar granule cells (Tremper-Wells and Vallano, 2005). High intracellular Ca^{2+} level not only triggers the activation of CaMKIIα, but also it could activate the proteolytic activity (Baudry et al., 2015; Goll et al., 2003; Kim et al., 2002; Liu et al., 2006). Calpain is also necessary for LTP formation (Baudry et al., 2013). Spectrin digestion by calpain facilitates an increase of glutamate receptors in postsynaptic densities (Baudry et al., 2015). Calpain splits the catalytic domain of CaMKII from the regulatory and association domains. So

degradation of CaMKII after autophosphorylation leaves the protein in active state independent of intracellular Ca^{2+} level (Baudry et al., 2013; Yoshimura et al., 1996). My results showed that the diffusion profile of CaMKII started to change 10 to 20 min after the onset of stimulation, which may imply digestion of the CaMKII holoenzyme by proteolytic activity or even dissociation of holoenzymes to smaller catalytic domains of the protein. This liberation of holoenzyme was irreversible, and CaMKII proteins did not show any tendency to recover even 40 min after washing out the stimuli. This interpretation was confirmed by the reduction in brightness of proteins upon stimulation. It is possible that CaMKIIα and CaMKIIβ were degraded to two major parts of catalytic domain and regulatory and association domains.

In addition to the structural change of CaMKII, it has been shown that the stimulation of neurons by Glu/Gly induces a couple of CaMKIIα translocation patterns. CaMKIIα is translocated to the post synaptic region (Otmakhov et al., 2004), where it associates with NMDA type glutamate receptors and plays an important role in the synaptic plasticity (Sanhueza and Lisman, 2013). CaMKIIα also forms aggregations in the soma and dendrites (Dosemeci et al., 2000; Grant et al., 2008; Hudmon et al., 2005, 1996; Shen and Meyer, 1999; Tao-Cheng et al., 2001) as was seen in this study. A protective role against over activation of the kinase activity of CaMKII has been proposed to this cluster formation (Dosemeci et al., 2000). These translocations may be carried out by CaMKII holoenzymes as a whole since they happens in few minutes after stimulation. Thus CaMKII holoenzyme responds to Glu/Gly stimulation by variety of responses, breaking up, translocation to postsynapse and cluster formation in the cytosol, leading to different consequences.

I examined the four different types of CaMKIIα mutants with the same stimulation protocol of wild type CaMKIIα. Although, in my experiments there was no clustering pattern for I205K and A302R mutants, the changes in diffusion pattern was almost the same among the mutants and normal protein. It showed that the structure of CaMKII protein changed regardless of its enzymatic role.

5.3 CaMKII in the nucleus

There have been a few researches on the existence and function of CaMKIIα and CaMKIIβ diffusion in the nucleus (Jing et al., 2015; Kutcher et al., 2003; Shen and Meyer, 1998). The idea that CaMKIIα and CaMKIIβ do not localize in the nucleus has been supported by the nuclear exclusion pattern of CaMKIIα and CaMKIIβ in immunohistochemistry and the expression pattern of fluorescent protein tagged CaMKIIα and CaMKIIβ (Kutcher et al., 2003; Srinivasan et al., 1994), which was also seen in this study.

According to my results, the difference between diffusion profile of CaMKIIα and CaMKIIβ in the cytosol and nucleus showed a possibility of existence of those proteins in monomeric form or small fragments in the nucleus of HEK293 cells and neurons. D_{fast} of CaMKIIα and CaMKIIβ in the nucleus was as large as that of mCaMKIIα in the nucleus and cytosol, and ε_{fast} of CaMKIIα and CaMKIIβ in the nucleus was about seven times lower than those in the cytosol in HEK293 cells. It is possible that not intact but degraded CaMKII proteins were detected due to the high sensitivity of the FCS method (Fig. 5-4).

The consensus view is that intracellular CaMKIIα is existing in its dodecameric form (Kolb et al., 1998; Lantsman and Tombes, 2005; Srinivasan et al., 1994). My results are showing possible existence of small fragments of CaMKIIα and CaMKIIβ in

the nucleus which are diffusing through nuclear pores according to their size. Since the CaMKI and CaMKIV, which always exist as monomer (Heist and Schulman, 1998), or CaMKIIγ, which contains NLS, translocate postsynaptic information to the nucleus, where they phosphorylate transcription factors and DNA binding proteins upon activation by Ca^{2+}/CaM (Heist and Schulman, 1998; Ma et al., 2015). So there is a possibility that small fragments of CaMKIIα and CaMKIIβ were involved in the nuclear functions. Therefore, the exact role and structure of CaMKIIα and CaMKIIβ in the nucleus is still open question.

5.4 CaMKII and the gene expression

CaMKII has more than 30 isoforms (Hudmon and Schulman, 2002a; Lantsman and Tombes, 2005; Takeuchi et al., 2002). CaMKII holoenzyme with hetero or homo-oligomeric structure is formed by polymerization of 6-12 subunits (Hoelz et al., 2003; Kanaseki et al., 1991; Kolodziej et al., 2000; Lantsman and Tombes, 2005). CaMKIIα, β, γ and δ are expressed in brain (Hudmon and Schulman, 2002b), and have different functions (Shen et al., 1998; Sun et al., 1994; Tombes et al., 2003). CaMKIIα and β have faster catalytic activity than γ (Gaertner et al., 2004). In the pathway from the plasma membrane to the nucleus, especially from the synapse to nucleus, still the role of CaMKII family proteins is not totally understood. However, it is known that CaMKII proteins are involved in gene expressions (Takeuchi et al., 2002). In case CaMKIIα and CaMKIIβ in the holoenzyme structure do not enter the nucleus, it is supposed that γ with NLS sequence is phosphorylated by CaMKIIα and β (Ma et al., 2015, 2014) and transduces the signals to the nucleus.

Histone deacetylase family proteins (HDACs) are target of CaMKII. IIa types of HDACs (HDAC4,5,7 and 9) play an important role in regulation of neuronal apoptosis

(Wei et al., 2015). In strongly stimulated neurons, HDACs are phosphorylated and exported from the nucleus, which affects the gene expression by leaving histone acetyltransferases in activated state in the nucleus, while they promote gene activation by acetylation of histones (Jing et al., 2015) or by dissociation from transcription factors such as myocyte enhancer factor-2 (Chawla et al., 2003). CaMKII has been implicated in this phosphorylation of HDACs in the nucleus (Chawla et al., 2003; McKinsey et al., 2001; Renthal et al., 2007). Also it has been reported that the nuclear export of HDAC5 is mediated by CaMKIIα, while the detailed mechanism is not known (Wei et al., 2015). My result that possibly small fragments of CaMKIIα exists in the nucleus could be an explanation to the phosphorylation of HDAC5 in the nucleus, which controls the gene expression and cell apoptosis.

5.5 The slower diffusing fraction

Consistent with the previously reported values, diffusion coefficient of the slower component of proteins was almost 10-20 times slower than the faster component (Johnson and Harms, 2016; Luby-Phelps et al., 1985). The reason for the existence of slower component could be aggregation of proteins, intracellular crowding effect or specific and non-specific interactions with other cellular proteins (Johnson and Harms, 2016).

At rest, almost half of CaMKIIα and CaMKIIβ subunits were included in the faster diffusing component in the cytosol (Φ_{fast}/Φ_{total} = 52.0 ± 2.0 and 58.7 ± 2.4% in the soma and 47.2 ± 2.2 and 47.6 ± 2.7% in the dendrite). D_{slow} of CaMKIIα in the cytosol was about 10-20 times smaller than D_{fast}, which is in accordance with previous reports (Johnson and Harms, 2016; Luby-Phelps et al., 1985). Ratio of ε_{slow} to ε_{fast} in the soma

of neurons was 5.4 ± 0.3 (n = 41) at rest, suggesting that presumably holoenzymes are forming aggregated superstructures (Dosemeci et al., 2000).

5.6 CaMKII in the dendrite

According to my findings, CaMKIIα and CaMKIIβ in the dendrite behaved almost the same as they did in the soma. The pattern of liberation after the stimulation was similar between soma and dendrite. D_{fast} and ε_{fast} were very close in these compartments. Φ_{fast}/Φ_{total} of CaMKIIα and CaMKIIβ was smaller in the dendrite than in the soma, and Φ_{total} as an index for total number of subunits was 2.9 and 4 times higher in the soma than dendrite for CaMKIIα and CaMKIIβ, respectively, indicating lower number of CaMKII holoenzymes in dendrite, while Φ_{total} was in the same order for mGFP and CaM in the soma and dendrite. So mGFP and CaM are diffusing in soma and dendrite evenly, but diffusion of bigger proteins such as CaMKIIα and CaMKIIβ might have some regulations to enter to the dendrite. In addition, my results showed two-fold difference of Φ_{total} for mCaMKIIα in soma and dendrite which could be a sign for different translocation mechanisms for dendritic diffusion.

5.7 Multi-point fluorescence correlation spectroscopy

In functionally compartmentalized cells such as neurons, it is fundamentally important to read out information in each functional compartment. I introduced the new method for multi-point FCS recording. Methods such as using parallel laser beams (Dittrich and Schwille, 2002; Ohsugi and Kinjo, 2009) or recruiting spinning disks (Needleman et al., 2009; Sisan et al., 2006) are technically difficult ways to adjust. The other methods such as using line scanning or loop scanning (Baum et al., 2014; Petrásek

and Schwille, 2008; Ries et al., 2009) are suffered from temporal resolution. Using spatial light modulators is also challenging because of possibility of cross-talk among the light beams (Kloster-Landsberg et al., 2012).

Reducing the number of recorded points and using two AODs instead of galvano mirrors increased the temporal resolution and avoided recording from unnecessary points. The high speed random access scanning setup was able to jump between the points in microsecond order. So, I recorded from three points with 15 kHz recording rate which was satisfying for study of intracellular diffusion of proteins.

My results showed that my method for recording from different points in the cell could be trusted in the same way as single point recordings. In neurons, I was able to record from soma, nucleus and dendrite simultaneously which has beneficial to save time while monitoring the changes of protein behavior at different compartments of the cell. How molecular dynamics are regulated in cellular compartments, such as spines, dendritic branches or axon terminals, is an important question in neuroscience, to which three-point FCS would effectively give answers.

5.8 Conclusion

Spatial distribution and function of the proteins are two important aspects for disclosing mystery of molecular signaling in the cells. CaM and CaMKII proteins have unique roles in encoding the extracellular signals via Ca^{2+} influx especially in the neuron. Phenomena such as LTP or LTD are influenced by activation of these two proteins as well as their distribution. I recruited two-photon fluorescence correlation spectroscopy to determine a view for the diffusion of CaM and CaMKII proteins in HEK293 cells and in hippocampal neurons. I detected existence of small fragments of

CaMKIIα and CaMKIIβ in the nucleus, which opens up new questions about the structure and role of these small fragments.

Also, I found changes in diffusion pattern of CaMKII proteins in persistent glutamatergic stimulations. My results showed that 10-20 min after stimulation, a faster diffusing CaMKII protein population was detected in the soma and dendrite which were 3.1 and 1.6 times less bright than those of CaMKIIα and CaMKIIβ at rest, respectively. It is a sign of probable digestion of CaMKII proteins by proteolytic activity via proteins such as calpain or any other liberation of subunits from holoenzyme which demands further investigations.

How CaMKIIα regulates the molecular pathways in stimulations is still unknown. Here I focused on the diffusion of the CaMKIIα, CaMKIIβ and CaM proteins. CaM as a first main receiver for extracellular stimulation diffused faster in all compartments of the neuron possibly because of dissociation from its substrates. Despite the previous report (Grant et al., 2008), in my results no aggregation or cluster formation was seen in the transfected neurons with mGFP-CaM. Intriguing properties of the CaM and CaMKII proteins in diffusion and assembly were revealed in this study. CaMKIIα digestion or dissociation changed the diffusion profile of CaMKII proteins in irreversible way. It was different from changes in the behavior of CaM. Changes in CaM diffusion was response to stimulation and possibly due to changes in its molecular interactions, while for CaMKII, the structure of protein was changed in response to the stimulation. These changes raise up new questions about the consequences of the function of CaMKII proteins in the non-active and active statues of neurons.

Acknowledgements

I would like to express my deepest gratitude and appreciation to my advisor Professor Takafumi Inoue for his support and guidance throughout the research.

I would also like to extend my appreciation to my committee members, Professor Toshio Ohshima and Professor Toru Asahi. And I deeply thank Professor Masataka Kinjo and Dr. Hideki Nakamura for valuable advices during my research, Dr. Paul De Koninck and Dr. Takeo Saneyoshi for the gifts of plasmids and all the members of Inoue laboratory for fruitful discussions and technical assistance.

Special thanks go to Nasrin Shafeghat, my wife and colleague, for her stop less support in all moments of this research and my family for giving encouragement to follow my dreams.

This work was done by a support of Yoshida Scholarship Foundation, and I was honored to receive YKK Leader 21 Scholarship during my research period.

Table of figures

References

Ashpole, N.M., Hudmon, A., 2011. Excitotoxic neuroprotection and vulnerability with CaMKII inhibition. Mol. Cell. Neurosci. 46, 720–730. doi:10.1016/j.mcn.2011.02.003

Axelrod, D., Koppel, D.E., Schlessinger, J., Elson, E., Webb, W.W., 1976. Mobility measurement by analysis of fluorescence photobleaching recovery kinetics. Biophys. J. 16, 1055–1069. doi:10.1016/S0006-3495(76)85755-4

Bagshaw, C.R., Cherny, D., 2006. Blinking fluorophores: what do they tell us about protein dynamics? Biochem. Soc. Trans. 34, 979–982. doi:10.1042/BST0340979

Banks, D.S., Fradin, C., 2005. Anomalous diffusion of proteins due to molecular crowding. Biophys. J. 89, 2960–2971. doi:10.1529/biophysj.104.051078

Bannai, H., Lévi, S., Schweizer, C., Inoue, T., Launey, T., Racine, V., Sibarita, J.-B., Mikoshiba, K., Triller, A., 2009. Activity-dependent tuning of inhibitory neurotransmission based on $GABA_AR$ diffusion dynamics. Neuron 62, 670–682. doi:10.1016/j.neuron.2009.04.023

Barcomb, K., Goodell, D.J., Arnold, D.B., Bayer, K.U., 2015. Live imaging of endogenous Ca^{2+}/calmodulin-dependent protein kinase II in neurons reveals that ischemia-related aggregation does not require kinase activity. J. Neurochem. 135, 666–673. doi:10.1111/jnc.13263

Baudry, M., Chou, M.M., Bi, X., 2013. Targeting calpain in synaptic plasticity. Expert Opin. Ther. Targets 17, 579–592. doi:10.1517/14728222.2013.766169

Baudry, M., Zhu, G., Liu, Y., Wang, Y., Briz, V., Bi, X., 2015. Multiple cellular cascades participate in long-term potentiation and in hippocampus-dependent learning. Brain Res. 1621, 73–81. doi:10.1016/j.brainres.2014.11.033

Baum, M., Erdel, F., Wachsmuth, M., Rippe, K., 2014. Retrieving the intracellular topology from multi-scale protein mobility mapping in living cells. Nat. Commun. 5, 4494. doi:10.1038/ncomms5494

Bayer, K.U., De Koninck, P., Leonard, A.S., Hell, J.W., Schulman, H., 2001. Interaction with the NMDA receptor locks CaMKII in an active conformation. Nature 411, 801–805. doi:10.1038/35081080

Bayer, K.U., Schulman, H., 2001. Regulation of Signal Transduction by Protein Targeting: The Case for CaMKII. Biochem. Biophys. Res. Commun. 289, 917–923. doi:10.1006/bbrc.2001.6063

Becker, 2013. TCSPC Handbook. 5th ed. Berlin. Becker and Hickl GmBH.

Berland, K.M., So, P.T., Gratton, E., 1995. Two-photon fluorescence correlation spectroscopy: method and application to the intracellular environment. Biophys. J. 68, 694–701.

Brinkmeier, M., Dörre, K., Stephan, J., Eigen, M., 1999. Two-beam cross-correlation: a method to characterize transport phenomena in micrometer-sized structures. Anal. Chem. 71, 609–616. doi:10.1021/ac980820i

Brock, R., Vàmosi, G., Vereb, G., Jovin, T.M., 1999. Rapid characterization of green fluorescent protein fusion proteins on the molecular and cellular level by fluorescence correlation microscopy. Proc. Natl. Acad. Sci. U. S. A. 96, 10123–10128.

Brocke, L., Chiang, L.W., Wagner, P.D., Schulman, H., 1999. Functional implications of the subunit composition of neuronal CaM kinase II. J. Biol. Chem. 274, 22713–22722.

Brown, R, 1828. . Ann. d. Phys. u. Chern 294–313.

Carisey, A., Stroud, M., Tsang, R., Ballestrem, C., 2011. Fluorescence recovery after photobleaching. Methods Mol. Biol. Clifton NJ 769, 387–402. doi:10.1007/978-1-61779-207-6_26

Chawla, S., Vanhoutte, P., Arnold, F.J.L., Huang, C.L.-H., Bading, H., 2003. Neuronal activity-dependent nucleocytoplasmic shuttling of HDAC4 and HDAC5. J. Neurochem. 85, 151–159.

Chen, H., Farkas, E.R., Webb, W.W., 2008. Chapter 1: In vivo applications of fluorescence correlation spectroscopy. Methods Cell Biol. 89, 3–35. doi:10.1016/S0091-679X(08)00601-8

Chen, Y., Müller, J.D., Ruan, Q., Gratton, E., 2002. Molecular brightness characterization of EGFP in vivo by fluorescence fluctuation spectroscopy. Biophys. J. 82, 133–144. doi:10.1016/S0006-3495(02)75380-0

Chen, Y., Müller, J.D., Tetin, S.Y., Tyner, J.D., Gratton, E., 2000. Probing ligand protein binding equilibria with fluorescence fluctuation spectroscopy. Biophys. J. 79, 1074–1084.

Chin, D., Means, A.R., 2000. Calmodulin: a prototypical calcium sensor. Trends Cell Biol. 10, 322–328.

Cimler, B.M., Andreasen, T.J., Andreasen, K.I., Storm, D.R., 1985. P-57 is a neural specific calmodulin-binding protein. J. Biol. Chem. 260, 10784–10788.

Colbran, R.J., 2004. Targeting of calcium/calmodulin-dependent protein kinase II. Biochem. J. 378, 1–16. doi:10.1042/BJ20031547

Coultrap, S.J., Vest, R.S., Ashpole, N.M., Hudmon, A., Bayer, K.U., 2011. CaMKII in cerebral ischemia. Acta Pharmacol. Sin. 32, 861–872.

doi:10.1038/aps.2011.68

De Koninck, P., Schulman, H., 1998. Sensitivity of CaM kinase II to the frequency of Ca^{2+} oscillations. Science 279, 227–230.

De Los Santos, C., Chang, C.-W., Mycek, M.-A., Cardullo, R.A., 2015. FRAP, FLIM, and FRET: Detection and analysis of cellular dynamics on a molecular scale using fluorescence microscopy. Mol. Reprod. Dev. 82, 587–604. doi:10.1002/mrd.22501

Deisseroth, K., Heist, E.K., Tsien, R.W., 1998. Translocation of calmodulin to the nucleus supports CREB phosphorylation in hippocampal neurons. Nature 392, 198–202. doi:10.1038/32448

Dickson, R.M., Cubitt, A.B., Tsien, R.Y., Moerner, W.E., 1997. On/off blinking and switching behaviour of single molecules of green fluorescent protein. Nature 388, 355–358. doi:10.1038/41048

Digman, M.A., Brown, C.M., Sengupta, P., Wiseman, P.W., Horwitz, A.R., Gratton, E., 2005. Measuring fast dynamics in solutions and cells with a laser scanning microscope. Biophys. J. 89, 1317–1327. doi:10.1529/biophysj.105.062836

Dittrich, P.S., Schwille, P., 2002. Spatial two-photon fluorescence cross-correlation spectroscopy for controlling molecular transport in microfluidic structures. Anal. Chem. 74, 4472–4479.

Dolino, D.M., Rezaei Adariani, S., Shaikh, S.A., Jayaraman, V., Sanabria, H., 2016. Conformational Selection and Submillisecond Dynamics of the Ligand-binding Domain of the N-Methyl-d-aspartate Receptor. J. Biol. Chem. 291, 16175–16185. doi:10.1074/jbc.M116.721274

Dosemeci, A., Reese, T.S., Petersen, J., Tao-Cheng, J.H., 2000. A novel particulate form of Ca^{2+}/calmodulin-dependent protein kinase II in neurons. J. Neurosci. Off. J. Soc. Neurosci. 20, 3076–3084.

Einstein, A, 1905. Investigations on the theory of the Brownian movement. Annalen der physik, 17:549.

Elowitz, M.B., Surette, M.G., Wolf, P.E., Stock, J.B., Leibler, S., 1999. Protein mobility in the cytoplasm of Escherichia coli. J. Bacteriol. 181, 197–203.

Elson, E.L., Magde, D., 1974. Fluorescence correlation spectroscopy. I. Conceptual basis and theory. Biopolymers 13, 1–27. doi:10.1002/bip.1974.360130102

Eriksen, J., Rasmussen, S.G.F., Rasmussen, T.N., Vaegter, C.B., Cha, J.H., Zou, M.-F., Newman, A.H., Gether, U., 2009. Visualization of dopamine transporter trafficking in live neurons by use of fluorescent cocaine analogs. J. Neurosci. Off. J. Soc. Neurosci. 29, 6794–6808. doi:10.1523/JNEUROSCI.4177-08.2009

Fick, A., 1855. Ueber Diffusion. Ann. Phys. 170, 59–86.

doi:10.1002/andp.18551700105

Fink, C.C., Meyer, T., 2002. Molecular mechanisms of CaMKII activation in neuronal plasticity. Curr. Opin. Neurobiol. 12, 293–299.

Fourier, J, 1822. The analytical theory of heat (Trans : Freeman A), Cambridge, UK. Cambridge University Press.

Gabelli, S.B., Yoder, J.B., Tomaselli, G.F., Amzel, L.M., 2015. Calmodulin and Ca^{2+} control of voltage gated Na^{+} channels. Channels 10, 45–54. doi:10.1080/19336950.2015.1075677

Gaertner, T.R., Kolodziej, S.J., Wang, D., Kobayashi, R., Koomen, J.M., Stoops, J.K., Waxham, M.N., 2004. Comparative analyses of the three-dimensional structures and enzymatic properties of α, β, γ and δ isoforms of Ca^{2+}-calmodulin-dependent protein kinase II. J. Biol. Chem. 279, 12484–12494. doi:10.1074/jbc.M313597200

Gaffield, M.A., Rizzoli, S.O., Betz, W.J., 2006. Mobility of synaptic vesicles in different pools in resting and stimulated frog motor nerve terminals. Neuron 51, 317–325. doi:10.1016/j.neuron.2006.06.031

Gauthier-Kemper, A., Weissmann, C., Reyher, H.-J., Brandt, R., 2012. Monitoring cytoskeletal dynamics in living neurons using fluorescence photoactivation. Methods Enzymol. 505, 3–21. doi:10.1016/B978-0-12-388448-0.00009-7

Gerendasy, D., 1999. Homeostatic tuning of Ca^{2+} signal transduction by members of the calpacitin protein family. J. Neurosci. Res. 58, 107–119. doi:10.1002/(SICI)1097-4547(19991001)58:1<107::AID-JNR11>3.0.CO;2-G

Gerendasy, D.D., Sutcliffe, J.G., 1997. RC3/neurogranin, a postsynaptic calpacitin for setting the response threshold to calcium influxes. Mol. Neurobiol. 15, 131–163.

Goll, D.E., Thompson, V.F., Li, H., Wei, W., Cong, J., 2003. The calpain system. Physiol. Rev. 83, 731–801. doi:10.1152/physrev.00029.2002

Goshima, N., Kawamura, Y., Fukumoto, A., Miura, A., Honma, R., Satoh, R., Wakamatsu, A., Yamamoto, J., Kimura, K., Nishikawa, T., Andoh, T., Iida, Y., Ishikawa, K., Ito, E., Kagawa, N., Kaminaga, C., Kanehori, K., Kawakami, B., Kenmochi, K., Kimura, R., Kobayashi, M., Kuroita, T., Kuwayama, H., Maruyama, Y., Matsuo, K., Minami, K., Mitsubori, M., Mori, M., Morishita, R., Murase, A., Nishikawa, A., Nishikawa, S., Okamoto, T., Sakagami, N., Sakamoto, Y., Sasaki, Y., Seki, T., Sono, S., Sugiyama, A., Sumiya, T., Takayama, T., Takayama, Y., Takeda, H., Togashi, T., Yahata, K., Yamada, H., Yanagisawa, Y., Endo, Y., Imamoto, F., Kisu, Y., Tanaka, S., Isogai, T., Imai, J., Watanabe, S., Nomura, N., 2008. Human protein factory for converting the transcriptome into an in vitro-expressed proteome,. Nat. Methods 5, 1011–1017.

Grant, P.A.A., Best, S.L., Sanmugalingam, N., Alessio, R., Jama, A.M., Török, K., 2008. A two-state model for Ca^{2+}/CaM-dependent protein kinase II (CaMKIIα) in response to persistent Ca^{2+} stimulation in hippocampal neurons. Cell Calcium 44, 465–478. doi:10.1016/j.ceca.2008.03.003

Griffith, L.C., Lu, C.S., Sun, X.X., 2003. CaMKII, an enzyme on the move: regulation of temporospatial localization. Mol. Interv. 3, 386–403. doi:10.1124/mi.3.7.386

Hajimohammadreza, I., Raser, K.J., Nath, R., Nadimpalli, R., Scott, M., Wang, K.K., 1997. Neuronal nitric oxide synthase and calmodulin-dependent protein kinase IIα undergo neurotoxin-induced proteolysis. J. Neurochem. 69, 1006–1013.

Haupts, U., Maiti, S., Schwille, P., Webb, W.W., 1998. Dynamics of fluorescence fluctuations in green fluorescent protein observed by fluorescence correlation spectroscopy. Proc. Natl. Acad. Sci. U. S. A. 95, 13573–13578.

Heidarinejad, M., Nakamura, H., Inoue, T., Stimulation-induced changes in diffusion and structure of calmodulin and calmodulin-dependent protein kinase II proteins in neurons. Neurosci. Res., in press. doi:10.1016/j.neures.2018.01.003

Heist, E.K., Schulman, H., 1998. The role of Ca^{2+}/calmodulin-dependent protein kinases within the nucleus. Cell Calcium 23, 103–114.

Heist, E.K., Srinivasan, M., Schulman, H., 1998. Phosphorylation at the nuclear localization signal of Ca^{2+}/calmodulin-dependent protein kinase II blocks its nuclear targeting. J. Biol. Chem. 273, 19763–19771.

Hell, J.W., 2014. CaMKII: claiming center stage in postsynaptic function and organization. Neuron 81, 249–265. doi:10.1016/j.neuron.2013.12.024

Henzler-Wildman, K.A., Lei, M., Thai, V., Kerns, S.J., Karplus, M., Kern, D., 2007. A hierarchy of timescales in protein dynamics is linked to enzyme catalysis. Nature 450, 913–916. doi:10.1038/nature06407

Hoeflich, K.P., Ikura, M., 2002. Calmodulin in action: diversity in target recognition and activation mechanisms. Cell 108, 739–742.

Hoelz, A., Nairn, A.C., Kuriyan, J., 2003. Crystal structure of a tetradecameric assembly of the association domain of Ca^{2+}/calmodulin-dependent kinase II. Mol. Cell 11, 1241–1251.

Hou, S.T., Jiang, S.X., Aylsworth, A., Ferguson, G., Slinn, J., Hu, H., Leung, T., Kappler, J., Kaibuchi, K., 2009. CaMKII phosphorylates collapsin response mediator protein 2 and modulates axonal damage during glutamate excitotoxicity. J. Neurochem. 111, 870–881. doi:10.1111/j.1471-4159.2009.06375.x

Hudmon, A., Aronowski, J., Kolb, S.J., Waxham, M.N., 1996. Inactivation and self-association of Ca^{2+}/calmodulin-dependent protein kinase II during autophosphorylation. J. Biol. Chem. 271, 8800–8808.

Hudmon, A., Lebel, E., Roy, H., Sik, A., Schulman, H., Waxham, M.N., De Koninck, P., 2005. A mechanism for Ca^{2+}/calmodulin-dependent protein kinase II clustering at synaptic and nonsynaptic sites based on self-association. J. Neurosci. Off. J. Soc. Neurosci. 25, 6971–6983. doi:10.1523/JNEUROSCI.4698-04.2005

Hudmon, A., Schulman, H., 2002a. Structure-function of the multifunctional Ca^{2+}/calmodulin-dependent protein kinase II. Biochem. J. 364, 593–611. doi:10.1042/BJ20020228

Hudmon, A., Schulman, H., 2002b. Neuronal CA^{2+}/calmodulin-dependent protein kinase II: the role of structure and autoregulation in cellular function. Annu. Rev. Biochem. 71, 473–510. doi:10.1146/annurev.biochem.71.110601.135410

Jing, Y.-P., Liu, W., Wang, J.-X., Zhao, X.-F., 2015. The steroid hormone 20-hydroxyecdysone via nongenomic pathway activates Ca^{2+}/calmodulin-dependent protein kinase II to regulate gene expression. J. Biol. Chem. 290, 8469–8481. doi:10.1074/jbc.M114.622696

Johnson, C.K., Harms, G.S., 2016. Tracking and localization of calmodulin in live cells. Biochim. Biophys. Acta 1863, 2017–2026. doi:10.1016/j.bbamcr.2016.04.021

Kanaseki, T., Ikeuchi, Y., Sugiura, H., Yamauchi, T., 1991. Structural features of Ca^{2+}/calmodulin-dependent protein kinase II revealed by electron microscopy. J. Cell Biol. 115, 1049–1060.

Kerchner, G.A., Nicoll, R.A., 2008. Silent synapses and the emergence of a postsynaptic mechanism for LTP. Nat. Rev. Neurosci. 9, 813–825. doi:10.1038/nrn2501

Khan, S., Reese, T.S., Rajpoot, N., Shabbir, A., 2012. Spatiotemporal maps of CaMKII in dendritic spines. J. Comput. Neurosci. 33, 123–139. doi:10.1007/s10827-011-0377-1

Kim, M.-J., Jo, D.-G., Hong, G.-S., Kim, B.J., Lai, M., Cho, D.-H., Kim, K.-W., Bandyopadhyay, A., Hong, Y.-M., Kim, D.H., Cho, C., Liu, J.O., Snyder, S.H., Jung, Y.-K., 2002. Calpain-dependent cleavage of cain/cabin1 activates calcineurin to mediate calcium-triggered cell death. Proc. Natl. Acad. Sci. U. S. A. 99, 9870–9875. doi:10.1073/pnas.152336999

Kim, S.A., Heinze, K.G., Schwille, P., 2007. Fluorescence correlation spectroscopy in living cells. Nat. Methods 4, 963–973. doi:10.1038/nmeth1104

Kim, S.A., Heinze, K.G., Waxham, M.N., Schwille, P., 2004. Intracellular calmodulin availability accessed with two-photon cross-correlation. Proc.

Natl. Acad. Sci. U. S. A. 101, 105–110. doi:10.1073/pnas.2436461100

Kloster-Landsberg, M., Herbomel, G., Wang, I., Derouard, J., Vourc'h, C., Usson, Y., Souchier, C., Delon, A., 2012. Cellular Response to Heat Shock Studied by Multiconfocal Fluorescence Correlation Spectroscopy. Biophys. J. 103, 1110–1119. doi:10.1016/j.bpj.2012.07.041

Köhler, R.H., Schwille, P., Webb, W.W., Hanson, M.R., 2000. Active protein transport through plastid tubules: velocity quantified by fluorescence correlation spectroscopy. J. Cell Sci. 113 (Pt 22), 3921–3930.

Kolb, S.J., Hudmon, A., Ginsberg, T.R., Waxham, M.N., 1998. Identification of domains essential for the assembly of calcium/calmodulin-dependent protein kinase II holoenzymes. J. Biol. Chem. 273, 31555–31564.

Kolodziej, S.J., Hudmon, A., Waxham, M.N., Stoops, J.K., 2000. Three-dimensional reconstructions of calcium/calmodulin-dependent (CaM) kinase IIα and truncated CaM kinase IIα reveal a unique organization for its structural core and functional domains. J. Biol. Chem. 275, 14354–14359.

Koppel, D.E., 1974. Statistical accuracy in fluorescence correlation spectroscopy. Phys. Rev. A 10, 1938–1945. doi:10.1103/PhysRevA.10.1938

Koppel, D.E., Morgan, F., Cowan, A.E., Carson, J.H., 1994. Scanning concentration correlation spectroscopy using the confocal laser microscope. Biophys. J. 66, 502–507.

Kortvely, E., Gulya, K., 2004. Calmodulin, and various ways to regulate its activity. Life Sci. 74, 1065–1070.

Koskinen, M., Bertling, E., Hotulainen, P., 2012. Methods to measure actin treadmilling rate in dendritic spines. Methods Enzymol. 505, 47–58. doi:10.1016/B978-0-12-388448-0.00011-5

Krichevsky, O., Bonnet, G., 2002. Fluorescence correlation spectroscopy: the technique and its applications. Rep. Prog. Phys. 65, 251. doi:10.1088/0034-4885/65/2/203

Kursula, P., 2014. The many structural faces of calmodulin: a multitasking molecular jackknife. Amino Acids 46, 2295–2304. doi:10.1007/s00726-014-1795-y

Kutcher, L.W., Beauman, S.R., Gruenstein, E.I., Kaetzel, M.A., Dedman, J.R., 2003. Nuclear CaMKII inhibits neuronal differentiation of PC12 cells without affecting MAPK or CREB activation. Am. J. Physiol. Cell Physiol. 284, C1334-1345. doi:10.1152/ajpcell.00510.2002

Lantsman, K., Tombes, R.M., 2005. CaMK-II oligomerization potential determined using CFP/YFP FRET. Biochim. Biophys. Acta 1746, 45–54. doi:10.1016/j.bbamcr.2005.08.005

Lee, S.-J.R., Escobedo-Lozoya, Y., Szatmari, E.M., Yasuda, R., 2009. Activation of CaMKII in single dendritic spines during long-term potentiation. Nature 458, 299–304. doi:10.1038/nature07842

Lin, Y.-C., Redmond, L., 2009. Neuronal CaMKII acts as a structural kinase. Commun. Integr. Biol. 2, 40–41.

Lisman, J., 1994. The CaM kinase II hypothesis for the storage of synaptic memory. Trends Neurosci. 17, 406–412.

Lisman, J., Schulman, H., Cline, H., 2002. The molecular basis of CaMKII function in synaptic and behavioural memory. Nat. Rev. Neurosci. 3, 175–190. doi:10.1038/nrn753

Lisman, J., Yasuda, R., Raghavachari, S., 2012. Mechanisms of CaMKII action in long-term potentiation. Nat. Rev. Neurosci. 13, 169–182. doi:10.1038/nrn3192

Liu, M.C., Akle, V., Zheng, W., Dave, J.R., Tortella, F.C., Hayes, R.L., Wang, K.K.W., 2006. Comparing calpain- and caspase-3-mediated degradation patterns in traumatic brain injury by differential proteome analysis. Biochem. J. 394, 715–725. doi:10.1042/BJ20050905

Lu, H.E., MacGillavry, H.D., Frost, N.A., Blanpied, T.A., 2014. Multiple spatial and kinetic subpopulations of CaMKII in spines and dendrites as resolved by single-molecule tracking PALM. J. Neurosci. Off. J. Soc. Neurosci. 34, 7600–7610. doi:10.1523/JNEUROSCI.4364-13.2014

Luby-Phelps, K., Hori, M., Phelps, J.M., Won, D., 1995. Ca^{2+} regulated dynamic compartmentalization of calmodulin in living smooth muscle cells. J. Biol. Chem. 270, 21532–21538.

Luby-Phelps, K., Lanni, F., Taylor, D.L., 1985. Behavior of a fluorescent analogue of calmodulin in living 3T3 cells. J. Cell Biol. 101, 1245–1256.

Ma, H., Groth, R.D., Cohen, S.M., Emery, J.F., Li, B., Hoedt, E., Zhang, G., Neubert, T.A., Tsien, R.W., 2014a. γCaMKII shuttles Ca^{2+}/CaM to the nucleus to trigger CREB phosphorylation and gene expression. Cell 159, 281–294. doi:10.1016/j.cell.2014.09.019

Ma, H., Li, B., Tsien, R.W., 2015. Distinct roles of multiple isoforms of CaMKII in signaling to the nucleus. Biochim. Biophys. Acta 1853, 1953–1957. doi:10.1016/j.bbamcr.2015.02.008

Magde, D., Elson, E., Webb, W.W., 1972. Thermodynamic Fluctuations in a Reacting System-Measurement by Fluorescence Correlation Spectroscopy. Phys. Rev. Lett. 29, 705–708. doi:10.1103/PhysRevLett.29.705

Maiti, S., Haupts, U., Webb, W.W., 1997. Fluorescence correlation spectroscopy: diagnostics for sparse molecules. Proc. Natl. Acad. Sci. U. S. A. 94, 11753–

11757.

McKinsey, T.A., Zhang, C.L., Olson, E.N., 2001. Identification of a signal-responsive nuclear export sequence in class II histone deacetylases. Mol. Cell. Biol. 21, 6312–6321.

Michelman-Ribeiro, A., Mazza, D., Rosales, T., Stasevich, T.J., Boukari, H., Rishi, V., Vinson, C., Knutson, J.R., McNally, J.G., 2009. Direct Measurement of Association and Dissociation Rates of DNA Binding in Live Cells by Fluorescence Correlation Spectroscopy. Biophys. J. 97, 337–346. doi:10.1016/j.bpj.2009.04.027

Mikuni, S., Tamura, M., Kinjo, M., 2007. Analysis of intranuclear binding process of glucocorticoid receptor using fluorescence correlation spectroscopy. FEBS Lett. 581, 389–393. doi:10.1016/j.febslet.2006.12.038

Misteli, T., 2001. Protein dynamics: implications for nuclear architecture and gene expression. Science 291, 843–847.

Mueller, F., Morisaki, T., Mazza, D., McNally, J.G., 2012. Minimizing the impact of photoswitching of fluorescent proteins on FRAP analysis. Biophys. J. 102, 1656–1665. doi:10.1016/j.bpj.2012.02.029

Müller, J.D., Chen, Y., Gratton, E., 2003. Fluorescence correlation spectroscopy. Methods Enzymol. 361, 69–92.

Mullineaux, C.W., Kirchhoff, H., 2007. Using fluorescence recovery after photobleaching to measure lipid diffusion in membranes. Methods Mol. Biol. Clifton NJ 400, 267–275. doi:10.1007/978-1-59745-519-0_18

Mullineaux, C.W., Nenninger, A., Ray, N., Robinson, C., 2006. Diffusion of Green Fluorescent Protein in Three Cell Environments in Escherichia Coli. J. Bacteriol. 188, 3442–3448. doi:10.1128/JB.188.10.3442-3448.2006

Myers, J.B., Zaegel, V., Coultrap, S.J., Miller, A.P., Bayer, K.U., Reichow, S.L., 2017. The CaMKII holoenzyme structure in activation-competent conformations. Nat. Commun. 8, 15742. https://doi.org/10.1038/ncomms15742

Needleman, D.J., Xu, Y., Mitchison, T.J., 2009. Pin-Hole Array Correlation Imaging: Highly Parallel Fluorescence Correlation Spectroscopy. Biophys. J. 96, 5050–5059. doi:10.1016/j.bpj.2009.03.023

Nguyen, T.A., Sarkar, P., Veetil, J.V., Davis, K.A., Puhl, H.L., Vogel, S.S., 2015. Covert Changes in CaMKII Holoenzyme Structure Identified for Activation and Subsequent Interactions. Biophys. J. 108, 2158–2170. doi:10.1016/j.bpj.2015.03.028

Nomura, Y., Tanaka, H., Poellinger, L., Higashino, F., Kinjo, M., 2001. Monitoring of in vitro and in vivo translation of green fluorescent protein and its fusion

proteins by fluorescence correlation spectroscopy. Cytometry 44, 1–6.

Ohsugi, Y., Kinjo, M., 2009. Multipoint fluorescence correlation spectroscopy with total internal reflection fluorescence microscope. J. Biomed. Opt. 14, 014030. doi:10.1117/1.3080723

Olofsson, M.H., Havelka, A.M., Brnjic, S., Shoshan, M.C., Linder, S., 2008. Charting calcium-regulated apoptosis pathways using chemical biology: role of calmodulin kinase II. BMC Chem. Biol. 8, 2. doi:10.1186/1472-6769-8-2

Orenbuch, A., Shalev, L., Marra, V., Sinai, I., Lavy, Y., Kahn, J., Burden, J.J., Staras, K., Gitler, D., 2012. Synapsin selectively controls the mobility of resting pool vesicles at hippocampal terminals. J. Neurosci. Off. J. Soc. Neurosci. 32, 3969–3980. doi:10.1523/JNEUROSCI.5058-11.2012

Otmakhov, N., Tao-Cheng, J.-H., Carpenter, S., Asrican, B., Dosemeci, A., Reese, T.S., Lisman, J., 2004. Persistent accumulation of calcium/calmodulin-dependent protein kinase II in dendritic spines after induction of NMDA receptor-dependent chemical long-term potentiation. J. Neurosci. Off. J. Soc. Neurosci. 24, 9324–9331. doi:10.1523/JNEUROSCI.2350-04.2004

Ouimet, C.C., Hemmings, H.C., Greengard, P., 1989. ARPP-21, a cyclic AMP-regulated phosphoprotein enriched in dopamine- innervated brain regions. II. Immunocytochemical localization in rat brain. J. Neurosci. 9, 865–875.

Peters, R., Peters, J., Tews, K.H., Bähr, W., 1974. A microfluorimetric study of translational diffusion in erythrocyte membranes. Biochim. Biophys. Acta 367, 282–294.

Petersen, N.O., 1986. Scanning fluorescence correlation spectroscopy. I. Theory and simulation of aggregation measurements. Biophys. J. 49, 809–815.

Petrásek, Z., Schwille, P., 2008. Precise measurement of diffusion coefficients using scanning fluorescence correlation spectroscopy. Biophys. J. 94, 1437–1448. doi:10.1529/biophysj.107.108811

Philip Nelson, 2003. Biological Physics: Energy, Information, Life. W.H. Freeman, New York.

Politz, J.C., Browne, E.S., Wolf, D.E., Pederson, T., 1998. Intranuclear diffusion and hybridization state of oligonucleotides measured by fluorescence correlation spectroscopy in living cells. Proc. Natl. Acad. Sci. U. S. A. 95, 6043–6048.

Price, E.S., Aleksiejew, M., Johnson, C.K., 2011. FRET-FCS detection of intralobe dynamics in calmodulin. J. Phys. Chem. B 115, 9320–9326. doi:10.1021/jp203743m

Price, E.S., DeVore, M.S., Johnson, C.K., 2010. Detecting intramolecular dynamics and multiple Förster resonance energy transfer states by fluorescence correlation spectroscopy. J. Phys. Chem. B 114, 5895–5902. doi:10.1021/jp912125z

Rakhilin, S.V., Olson, P.A., Nishi, A., Starkova, N.N., Fienberg, A.A., Nairn, A.C., Surmeier, D.J., Greengard, P., 2004. A Network of Control Mediated by Regulator of Calcium/Calmodulin-Dependent Signaling. Science 306, 698–701. doi:10.1126/science.1099961

Renthal, W., Maze, I., Krishnan, V., Covington, H.E., Xiao, G., Kumar, A., Russo, S.J., Graham, A., Tsankova, N., Kippin, T.E., Kerstetter, K.A., Neve, R.L., Haggarty, S.J., McKinsey, T.A., Bassel-Duby, R., Olson, E.N., Nestler, E.J., 2007. Histone deacetylase 5 epigenetically controls behavioral adaptations to chronic emotional stimuli. Neuron 56, 517–529. doi:10.1016/j.neuron.2007.09.032

Renz, M., Langowski, J., 2008. Dynamics of the CapG actin-binding protein in the cell nucleus studied by FRAP and FCS. Chromosome Res. Int. J. Mol. Supramol. Evol. Asp. Chromosome Biol. 16, 427–437. doi:10.1007/s10577-008-1234-6

Ries, J., Chiantia, S., Schwille, P., 2009. Accurate determination of membrane dynamics with line-scan FCS. Biophys. J. 96, 1999–2008. doi:10.1016/j.bpj.2008.12.3888

Rostas, J.A., Dunkley, P.R., 1992. Multiple forms and distribution of calcium/calmodulin-stimulated protein kinase II in brain. J. Neurochem. 59, 1191–1202.

Ruan, Q., Cheng, M.A., Levi, M., Gratton, E., Mantulin, W.W., 2004. Spatial-temporal studies of membrane dynamics: scanning fluorescence correlation spectroscopy (SFCS). Biophys. J. 87, 1260–1267. doi:10.1529/biophysj.103.036483

Salomé, R., Kremer, Y., Dieudonné, S., Léger, J.-F., Krichevsky, O., Wyart, C., Chatenay, D., Bourdieu, L., 2006. Ultrafast random-access scanning in two-photon microscopy using acousto-optic deflectors. J. Neurosci. Methods 154, 161–174. doi:10.1016/j.jneumeth.2005.12.010

Sanabria, H., Digman, M.A., Gratton, E., Waxham, M.N., 2008. Spatial diffusivity and availability of intracellular calmodulin. Biophys. J. 95, 6002–6015. doi:10.1529/biophysj.108.138974

Sanabria, H., Kubota, Y., Waxham, M.N., 2007. Multiple diffusion mechanisms due to nanostructuring in crowded environments. Biophys. J. 92, 313–322. doi:10.1529/biophysj.106.090498

Sanabria, H., Swulius, M.T., Kolodziej, S.J., Liu, J., Waxham, M.N., 2009. CaMKIIβ regulates actin assembly and structure. J. Biol. Chem. 284, 9770–

9780. doi:10.1074/jbc.M809518200

Sanabria, H., Waxham, M.N., 2010. Transient anomalous subdiffusion: effects of specific and nonspecific probe binding with actin gels. J. Phys. Chem. B 114, 959–972. doi:10.1021/jp9072153

Sanhueza, M., Lisman, J., 2013. The CaMKII/NMDAR complex as a molecular memory. Mol. Brain 6, 10. doi:10.1186/1756-6606-6-10

Schlessinger, J., Axelrod, D., Koppel, D.E., Webb, W.W., Elson, E.L., 1977. Lateral transport of a lipid probe and labeled proteins on a cell membrane. Science 195, 307–309.

Schulman, H., Hanson, P.I., 1993. Multifunctional Ca^{2+}/calmodulin-dependent protein kinase. Neurochem. Res. 18, 65–77.

Schwille, P., 2001. Fluorescence correlation spectroscopy and its potential for intracellular applications. Cell Biochem. Biophys. 34, 383–408. doi:10.1385/CBB:34:3:383

Schwille, P., Haupts, U., Maiti, S., Webb, W.W., 1999. Molecular dynamics in living cells observed by fluorescence correlation spectroscopy with one- and two-photon excitation. Biophys. J. 77, 2251–2265. doi:10.1016/S0006-3495(99)77065-7

Schwille, P., Meyer-Almes, F.J., Rigler, R., 1997. Dual-color fluorescence cross-correlation spectroscopy for multicomponent diffusional analysis in solution. Biophys. J. 72, 1878–1886.

Scott, D., Roy, S., 2012. α-Synuclein inhibits intersynaptic vesicle mobility and maintains recycling-pool homeostasis. J. Neurosci. Off. J. Soc. Neurosci. 32, 10129–10135. doi:10.1523/JNEUROSCI.0535-12.2012

Shafeghat, N., Heidarinejad, M., Murata, N., Nakamura, H., Inoue, T., 2016. Optical detection of neuron connectivity by random access two-photon microscopy. J. Neurosci. Methods 263, 48–56. doi:10.1016/j.jneumeth.2016.01.023

Shen, K., Meyer, T., 1999. Dynamic control of CaMKII translocation and localization in hippocampal neurons by NMDA receptor stimulation. Science 284, 162–166.

Shen, K., Meyer, T., 1998. In vivo and in vitro characterization of the sequence requirement for oligomer formation of Ca^{2+}/calmodulin-dependent protein kinase IIalpha. J. Neurochem. 70, 96–104.

Shen, K., Teruel, M.N., Subramanian, K., Meyer, T., 1998. CaMKIIβ functions as an F-actin targeting module that localizes CaMKIIα/β heterooligomers to dendritic spines. Neuron 21, 593–606.

Shtrahman, M., Yeung, C., Nauen, D.W., Bi, G., Wu, X., 2005. Probing Vesicle

Dynamics in Single Hippocampal Synapses. Biophys. J. 89, 3615–3627. https://doi.org/10.1529/biophysj.105.059295

Silver, P.A., 1991. How proteins enter the nucleus. Cell 64, 489–497.

Simon, B., Huart, A.-S., Wilmanns, M., 2015. Molecular mechanisms of protein kinase regulation by calcium/calmodulin. Bioorg. Med. Chem. 23, 2749–2760. doi:10.1016/j.bmc.2015.04.051

Sinnecker, D., Voigt, P., Hellwig, N., Schaefer, M., 2005. Reversible photobleaching of enhanced green fluorescent proteins. Biochemistry (Mosc.) 44, 7085–7094. doi:10.1021/bi047881x

Sisan, D.R., Arevalo, R., Graves, C., McAllister, R., Urbach, J.S., 2006. Spatially Resolved Fluorescence Correlation Spectroscopy Using a Spinning Disk Confocal Microscope. Biophys. J. 91, 4241–4252. doi:10.1529/biophysj.106.084251

Slade, K.M., Baker, R., Chua, M., Thompson, N.L., Pielak, G.J., 2009. Effects of recombinant protein expression on green fluorescent protein diffusion in Escherichia coli. Biochemistry (Mosc.) 48, 5083–5089. doi:10.1021/bi9004107

Srinivasan, M., Edman, C.F., Schulman, H., 1994. Alternative splicing introduces a nuclear localization signal that targets multifunctional CaM kinase to the nucleus. J. Cell Biol. 126, 839–852.

Stratton, M., Lee, I.-H., Bhattacharyya, M., Christensen, S.M., Chao, L.H., Schulman, H., Groves, J.T., Kuriyan, J., 2014. Activation-triggered subunit exchange between CaMKII holoenzymes facilitates the spread of kinase activity. eLife 3, e01610. doi:10.7554/eLife.01610

Sun, P., Enslen, H., Myung, P.S., Maurer, R.A., 1994. Differential activation of CREB by Ca^{2+}/calmodulin-dependent protein kinases type II and type IV involves phosphorylation of a site that negatively regulates activity. Genes Dev. 8, 2527–2539.

Takeuchi, Y., Fukunaga, K., Miyamoto, E., 2002. Activation of nuclear Ca^{2+}calmodulin-dependent protein kinase II and brain-derived neurotrophic factor gene expression by stimulation of dopamine D2 receptor in transfected NG108-15 cells. J. Neurochem. 82, 316–328.

Takeuchi, Y., Yamamoto, H., Fukunaga, K., Miyakawa, T., Miyamoto, E., 2000. Identification of the isoforms of Ca^{2+}/Calmodulin-dependent protein kinase II in rat astrocytes and their subcellular localization. J. Neurochem. 74, 2557–2567.

Tao-Cheng, J.H., Vinade, L., Smith, C., Winters, C.A., Ward, R., Brightman, M.W., Reese, T.S., Dosemeci, A., 2001. Sustained elevation of calcium induces Ca^{2+}/calmodulin-dependent protein kinase II clusters in hippocampal neurons.

Neuroscience 106, 69–78.

Terada, N., Tadakuma, H., Ishihama, Y., Yamagishi, M., Zako, T., Funatsu, T., 2005. Analysis of Nuclear Microenvironments by Translational Diffusion of GFP Using Fluorescence Correlation Spectroscopy. bioimages 13, 1–10. doi:10.11169/bioimages.13.1

Terada, S., Kinjo, M., Hirokawa, N., 2000. Oligomeric tubulin in large transporting complex is transported via kinesin in squid giant axons. Cell 103, 141–155.

Thorogate, R., Török, K., 2004. Ca^{2+}-dependent and -independent mechanisms of calmodulin nuclear translocation. J. Cell Sci. 117, 5923–5936. doi:10.1242/jcs.01510

Tidow, H., Nissen, P., 2013. Structural diversity of calmodulin binding to its target sites. FEBS J. 280, 5551–5565. doi:10.1111/febs.12296

Tombes, R.M., Faison, M.O., Turbeville, J.M., 2003. Organization and evolution of multifunctional Ca^{2+}/CaM-dependent protein kinase genes. Gene 322, 17–31.

Tremper-Wells, B., Vallano, M.L., 2005. Nuclear calpain regulates Ca^{2+}-dependent signaling via proteolysis of nuclear Ca^{2+}/calmodulin-dependent protein kinase type IV in cultured neurons. J. Biol. Chem. 280, 2165–2175. doi:10.1074/jbc.M410591200

Tsuriel, S., Geva, R., Zamorano, P., Dresbach, T., Boeckers, T., Gundelfinger, E.D., Garner, C.C., Ziv, N.E., 2006. Local sharing as a predominant determinant of synaptic matrix molecular dynamics. PLoS Biol. 4, e271. doi:10.1371/journal.pbio.0040271

Vosler, P.S., Brennan, C.S., Chen, J., 2008. Calpain-mediated signaling mechanisms in neuronal injury and neurodegeneration. Mol. Neurobiol. 38, 78–100. doi:10.1007/s12035-008-8036-x

Watanabe, N., Mitchison, T.J., 2002. Single-molecule speckle analysis of actin filament turnover in lamellipodia. Science 295, 1083–1086. doi:10.1126/science.1067470

Waters, J.C., 2007. Live-cell fluorescence imaging. Methods Cell Biol. 81, 115–140. doi:10.1016/S0091-679X(06)81007-1

Watson, J.B., Sutcliffe, J.G., Fisher, R.S., 1992. Localization of the protein kinase C phosphorylation/calmodulin-binding substrate RC3 in dendritic spines of neostriatal neurons. Proc. Natl. Acad. Sci. 89, 8581–8585. doi:10.1073/pnas.89.18.8581

Weber, J.T., 2007. Green Fluorescent Protein: Properties, Applications, and Protocols. 2nd Edition Edited by M. Chalfie and S. R. Kain. Wiley-Interscience, Hoboken. 2006. xv + 443 pp.

Wei, J.-Y., Lu, Q.-N., Li, W.-M., He, W., 2015. Intracellular translocation of

histone deacetylase 5 regulates neuronal cell apoptosis. Brain Res. 1604, 15–24. doi:10.1016/j.brainres.2015.01.043

Weissman, M., Schindler, H., Feher, G., 1976. Determination of molecular weights by fluctuation spectroscopy: application to DNA. Proc. Natl. Acad. Sci. U. S. A. 73, 2776–2780.

Wohland, T., Rigler, R., Vogel, H., 2001. The standard deviation in fluorescence correlation spectroscopy. Biophys. J. 80, 2987–2999. doi:10.1016/S0006-3495(01)76264-9

Xia, Z., Storm, D.R., 2005. The role of calmodulin as a signal integrator for synaptic plasticity. Nat. Rev. Neurosci. 6, 267–276. doi:10.1038/nrn1647

Yang, F., Moss, L.G., Phillips, G.N., 1996. The molecular structure of green fluorescent protein. Nat. Biotechnol. 14, 1246–1251. doi:10.1038/nbt1096-1246

Yoshimura, Y., Nomura, T., Yamauchi, T., 1996. Purification and characterization of active fragment of Ca^{2+}/calmodulin-dependent protein kinase II from the post-synaptic density in the rat forebrain. J. Biochem. (Tokyo) 119, 268–273.

Zacharias, D.A., Violin, J.D., Newton, A.C., Tsien, R.Y., 2002. Partitioning of lipid-modified monomeric GFPs into membrane microdomains of live cells. Science 296, 913–916. doi:10.1126/science.1068539

Zhou, H.-X., Rivas, G., Minton, A.P., 2008. Macromolecular crowding and confinement: biochemical, biophysical, and potential physiological consequences. Annu. Rev. Biophys. 37, 375–397. doi:10.1146/annurev.biophys.37.032807.125817

早稲田大学 博士(理学) 学位申請 研究業績書

(List of research achievements for application of doctorate (Dr. of Science), Waseda University)

氏名 Seyed Morteza Heidarinejad Mohammadi 印(seal or signature)

（As of February, 2018 ）

種類別 (By Type)	題名、 発表・発行掲載誌名、 発表・発行年月、 連名者（申請者含む） (theme, journal name, date & year of publication, name of authors inc. yourself)
Academic paper	○1. Heidarinejad, M., Nakamura, H., Inoue, T., 2018. Stimulation-induced changes in diffusion and structure of calmodulin and calmodulin-dependent protein kinase II proteins in neurons. Neuroscience Research, in press.
Academic paper	2. Shafeghat, N., Heidarinejad, M., Murata, N., Nakamura, H., Inoue, T., 2016. Optical detection of neuron connectivity by random access two-photon microscopy. J. Neurosci. Methods 263, 48–56.
Oral presentation in academic meeting	3. Heidarinejad, M, Inoue, T., Multi-point fluorescence correlation spectroscopy by AOD-driven two photon microscopy, 8th bio-optics research conference, Riken symposium, Kitasato University, December 2011, Kanagawa, Japan